UNIVERSITETET
I OSLO

Master Thesis

Identification of chromatin regulators involved in the maintenance of transcriptional homeostasis by centromeres and mitotic chromatin in *Saccharomyces cerevisiae*

Juna Steinnes

Genetics and developmental biology

60 credits

Section of Molecular Biology and Biochemistry

Faculty of Mathematics and Natural Sciences,
Department of Biosciences

2023

Identification of chromatin regulators involved in the maintenance of transcriptional homeostasis by centromeres and mitotic chromatin in *Saccharomyces cerevisiae*

Juna Steinnes

http://www.duo.uio.no/

Printing: Reprosentralen, Universitetet i Oslo

Acknowledgements

I would like to express my sincere gratitude to my primary advisor, Pierre Chymkowitch, for his invaluable guidance and support throughout my master's thesis. Despite his busy schedule as a PI, he always made time to answer my questions and provide valuable feedback that greatly enhanced the quality of my work.

I would also like to thank my secondary advisor, Lucia Ramos-Alonso, for her patience and thorough training in yeast culture and methods. Her expertise and encouragement were vital in enabling me to carry out my experiments and achieve the desired results. Her optimism and professionality have been fundamental in shaping my research experience.

I am also grateful to the Chymkowitch lab group for their collaborative and supportive environment, which fostered my growth as a researcher. I am grateful to my fellow lab mates; Xu, Yunna, Patrizia and Sophia for their inspiring discussions in both biology-related and unrelated content, helpful comments, and technical assistance.

I would like to extend my appreciation to the faculty and staff at the Faculty of Mathematics and Natural Sciences, Department of Biosciences for providing me with the necessary resources and infrastructure to pursue my research interests.

Finally, I would like to acknowledge the support of my family and friends, many of whom I met during my studies at UiO, who have encouraged and motivated me throughout my academic journey. Their love and encouragement have been a constant source of strength and inspiration.

Abstract

Chromatin is the complex of DNA and nucleosomes that makes up chromosomes and is responsible for packaging and protecting genetic information. Chromatin architecture and functions are dramatically affected during the cell cycle. During the S phase, the genome duplicates, which involves the dissociation of nucleosomes from the DNA, and during M phase, the chromatids contract and condense to a state that facilitates segregation to each daughter cell after cell division.

Recent studies have highlighted the central role of the centromere in regulating chromatin structure and gene expression at mitosis. Strikingly, evidence shows that the centromeres license the mitotic condensation of entire chromosome arms in *Saccharomyces cerevisiae.* Some of the factors involved include Aurora B, triggering condensation in late metaphase, and the histone deacetylase Hst2, acting together with Shugoshin to propagate the signal outwards from the centromere to chromosome arms. A mechanism found to act strictly in *cis*, and centromere-less chromatin fails to condense during mitosis. A recent study from the Chymkowitch lab found that when a chromosome fails to condense during mitosis, it remains unable to reset transcriptional homeostasis during the subsequent interphase, showing that mitotic condensation also acts as a vital protective mechanism of transcriptional fidelity. However, it is not established that the identified proteins, Aurora B, Bub1, Shugoshin and Hst2 are solely responsible for this chromosome-wide signal.

To identify factors involved in the regulation of transcription by centromeres, the first part of this project intended generation of yeast strains lacking genes encoding chromatin regulators: *DOT1, HAT1, RPD3, RTT109, SAS2, SAS3, SET1, SET2* and *SNF2.* Secondly, using qPCR in synchronized cells, I assessed the expression of selected genes in these deletion mutants before and after centromere-excision to identify chromatin regulators involved in maintenance of transcriptional homeostasis during interphase.

The work from this thesis identified a possible role of histone methyltransferase Set2, which may aid the centromere in transcriptional homeostasis via function outside its canonical role as a repressor of cryptic transcription. This thesis also identified the acetyltransferase Rtt109 and the deacetylase Hst2 as regulators worth further investigation.

Contents

Figures

Tables

1 Introduction

This chapter contains an introduction to the different topics that will be addressed throughout the study. Starting with eukaryotic chromatin organization, epigenetic markers with a focus on histone acetylation and methylation, an introduction to chromatin regulators used in this study and their function (marked with **bold** for clarity). Then moving on to the budding yeast cell cycle, centromere function and the aim of this study: **Identification of chromatin regulators involved in the maintenance of transcriptional homeostasis by centromeres and mitotic chromatin in *Saccharomyces cerevisiae*.**

1.1 Chromatin

The *genome* is the entire genetic information of an organism. It is made of relatively long strands of DNA which must be packed on different levels to be able to fit inside the cell. Each DNA strand consists of nucleotides that are covalently bound together with phosphodiester bonds forming an alternating deoxyribose-phosphate backbone with the nitrogenous bases; adenine with thymine (A - T), and cytosine with guanine (C - G) linking the strands together to form a double helix. The DNA molecule is negatively charged and rigid due to electrostatic repulsion between the phosphodiester bonds.

To be able to fold neatly inside the nucleus, the DNA double helix is at first level wrapped 145-147 bp, or 1.7 times around a positively charged protein octamer consisting of two times core histones H2A, H2B, H3 and H4. H2A forms a dimer with H2B, and H3 with H4 respectively (Luger et al., 1997). The negative DNA phosphate interacts through electrostatic bonding to the positively charged histone fold, while deoxyribose interacts with the fold through hydrogen bonding (Arents et al., 1991). This complex of DNA attached around core histones is called a *nucleosome* (see **Figure 1** for schematic) and it makes up the chromatin in the cell (Kornberg, 1977).

Each nucleosome is connected by 10-60 bp linker DNA and forms “beads-on-a-string” referred to as the 10nm fibre. In addition to the core histones, an H1 linker histone keeps the string in place around the core by binding the DNA entry/exit points. The nucleosomes with the H1 linker histone form the *chromatosome* (Allan et al., 1980; Zhou et al., 2015).

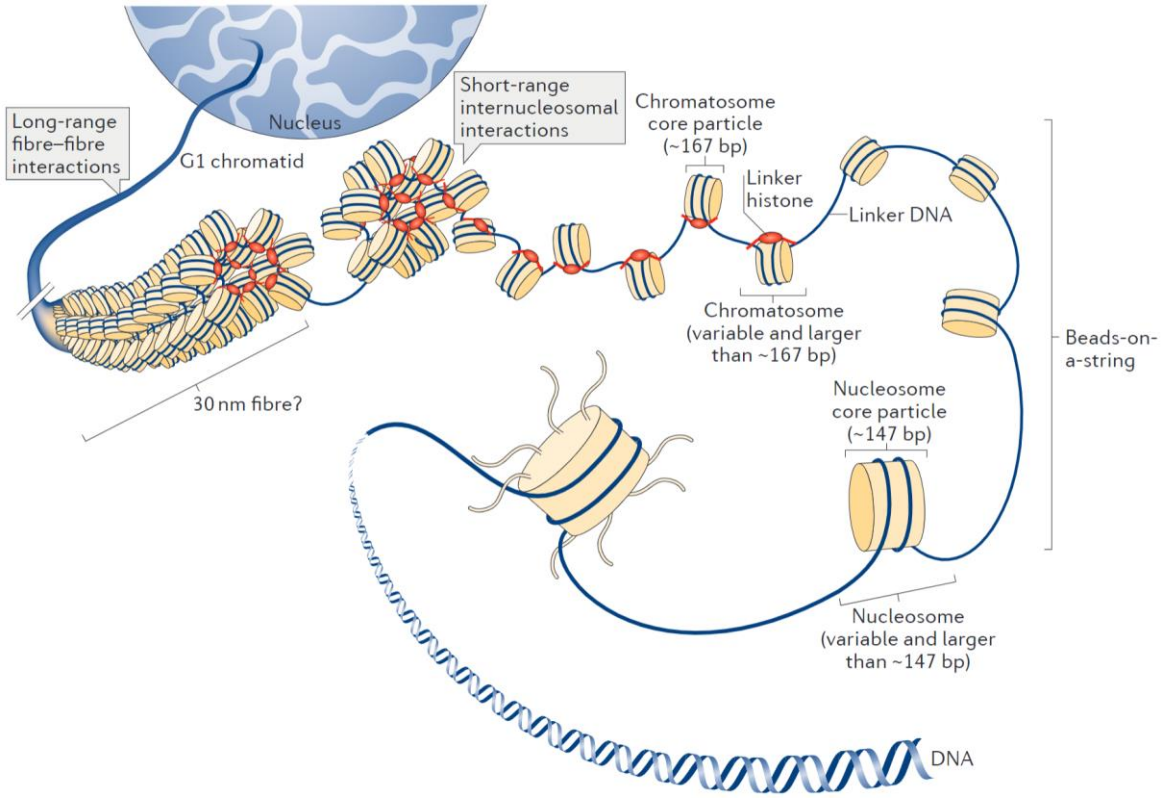

Figure 1. Various levels of chromatin folding. During interphase, DNA compaction within the nucleus involves multiple levels of histone-mediated folding. These include the formation of the nucleosome core particle, nucleosomes in a "bead-on-a-string arrangement", and the chromatosome core particle. The 30 nm fibre is debated in vivo and may only be relevant as short-range internucleosomal interactions of chromatin. The interaction of these fibres eventually forms tertiary structures (Fyodorov et al., 2018).

In vitro, the 10nm fibre can fold into a helical structure called the 30nm fibre at low salt concentrations (Arents et al., 1991; Finch & Klug, 1976). The H1 histone can stabilize this structure (Bednar et al., 1998), but a continuous 30nm fibre has not been observed *in vivo* (Efroni et al., 2008; Fyodorov et al., 2018; Ricci et al., 2015; Song et al., 2014).

Instead, it has been proposed that the chromatosomes form globular nucleosome clutches as short fragments of the 30nm fibre (Ricci et al., 2015) described as "short-range internucleosomal interactions" in Figure 1. Long-range fibre- fibre loops by condensin, cohesin and other nuclear proteins further condense the chromatin to a diameter of 50-1000nm (Fyodorov et al., 2018; Maeshima et al., 2016). The chromatin forms distinct chromosomes within the cell's nucleus.

Chromatin can be divided into two different types, decondensed and actively transcribed euchromatin and more condensed and transcriptionally silent heterochromatin.

1.1.1 Epigenetics, above the genome

The Greek word "*epi*" means over/above which means that *epigenetics* translates to "*above the genome*". Genomes of individual organisms are different, but all somatic cells within an organism share the same genetic code except for mutations that occur during its lifespan. The study of epigenetics has become a fascinating field that has captured the attention of scientists for many years. The interplay that occurs within the cell is in a delicate balance between the modifications inside the chromatin and the cellular machinery that reads and interprets these modifications. Factors such as nutrient availability, temperature, tissue type or cell cycle affect the cell's gene expression program. The gene expression does not arise from alterations in the DNA sequence, but rather from epigenetic marks like histone modifications, noncoding RNA (ncRNA) or DNA methylation. A small change can result in a wide range of biological outcomes important for understanding differentiation and development, but also an abnormal expression of genes due to improper epigenetic regulation, causing diseases, including cancer and neurological disorders.

Transcription by RNA Polymerase II is conserved from yeast to higher eukaryotes and involves the assembly of general transcription factors (GTFs): TFII-A, -B, -D, -E and -H with RNAPII on promoters, which forms the pre-initiation complex (PIC). The mediator complex aids in transmitting signals from transcription- and co-factors bound to enhancers to the transcriptional machinery on promoters. RNAPII's biggest subunit Rpb1 is then consecutively phosphorylated by CDKs which allow mRNA synthesis by RNAPII, and also chromatin modification during elongation and termination.

The accessibility of chromatin highly impacts gene expression. Condensed heterochromatin is tightly packed and hardly accessible for the transcriptional machinery. Heterochromatin can be *facultative*; meaning it can change states between heterochromatin and euchromatin depending on the cell's environment and cell fate. Or it can be *constitutive*; meaning it remains condensed through the organism's life cycle and mainly consists of tandem repeats inside telomeres and the centromere. Other than the condensed state, chromatin can be identified by its histone modification identity (Grunstein & Gasser, 2013).

Euchromatin holds a more complex and greater amount of histone modifications and contains regions that are more gene-rich and actively transcribed than heterochromatin. Heterochromatin usually localizes near the periphery of the nucleus or closer to the nucleolus,

while euchromatin occupies the remaining space (Gotta et al., 1996; Grunstein & Gasser, 2013). There are popular model organisms within mammalian or vertebrate species, but the most basic understandings have come from the single-celled organism *Saccharomyces Cerevisiae,* also called budding yeast which is used in this study (Rando & Winston, 2012).

1.1.2 *Saccharomyces Cerevisiae*: A key model organism to understand epigenetic marks

The budding yeast *S. cerevisiae* is the most used model organism for studying genetics, epigenetics, and chromatin state in the last two decades, but why?

Some characteristics include:

- Diploids can reproduce sexually, or haploids can reproduce vegetatively by budding, hence its name "budding yeast".
- Easily cultured in the laboratory with a generation time of about 90 minutes, depending on environmental and genetic factors.
- Small genome, well-established genetics, and easily mutated.
- Availability of genetic tools such as genetic libraries, mutant strains, and techniques developed to manipulate gene expression.
- Many cellular processes in cell cycle regulation, DNA repair, and regulation of gene expression, are conserved in higher eukaryotes.
- Has one of the simplest eukaryotic epigenomes, lacking repressive histone H3K9 methylation, 5mC DNA methylation and RNA interference (RNAi) machinery. Making a valuable model for simplified studies on remaining epigenetic markers.

(Comparative studies of DNA methylation in eukaryotes suggest that budding yeast lost this epigenetic pathway early during evolution, thus relying on histone modifications to define epigenetic states. However, opposing findings make it inconclusive if DNA methylation exists in budding yeast (Buitrago et al., 2021; Proffitt et al., 1984; Tang et al., 2012), it will not be focused on further in this study.)

Also, budding yeast only have two copies of the core histone genes, making a strain with only a single copy easy to engineer, allowing for mutagenic analysis of histone proteins, and histone-tagging experiments. It is also unique in that it lacks canonical linker histones H1 and

H5 and has a shorter nucleosomal repeat length of 165 bp. This makes it an excellent model for studying histone modification and chromatin states through the cell cycle (Taddei & Gasser, 2012). An important advantage utilized in this study is the properties of the centromere, which is conserved. The centromere plays an essential role in cell division and will be discussed in more detail later in **Chapter 1.4 The functions of the centromere**.

All properties mentioned are used towards a basic understanding of the complexities of genetic processes, including gene regulation, mechanisms of the cell cycle and epigenetics. Insights from yeast can be applied to the study of similar processes in more complex organisms (Rando & Winston, 2012).

1.1.3 Histone post-translational modifications and modulators

The properties of histones, and therefore nucleosomes, can be altered by small chemical modifications on the histone tails called histone post-translational modifications (HPTMs) (**Figure 2**), such as acetylation, methylation, phosphorylation, sumoylation and ubiquitination groups. As each core histone can be modified at several amino-acid residues, it is believed that the combinations of HPTMs at specific genetic loci lead to differences in gene expression programs by activation or repression (Millar & Grunstein, 2006).

This study focuses on histone acetylation and methylation. Histone modifiers include "writers" that deposit marks, "erasers" that remove them and "readers" that recognize marks via specific domains. Writers and erasers for acetyl groups are called histone acetyltransferases (HATs) and histone deacetylases (HDACs), while writers and erasers for methyl groups are called histone methyltransferases (HMTs) and histone demethylases (HDMs). Readers recognize acetylated histones by bromodomains or methylated histones by chromodomains respectively. See **Table 1** for an overview of histone modulators with their known substrates.

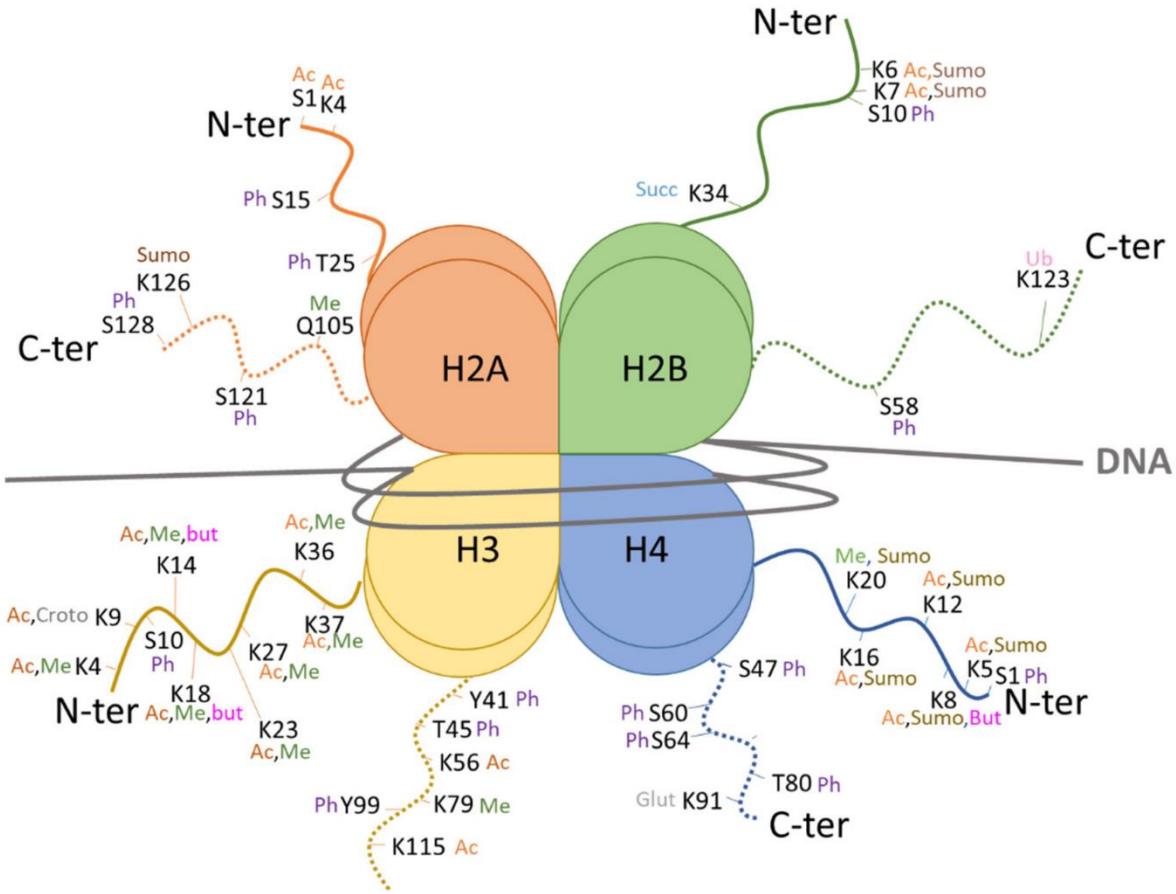

Figure 2. Histone post-translational modifications are frequently reported in *S. cerevisiae* (Etier et al., 2022). Schematic representation of a nucleosome containing DNA (in grey) wrapped around the canonical histone octamer. The N- (N-ter) and C-terminal (C-ter) tails of these histones are marked at specific amino acid residues (K, S, T, Q) with the following HPTMs; Acetylation (Ac), Methylation (Me), Phosphorylation (Ph), Sumoylation (Sumo), Ubiquitylation (Ub), Succinylation (Succ), Butyrylation (But), Glutarylation (Glut).

HATs are widely associated with transcriptional activation because acetyl groups added to nucleosomes neutralize the positive charge of histones. This weakens the DNA/histone interaction which leads to the opening of the chromatin. Examples of HATs in *S. cerevisiae* are **Hat1**, the first HAT to be identified and a subunit of **Hat1**/Hat2 and NuB4 complex. **Hat1** acetylates newly synthesized histones to mark them for deposition by chromatin chaperones, thought to be important in double-stranded DNA break (DSB) repair (Hammond et al., 2017). Another HAT important for DSB repair and nucleosome assembly is **Rtt109** which signals the completion of the repair, critical for turning off the DNA damage checkpoint in S phase, allowing cell cycle re-entry towards mitosis (Chen et al., 2008). Acetylation by **Sas2** however, represses telomeric silencing by the silent information regulator (SIR) complex (O'Kane & Hyland, 2019). **Sas3**, which is the catalytic subunit of Nucleosomal Acetyltransferase of histone H3 (NuA3 complex) promotes transcription or replication

elongation through nucleosomes together with other complexes through coupled acetyltransferase activity (Gilbert et al., 2014).

HDACs on the other hand, have the opposite activity of HATs and remove acetyl marks which leads to the repression of transcription. The Sir2 homolog **Hst2** contributes to mitotic condensation (Kruitwagen et al., 2018), while **Rpd3** is a more promiscuous deacetylase, with reported activity on all four histone proteins **(Table 1**).

An example of a reader of acetylated histones is the ATP-dependent chromatin remodelling complex Switch/Sucrose Non-Fermenting (SWI/SNF), which contains 12 subunits including the catalytic subunit Swi2/**Snf2**. **Snf2** also holds the bromodomain that recognizes (reads) acetylated lysines in histone 3 and histone 4 (H3 and H4) deposited by SAGA and NuA4 complexes.

Contrary to acetylation, methylation does not alter DNA/histone interaction. Instead, it recruits readers that recognize either mono-/di-/tri-methylation. The activity depends on the combination of histone, residue, or methylation state the nucleosome holds. This may lead to both activation or repression of transcription. Histone methyl modulators also tend to be more specific, with most known modulators only acting on a specific residue. Some important HMTs include **Set1**, a subunit of Complex of Proteins Associated with Set1 (COMPASS complex). **Set2**, which associates with the C-terminal domain (CTD) of RNAPII and methylates actively transcribed genes during elongation. **Dot1** deposits marks that inhibit telomeric silencing by the Silent Information Regulator (SIR) complex (Separovich & Wilkins, 2021).

Table 1. Histone modifications (acetylation and methylation) in *S. cerevisiae*. Histone modifiers used in this study are marked with orange for reference. The information for this table came from (Etier et al., 2022; Frigerio et al., 2023; Guillemette et al., 2011; Krebs, 2007; Pöpsel, 2015; Rando & Winston, 2012; Separovich & Wilkins, 2021). Not a complete table.

Histone	Residue	Mark	HATs	HDACs	HMTs	HDMs
H2A	K5	Ac	Esa1	Rpd3		
	K8	Ac	Esa1, Hat1	Rpd3		
H2B	K11	Ac	Esa1	Rpd3, Hda1, Hos3		
	K16	Ac	Esa1, Gcn5	Rpd3, Hda1		
H3	K4	Me, Ac	Gcn5, Rtt109		Set1	Jhd2
	K9	Ac	Gcn5, Rtt109*	Rpd3, Hos2, Hda1		
	K14	Ac	Gcn5, Sas3	Rpd3, Hos2, Hos3, Hda1		
	K18	Ac	Gcn5	Rpd3, Hos2, Hda1		
	K23	Ac	Gcn5, Rtt109	Rpd3, Hos2, Hda1		
	K36	Me			Set2	Jhd1, Rph1
	R37**	Me				
	K42	Me				
	K49**	Ac	Gcn5			
	K56	Ac	Rtt109*, Spt10	Hst3, Hst4		
	K79	Me			Dot1	
H4	R3	Me				
	K5	Ac, Me	Esa1, Hat1*	Rpd3, Hos2	Set5	
	K8	Ac, Me	Esa1, Hat1	Rpd3, Hos2	Set5	
	K12	Ac, Me	Esa1, Hat1*	Rpd3, Hos2	Set5	
	K16	Ac	Esa1, Sas2	Sir2, Hos2, Hst1, Hst2		
	K20	Ac, Me	Esa1, Sas2	Sir2, Hos2, Hst1		
	K31	Me				

* on free histones. **Centromeric H3 (CenH3).

1.2 The interplay between histone modifications, chromatin structure and transcription.

In this chapter, I will introduce the chromatin regulators used in this study and some of their functions.

1.2.1 Set2/Rpd3 has a role in transcriptional elongation and DNA replication

The HMT **Set2** is responsible for mono-, di-, or tri-methylation of histone 3 lysine 36 (H3K36). This modification is important for regulating gene expression by facilitating transcriptional elongation, preventing cryptic transcription, DNA replication, timely progression of the cell cycle and additionally, a role in transcriptional silencing (more in **Chapter 1.2.3 Telomeric silencing**).

During transcriptional elongation, **Set2** is recruited to RNAPII's phosphorylated C-terminal tail and deposits H3K36me3 (tri-methylation) during the elongation, marking recently transcribed genes with enrichment at the 5'-end of the ORF. The chromodomain of Eaf3, a subunit of **Rpd3**S recognises and binds to H3K36me3 and can deacetylate multiple residues across all histone proteins (**Table 1**). Deacetylation leads to transcriptional repression of recently transcribed genes. It also suppresses intragenic transcriptional initiation of both sense- and antisense RNAs, thus preventing cryptic transcripts (Carrozza et al., 2005; Dronamraju et al., 2018; Venkatesh et al., 2016).

Set2 also plays a role in DNA replication. One study found that H3K36 methylation regulates the timing of Cdc45 binding to replication origins. H3K36me1 coupled histone acetylation facilitates early binding of Cdc45 to replication origins, while H3K36me3 coupled with histone deacetylation by **Rpd3** inhibit this association, delaying Cdc45 binding. The absence of H3K36 methylation results in a disruption of cell cycle control and impairments in the fidelity of cell cycle regulatory gene transcripts, which tend to be long and thus rely on **Set2** activity for accurate transcription. **Set2** levels also differ during the cell cycle, with a decrease in G1/S phase compared with G2/M, and it was found that **Set2** is specifically targeted for destruction after mitosis by the APC/C/Cdc20 complex. A non-degradable form of **Set2** also caused transcriptional defects in cell cycle regulated genes, showing that the cyclical activity of **Set2** is important for proper cell cycle progression. Deletion of **Set2** or **Rpd3** leads to

increased cryptic transcription activity and earlier Cdc45 binding, resulting in a more rapid S phase progression. These results show that the timing of firing replication origins during S phase is important for genome stability (Carrozza et al., 2005; Dronamraju et al., 2018; Pryde et al., 2009).

1.2.2 The COMPASS Complex and transcription at COMPASS-regulated genes

Another example of the interplay between writers, erasers and readers is the regulation of transcription at genes regulated by the HMT activity of the Complex of Proteins Associated with **Set1** (COMPASS complex). COMPASS consists of **Set1** and seven other polypeptides including Cps35. The Cps35 subunit recognizes (reads) and binds to mono-ubiquitinated histone H2B lysine 123 (H2BK123ub1) at COMPASS-regulated gene promoters.

COMPASS activity involves mono-/di- or tri-methylation of H3K4. It was thought that H2BK123ub1 was required for the methyl deposition by both COMPASS and the methyl transferase **Dot1** in both H3K4 and H3K79 respectively, but studies found that mono-methylation by the two HMTs occurred independently at both residues. However, no di- or tri-methylation occurred, suggesting that the recognition of H2BK123ub1 by Cps35 is only required for the deposition of additional methyl groups by **Set1** and **Dot1**. This might explain why H3K4me1 is found at enhancers and H3K4me2/3 is found at promoters and transcription start sites (TSS). Interestingly, methylation of H3K79 by **Dot1** is known to repress transcriptional silencing (more in **Chapter 1.2.3 Telomeric silencing**), so the COMPASS complex aids **Dot1** by enabling di- and tri-methylation at the location of actively transcribed genes, with H3K79 methylation enriched on the 3'-end of ORFs (Lee et al., 2007; Nakanishi et al., 2009; Shahbazian et al., 2005).

As mentioned, H3K4me3 especially is known to provide a docking site for proteins that promote transcription. One such complex is the NuA3 complex where the Yng1 subunit has a specific binding affinity for H3K4me3 at promoters through a plant homeodomain (PHD) finger. As a result, the complex catalyses the acetylation of H3K14 through the **Sas3** HAT domain. This leads to the opening of the chromatin and transcriptional initiation at COMPASS-regulated promoters (Gilbert et al., 2014). H3K14 acetylation is performed by **Sas3** or Gcn5, as loss of either protein only has a minor effect on the acetylation of H3K14 at different genes while a double mutant loses H3K14 acetylation and is lethal due to cell cycle

arrest in S phase of the cell cycle (more in **Chapter 1.2.4. Nucleosome assembly during replication**) (Lafon et al., 2012).

The H3K4 residue can also be acetylated by both HATs Gcn5 and **Rtt109**, but acetylation and methylation marks do not exist simultaneously on the same residue. At promoters, this acetylation is typically found just upstream of H3K4me3 and leads to the opening of chromatin and an increase in transcription (Guillemette et al., 2011).

The COMPASS complex is also known to methylate various proteins, including kinetochore protein Dam1. This methylation is also regulated by H2BK123ub1, like H3K4 methylation. Specifically, Dam1 di-methylation on K233 inhibits the phosphorylation of surrounding serines by the Aurora^{Ipl1} (Zhang et al., 2005). During mitosis, Aurora^{Ipl1} phosphorylates several kinetochore proteins, leading to stabilizing of the kinetochore structure (more in **Chapter 1.4.1 An anchor for the kinetochore** & **1.3.1 G1 phase**).

Previous studies have indicated that **Set1** opposes the functions of Aurora^{Ipl1} during mitosis. The deletion of ***SET1*** was found to lessen the abnormal chromosome segregation seen in cells with a temperature-sensitive Aurora^{Ipl1} mutation. Strikingly, this suppression is not tied to H3 methylation. Mutation of H2BK123ub1 does not produce Aurora^{Ipl1} repression, indicating that **Set1** has unexpected functions during mitosis that are separate from its role in transcription initiation and early elongation. A later study showed that **Set1** play a crucial role in regulating the release of SAC (**Chapter 1.4.1 An anchor for the kinetochore**), which prevents activation of the anaphase-promoting complex/cyclosome (APC/C). They suggest that the loss of H3K4 methylation enables sustained inhibition of Cdc20, an inhibitor of APC/C, resulting in a delay in the release of the SAC. This means that maintaining a proper balance of Dam1 methylation and phosphorylation is crucial for normal chromosome segregation and cell survival (Schibler et al., 2016; Zhang et al., 2005).

1.2.3 Telomeric silencing

One of the most characterized epigenetic events in budding yeast is telomeric silencing, which is the spreading of heterochromatin ~3 kb from telomeric regions (Lowell & Pillus, 1998). In the establishment phase, telomere-binding proteins Rap1 and yKu70/80 bind to telomeric TG1–3 DNA repeats which recruit Sir4, followed by Sir2 and Sir3 which are sirtuin components of the SIR complex. Cooperative interactions between Sir2, Sir3, and different

histone modifiers spreads the signal along the telomere, leading to heterochromatic silencing. The signal is mainly regulated by two specific histone modifications; H4K16 acetylation by HAT **Sas2** and H3K79 methylation by HMT **Dot1** (O'Kane & Hyland, 2019).

Sir2 targets acetylated H4K16 nucleosomes for deacetylation while Sir3 selectively binds deacetylated H4K16 nucleosomes. Sir2 deacetylation also produces O-acetyl-ADP-ribose (OAADPr), a by-product that increases affinity for SIR complex-nucleosome binding. Together, this generates a positive feedback mechanism that facilitates the shifting of the SIR complex along telomeres. The spreading of heterochromatin through Sir2 deacetylase activity is limited by the competing activity of **Sas2** at adjacent euchromatin, disrupting Sir3 binding. Also, the activity of **Sas2** favours the recruitment of **Dot1**, which binds to H4K16ac nucleosomes and methylates H3K79. This methylation state weakens the interaction of Sir3's bromo-adjacent homology (BAH) to nucleosomes which inhibits the spreading of heterochromatin. This means that the modification states of H4K16 and H3K79 define the specificity of locations on the chromosomes that facilitate SIR complex binding, and propagation of the telomeric silencing signal.

Another HDAC able to deacetylate H4K16 is the Sir2 homolog **Hst2**, which is an important factor for chromosome condensation during mitosis and primarily locates to the cytoplasm (more in **Chapter 1.4.3 Chromosome condensation; compaction and contraction during mitosis**), though also important for repression of subtelomeric genes. Research has shown that they compete for a shared ligand that is required by Sir2 for telomeric silencing (Perrod et al., 2001).

Interestingly, the HDAC complex **Rpd3**L is thought to outline silent chromatin boundaries indirectly through its broad activity. The unspecific deacetylation activity (**Table 1**) may remove SIR complex acetyl substrates, inhibiting Sir2 from producing OAADPr and hindering SIR complex to spread beyond true heterochromatic regions (Ehrentraut, 2010). Alternatively, **Rpd3**L's removal of acetylation marks on H2B and H4 may reinforce a chromatin configuration that inhibits the SIR complex (Zhou et al., 2009).

It has also been found that H3K36me by **Set2** is essential in protecting subtelomeric euchromatin from erroneous silencing by the SIR complex. The absence of **Set2** causes a

significant decrease in the expression of genes located within ~20 kb of telomeres (Tompa & Madhani, 2007).

Another study also found that the COMPASS complex and **Set1**'s catalytic activity toward H3K4me2/3 is essential for the correct regulation of telomere maintenance factors, while telomere length regulation also relies on **Set1**'s catalytic activity but is likely independent of its H3K4 modification activity (Jezek et al., 2023).

Together, the balance between the activity of **Sas2**, **Dot1, Set1, Set2, Rpd3** and the SIR complex determines the silent chromatin boundaries along with factors such as barrier elements, other HPTMs and chromatin remodelling (O'Kane & Hyland, 2019).

1.2.4 Nucleosome assembly during replication

During S phase, HAT **Rtt109** acetylates H3K56 in newly synthesized histones in collaboration with the chaperone Asf1. Asf1 then transports the free H3K56ac/H4 dimer into the nucleus. Asf1 also has a physical interaction with the nuclear **Hat1**/Hat2/Hif1 complex which acetylates H4K5 and K12. Studies show that Asf1 assembles H3K56-H4K5/K12 acetylated dimers into chromatin behind replication forks (Ai & Parthun, 2004). Another study found that a wave of histone H3K9 acetylation by **Rtt109** progresses ~3-5 kb ahead of the replication fork. This slows replication velocity by promoting the replacement of nucleosomes evicted by the incoming fork, meaning that **Rtt109** acetylation protects genome integrity in two different pathways (Bar-Ziv et al., 2020; Frigerio et al., 2023).

The opposing deacetylation to **Rtt109** occurs via the HDAC activity of sirtuins Hst3 and Hst4 at G2/M phase entry in addition to post-DNA damage, while the opposing activity of **Hat1** is **Rpd3**. Since all histones have been deacetylated on mentioned residues in the previous cell cycle, unmarked histones are mixed with newly synthesized H3K56ac histones. This provides the ability to recognize the directionality of the replication fork, also aiding in genome stability. As the H3K56 residue is located near the entry/exit points in the nucleosome, acetylation by **Rtt109** opens the chromatin, this leads to the recruitment of DNA repair proteins, facilitates DNA unwrapping from the nucleosome and increases interaction between histones and chaperones that restores the chromatin structure (Chen et al., 2008; Frigerio et al., 2023; Gershon & Kupiec, 2021).

1.2.5 DNA Damage Response (DDR)

Interestingly, both H3K56 hypo- and hyperacetylation result in genomic instability. The acetylation state is utilized in the S phase checkpoint and prevents cells from proceeding with the cell cycle in response to DNA damage such as double-stranded breaks (DSBs). The S phase checkpoint can be inactivated either when DNA damage has been repaired (recovery) or in the presence of persistent DNA damage (adaptation). In the first case, inhibitors of the checkpoint proteins are repressed when the DSB is repaired. Cells lacking either **Rtt109** or Asf1 are incapable of reassembling chromatin following DSB repair. In this case, the DNA checkpoint remains active, and the cells are delayed in proceeding through the cell cycle even after DNA has been repaired (Chen et al., 2008; Gershon & Kupiec, 2021).

The HO pathway is the major pathway for DSB repair during replication and is named after *HO* endonuclease which cleaves damaged DNA, making a DSB/HO-lesion. The balance of H3K56 acetylation state during DNA replication is also required by the recombination machinery in choosing the right sister chromatid during homologous recombination. Hypoacetylation increases the exchange of sister chromatids during HO. H3K14ac by **Sas3** is associated with transcriptionally active chromatin but is also altered by the HO pathway triggered by DSB. H3K14ac is induced at the DSB site, recruiting the RSC complex via its bromodomain which facilitates the recruitment of subsequent DDR protein complexes to the break site. The absence of acetylation decreases accessibility to nucleosome-bound DNA and prevents nucleosome eviction, impairing nucleosome assembly pathways. This may also explain the sensitivity of both H3K56ac- and H3K14ac-related mutants to hydroxyurea (HU) and other DNA-damaging agents. Interestingly, **Rpd3** is found to repress activation of the *HO* gene and deletion of **Rpd3** cause elevated *HO* expression (Zhang et al., 2013).

The second major pathway in DSB repair is the non-homologous end-joining pathway (NHEJ). This response involves the methylation of H3 residues K4 by **Set1**, K36 by **Set2**, and K79 by **Dot1** mentioned earlier. Rad9 is a master regulator of DSB repair by NHEJ and binds to phosphorylated H2AS129 and H3K79me. H2BK123ub1 dependent di- and tri-methylation of H3K4 and K36 residues likely stabilize the interaction between Rad9 and the chromatin. leading to the upregulation of dNTPs, inhibition of late-firing origins, fork stabilization, and the activation of repair genes (Frigerio et al., 2023; Gershon & Kupiec, 2021).

In summary, precise and timely regulation of the H3 modifications; K56 by **Rtt109** enabled by Asf1, and K14 acetylation by **Sas3** in the HO pathway, together with modifications like K4me by **Set1**, K36me by **Set2** and K79me by **Dot1** in the NHEJ pathway is crucial for cell survival following DNA damage (Aricthota et al., 2022).

1.2.1 The chromatin remodelling SWI/SNF complex

Transcription of genes is linked to changes between the two types of chromatin structures described earlier, but changes in transcription are also due to smaller changes in nucleosomal positioning. By comparing repressed and activated gene expression in different growth conditions, it has been shown that increased transcription rates are accompanied by eviction of the -1 nucleosome from the transcription start site (TSS), more nucleosome-free regions (NFR) and increasingly delocalized nucleosomes in coding regions due to increased access to the chromatin (Rando & Winston, 2012). Many of these changes in nucleosome position are caused by chromatin remodelers recruited by transcription factors or by RNAPII, and RNAPII passage itself can also affect nucleosome positioning (Weiner et al. 2010). One important chromatin regulator containing a bromodomain (a "reader" mentioned earlier) is the SWI/SNF complex.

The 12 subunit SWI/SNF complex is responsible for controlling the mRNA levels of ~5% of all yeast genes. Interestingly, the affected genes do not belong to any specific functional category, but it was discovered that SWI/SNF plays a crucial role in transcription during the M phase. SWI/SNF was discovered via histone cross-linking studies via the association of the subunit Swi2/**Snf2** to nucleosomes. The ATPase activity of the Swi2/**Snf2** subunit is critical for the transcriptional activation and chromatin remodelling functions. SWI/SNF facilitate the access by transcription factors to the promoter regions in the chromatin by sliding and evicting nucleosomes in an ATP-dependent way. As a result, this complex plays a key role in both gene activation and repression (Dechassa et al., 2008).

The bromodomain of **Snf2** recognizes hyperacetylation by Gcn5, a catalytic subunit of multiple complexes like the SAGA complex, and Esa1 catalytic subunit of NuA4 complex (Allard et al., 1999). The binding of the bromodomain helps stabilize the association of SWI/SNF to the acetylated promoter nucleosomes. Without it, SWI/SNF can only do partial remodelling on nucleosomes even when ATPase function is intact. The bromodomain is also

needed for displacement of SAGA from the nucleosome (Awad & Hassan, 2008; Hassan et al., 2006).

Swi2/**Snf2** is also acetylated directly by Gcn5, this prevents the bromodomain from interacting with acetylated histones, acting as a regulatory switch to release SWI/SNF from already remodelled chromatin, allowing for the complex to be recycled for the next round of transcription (Strahl & Briggs, 2021).

1.3 Cell cycle

The cell cycle is controlled by the interaction between cyclin-dependent kinases (CDKs) and cyclins. Cyclins, which are named for their cyclical expression bind to CDKs and regulate their phosphorylation of target proteins. Both CDKs and cyclins are themselves regulated through phosphorylation. Regulation of CDK/Cyclin expression orchestrates cell cycle progression and is conserved between *S. cerevisiae* and higher eukaryotes. In *S. cerevisiae* the cell cycle is divided into three phases in budding yeast; G1 phase, S phase and G2/M phase.

1.3.1 G1 phase

During G1 phase, the cell expresses genes that prepare it for the following cell cycle stages. The chromatin is identified by its open state and epigenetic marks that facilitate transcription and gene expression. The cell monitors internal and external factors such as the availability of nutrients to determine whether it is appropriate to progress to the S phase, where DNA synthesis occurs.

One of *S. cerevisiae's* control mechanisms requires the cell to grow to a specific cell size in G1 before cell cycle progression to S phase (**Figure 3**). Reaching this size enables the cell to reach the START point, where it irreversibly commits to the mitotic cell cycle.

Therefore, it is thought that the cells only switches between G1, and S/G2/M phase. There are other

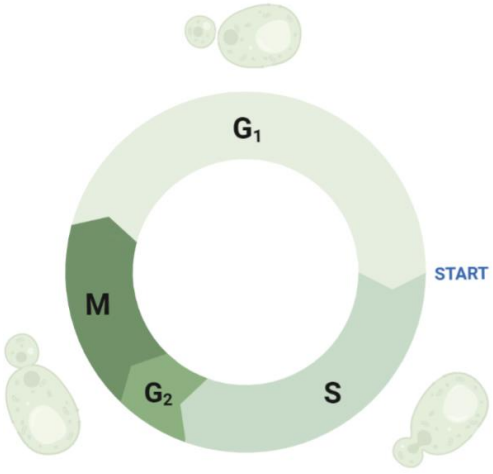

Figure 3. A simple schematic of cell cycle progression in budding yeast. The cell grows in G1-phase until reaching START. Bud emergence and duplication of cell components during S-phase. G2/M phase. The length of cell cycle stages are not measurable (made using Biorender).

checkpoints during the cell cycle but they only delay progression into subsequent stages. As a result, the cells cannot reverse into G1 without undergoing the last step of mitosis, cytokinesis. This size threshold at START prevents any decrease in cell size caused by premature cell cycle progression. Although the exact mechanisms are not understood, START involves some of the same CDKs and cyclins that control the cell cycle (Dungrawala et al., 2012)

1.3.1 S phase

During the S phase of the cell cycle, DNA is duplicated together with a higher transcription of histone proteins, chromatin chaperones, and S phase-specific signal proteins like cyclins. When DNA replication occurs, ribonucleotide reductase (RNR) catalyzes the reduction of ribonucleotides to deoxyribonucleotides (deoxynucleoside triphosphates (dNTPs))., which are then incorporated into the growing DNA strand or for DNA damage repair. Newly synthesised histone proteins are incorporated into newly replicated DNA by chaperones. This chromatin lacks epigenetic markers crucial for maintaining gene expression patterns, proper chromatin state and genome stability. The newly synthesized chromatin must be correctly marked at replication forks by histone modulators to maintain the epigenetic integrity through cell division. Euchromatin appears to be replicating prior to heterochromatin which is replicated in late S phase and is localised at the nuclear periphery (Howe et al., 2001).

The spindle pole body (SPB) which functions equivalent to the centrosome in higher eukaryotes is also duplicated in S phase and repositions to each side of the cell wall. SPB is embedded in the nuclear envelope, which does not break down in budding yeast compared to many eukaryotes (Fraschini, 2019). Already in S phase, a bipolar spindle of microtubules is formed alongside DNA replication and is associated with segregation factor kinesin-5 (Eg5) and the dynein motor protein which eventually allow positioning of the spindle and chromatin in the cell. Cohesin attaches to the sister-chromatids at the centromere and is protected from degradation.

Studies show that the kinetochore is attached to the microtubule during the whole cell cycle except for a brief moment in early S phase when the centromere is being replicated. The kinase Aurora B^{Ipl1} is recruited to the centromere and phosphorylates outer kinetochore complexes, enabling the assembly of the inner kinetochore (Kitamura et al., 2007). The existence of spindles during S phase has led to uncertainty about whether *S. cerevisiae* has a

proper G2 phase. Hence, many researchers studying *S. cerevisiae* refer to it as "G2/M" (Dörter & Momany, 2016).

1.3.1 M phase, cell division by budding

In G2/M, the chromosomes undergo major condensation and compaction where it is coiled and folded by condensin into a highly organized structure that is essential for proper segregation of sister-chromatids (more in **1.4.3 Chromosome condensation; compaction and contraction during mitosis**). During pro- and metaphase, sister-chromatids are not aligned in the centre of the cell, forming a metaphase-plate like in other eukaryotes (Straight et al., 1997), but they are still held in position by the spindle fibres. The Spindle assembly checkpoint (SAC) proteins promote attachment of the kinetochores to the sister-chromatids in a bi-polar way. Meanwhile, during SAC, unattached kinetochores catalyse the formation of the mitotic checkpoint complex (MCC) which inhibits the anaphase-promoting complex (APC/C) (Morgan, 2014). The spindle then exerts tension to monitor the proper attachment of chromosomes to kinetochores.

When proper biorientation and spindle tension is sensed and spindle assembly is satisfied, MCC disintegrates and SAC is uplifted. Cdc20, a part of MCC together with mitotic CDK/cyclin activates APC/C which leads to the degradation of securin, an inhibitor of separase. Separase cleaves off cohesin rings holding the sister-chromatids together, leading to the segregation event in anaphase. The sister chromatids separate and are pulled towards opposite poles of the cell by motor proteins and segregation factors, ensuring that each daughter cell will receive a complete set of chromosomes.

In budding yeast, the “budding neck” acts as the cleavage site at cytokinesis, separating the mother cell from the daughter cell. The spindle must be correctly positioned and aligned with the mother-bud axis. The bud neck may be established by polarity factors already in G1 before DNA replication and spindle formation, but timing is not established (Dörter & Momany, 2016; Fraschini, 2019; Juanes & Piatti, 2016). During telophase, the cell membrane grows inward along the budding neck, this process involves the assembly and constriction of the contractile actomyosin ring, which pinches the cell membrane inward until cytokinesis. Septins, a type of filamentous protein, help to maintain the shape of the division site and contribute to the stability of the daughter cells followed by synthesis of the missing cell wall and completes the formation of two separate daughter cells (Dörter & Momany, 2016).

The two cells then enter G1 phase where it needs to restore interphase transcription by opening the chromatin. Histone modifications play a critical role in this process by facilitating the re-establishment of euchromatin. Previous studies link both mitotic chromosome condensation, as well as transcriptional reset to the centromere (Kruitwagen et al., 2018; Ramos Alonso et al., 2023).

1.4 The functions of the centromere

In budding yeast, the centromere is identified by a 120-140 bp DNA sequence, and a centromere-specific histone 3 variant Cse4, also known as centromeric H3 (CenH3) and is commonly referred to as a "point-centromere". On the contrary, "regional centromeres" of most other eukaryotes can be 200 to 5000 Kb long, repetitive and mostly regulated by epigenetic markers such as histone modifications and DNA methylation patterns, rather than by specific DNA sequences. Regional centromeres are also able to relocate as an adaption to environmental signals (Tolomeo et al., 2017). Point-centromeres have a stable and consistent location on the chromosome and are well assembled in reference genomes. It also lacks H3K9 methylation often found in higher eukaryotes (Taddei & Gasser, 2012). This makes it easier to study the molecular mechanisms involved in centromere function, which is important in this study.

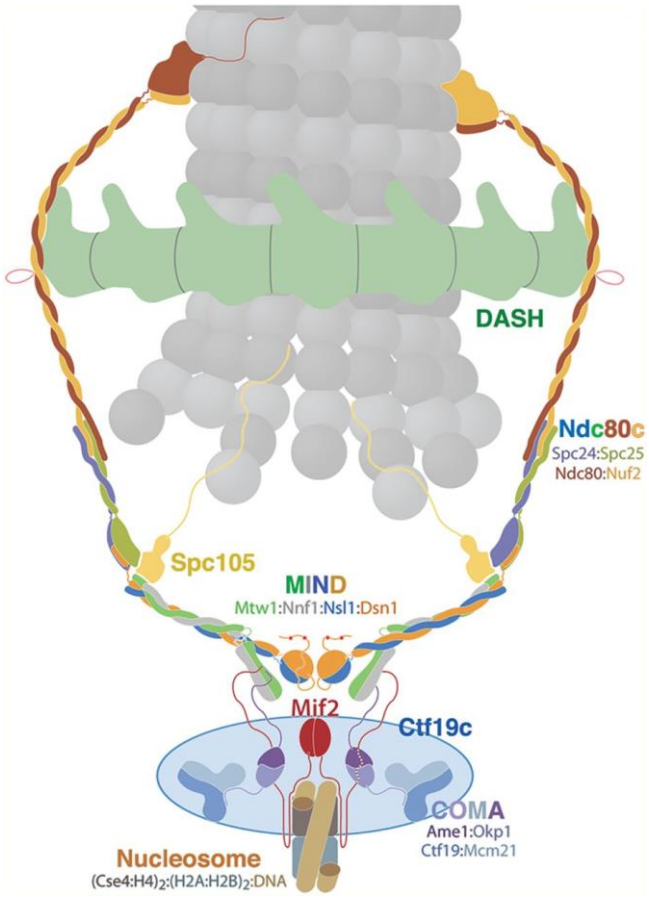

Figure 4. Two-dimensional schematic diagram of the principal components of yeast kinetochore: This representation does not show relative stoichiometries. Per nucleosome and microtubule, there are four to six MIND complexes and approximately eight Ndc80 complexes distributed around the DASH/Dam1c ring. The Ctf19 complex includes a total of 13 components (not shown). (Jenni et al., 2017).

1.4.1 An anchor for the kinetochore

The most known mechanism of the centromere is during mitosis by acting as an anchor for the kinetochore, ensuring

proper segregation of sister chromatids, with providing each cell with a complete copy of the genome.

The kinase Aurora B^{Ipl1} is recruited to the centromere and phosphorylates outer kinetochore complexes Ndc80c and DASH complex, enabling MIND's assembly of the inner kinetochore components Mif2 and COMA (Figure 4). $Shugoshin^{Sgo1}$ then promotes attachment of the kinetochores to the sister-chromatids in a bi-polar way by recruiting $PP2A^{Rts1}$ (Morgan, 2014).

Cohesin attached to the sister-chromatids at the centromere is protected from degradation until the separation event in mitosis. The spindle then exerts tension to monitor the proper attachment of chromosomes to kinetochores. When spindle assembly is satisfied, securin, an inhibitor of separase degrades leading to separase cleaving off cohesin rings holding the sister-chromatids together, causing the segregation event in anaphase. The sister chromatids separate and are pulled towards opposite poles of the cell by motor proteins and segregation factors, ensuring that each daughter cell will receive a complete set of chromosomes.

As the genes provide all vital information for the organism, the loss of a whole chromosome is fatal to the cell. This makes it difficult to study other possible roles of the centromere because the effect of loss, mutations or inhibition of a centromere has cascading effects on the cell in a global and dramatic way.

1.4.2 Non-canonical functions

Chromosome organization during interphase

Besides being an anchor for the kinetochore, in *S. cerevisiae* it has been observed that during interphase, centromeres cluster in the form of a rosette with the SPB at its centre. The opposite pole is occupied by the nucleolus, and chromosome arms continue from the centromeric pole towards the other pole. Studies have shown that this clustering is actively supported by microtubules during interphase, showing that centromeres are important for chromosome organization also outside of mitosis (Jin et al., 2000; Taddei & Gasser, 2012).

Separating species

Another study found that centromeric regions have higher mutation rates than any other part of the chromosome and the same has also been reported in multicellular plants and animals. Higher organisms regional centromeres are identified by epigenetic marks, and this could be an adaptation to maintain function despite of high mutation rates (Bensasson et al., 2008). On the other hand, the rapid evolvement of centromeres may cause incompatibilities between hybrid species and lead to reproductive isolation, giving centromeres a role in generating new species (Henikoff et al., 2001).

Maintaining transcriptional homeostasis

Due to chromatin condensation, gene expression nearly shuts down at mitosis. The prevention of transcription factors and *cis*-regulatory elements by the changed state of the chromatin silence expression of interphase genes (Vagnarelli, 2013). However, some active RNAPII remains active in housekeeping genes through mitosis to maintain advancement in the cell cycle and basic cellular functions (Palozola et al., 2017). After mitosis, proper regulation ensures that interphase gene expression is obtained. This study from our group found that when a chromosome fails to condense during mitosis, it remains unable to reset transcriptional homeostasis during the subsequent interphase, showing that mitotic condensation also acts as a vital protective mechanism of transcriptional fidelity (Ramos Alonso et al., 2023) and more in **Chapter 1.4.5 Centromere-regulated transcription**.

Identifying harmful genetic material

Another study from our group links mitotic condensation to the centromere by showing that the centromere is responsible for the mitotic condensation in yeast chromosome arms acting strictly in *cis*. Artificially condensed DNA circles, passively diffused to daughter cells without microtubule or kinetochore, suggesting that spreading of the condensation signal from centromeres is a critical mechanism for yeasts to protect their offspring from harmful genetic material introduced by viruses since centromeric endogenic chromatin can be distinguished from exogenous chromatin (Kruitwagen et al., 2018).

1.4.3 Chromosome condensation; compaction and contraction during mitosis

It has been proposed that mitotic chromosome condensation is divided into two parallel processes: short-range chromatin compaction due to changes in histone post-translational modifications coupled with the long-range condensin-facilitated (axial) contraction of chromosome arms.

The short-range chromatin compaction signal (**Figure 5**) is dependent on the phosphorylation of histone H3S10 in pericentromeric regions by Aurora B^{Ipl1} kinase, which is recruited to an unknown structure/factor located near the inner kinetochore regardless of other kinetochore functions or centromere locus. The SAC protein Bub1 then phosphorylates histone H2A on S121. This mediates a high-affinity binding-site for the recruitment of Shugoshin^{Sgo1} to pericentromeric chromatin. This signals the recruitment of the HDAC **Hst2** to chromatin, leading to the deacetylation of H4K16 from the centromere outwards to chromosome arms (Kruitwagen et al., 2018). A recent study found that **Hst2** depend on the 14-3-3 protein Bmh1 (not shown in **Figure 5**). They demonstrated that H3S10 phosphorylation by Aurora B^{Ipl1} recruited Bhm1, which simultaneously binds the H3 tail and phosphorylated C-terminal of **Hst2**, and this binding is essential for spreading the signal (Jain et al., 2021). However, H3S10p only remains high in pericentromeric regions, and the signal is also dependent on Shugoshin^{Sgo1} because H3S10p alone is not sufficient to initiate condensation (Kruitwagen et al., 2018). Therefore, the interaction between Shugoshin^{Sgo1} and **Hst2**/Bhm1 in the spreading of the signal is still unknown.

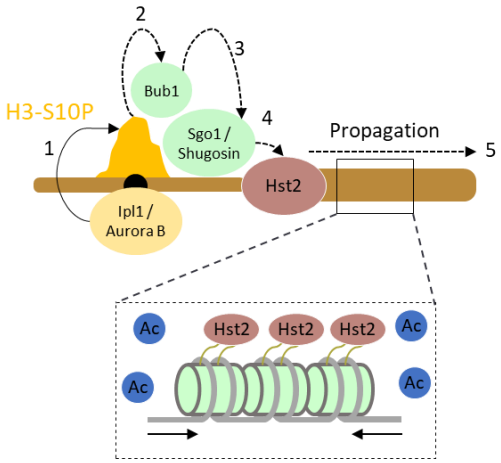

Figure 5. Mitotic chromosome condensation. Aurora B^{Ipl1} is recruited to the centromeres and phosphorylates pericentromeric regions (1, yellow) which activates Bub1 (2). Shugoshin (3) and Hst2 (4) deacetylates H4K16 which propagates the compaction-signal to chromosome arms in a Shugoshin-dependent manner (5).

Deacetylation of H4K16 leads to stronger *intra*-nucleosomal histone/DNA interactions, promoting short-range compaction. However, this interaction is not observed in highly condensed chromatin. It is thought that H4 tail's interaction on *intra*-nucleosomal DNA self-mediates shifting to the *inter*-nucleosomal H2A/H2B acidic pocket, and then to both DNA

and the acidic pocket in more condensed chromatin structures. The N-terminal tail of H3 is also thought to shift its interaction between *intra*-nucleosomal to *inter*-nucleosomal DNA in the presence of cations like Mg^{2+}. These interactions are essential for the formation of disulphide bridges and the 30nm fibre (Gordon et al., 2005).

Since a portion of these *inter*-nucleosome contacts was found in further condensed arrays of chromatin, they are thought to facilitate long-range condensation by the ring-shaped ATP-dependent complex called condensin, which compact chromatin more than 100-fold into consecutive coiled arrays coined loop extrusions (Goloborodko et al., 2016). However, mitotic condensation still occurs when condensin is disrupted. So more research is needed to characterize unknown factors for a complete model of long-range array interactions.

1.4.4 Centromere excision assay

Findings from papers with authors from the Chymkowitch group (Kruitwagen et al., 2018; Ramos Alonso et al., 2023), as well as this thesis utilized the centromere excision assay to study gene expression in relation to chromosome condensation. Apart from chromosome XII, which contains the 1-2 Mb rDNA cluster, chromosome IV is the longest chromosome (Jacq et al., 1997). And was chosen for excising because it was thought to have the biggest impact on resulting data and contains important genes regulating all cellular functions. The findings using the centromere excision assay highlight the importance of chromosome condensation in regulating gene expression, also providing insights into mechanisms that promote timely reactivation of gene expression and safeguarding of cell identity and homeostasis during interphase.

All yeast strains in this study (**Appendix C**) express Cre recombinase fused to an estradiol-binding domain (Cheng et al., 2000; Lindstrom & Gottschling, 2009). This protein (Cre-EBD) confines in the cytoplasm, but when 1 μM β-estradiol is added to the cell culture it triggers nuclear import and activates the Cre recombinase to excise DNA at loxP sites.

The centromere of chromosome IV is referred to as *CEN4*. Constructed by (Warsi et al., 2008), native *CEN4* was replaced by *CEN1*, followed by a kanamycin resistance cassette, flanked by lox recombination sites; *loxP(CEN1:kanMX4)loxP*. This genotype is referred to as *lox-CEN4-lox::KanMX*, or *CEN4** before excision and *cen4-* after excision (**Figure 6 A**). One

control strain does not have loxP sites flanking *CEN4* and is referred to as *CEN4* which is used to eliminate independent effects of Cre-EBD.

(Please note that the abbreviation "*CEN4"* is used to refer to both the centromere on chromosome IV, and the strain without loxP sites flanking *CEN4*.)

To assess excision efficiency, two different primer pairs were constructed. P1 with P2 only amplify before excision, and P3 with P4 only amplify after excision (**Figure 6 B**). A waiting time of 1.5 h ensures that most (97.41%) of the *CEN4** strains have their centromere removed (**Figure 6 C**).

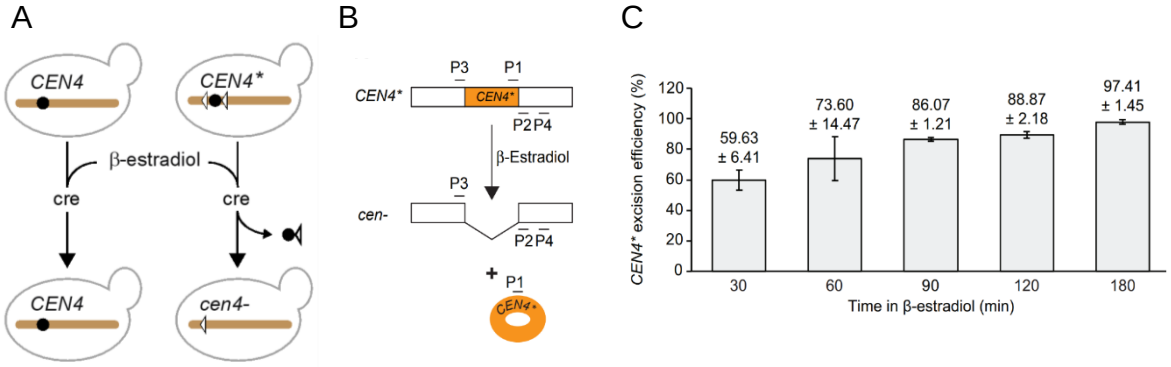

Figure 6. The centromere excision and efficiency assay (Kruitwagen et al., 2018; Ramos Alonso et al., 2023). A: Both *CEN4* (left) and *CEN4** (right) strains express Cre-EBD, but only *CEN4** has loxP sites flanking the centromere of chromosome IV (*CEN4*). When β-estradiol is added, it fuses to Cre-EBD which excises *CEN4* in the *CEN4** strain, becoming *cen4-*. **B:** Genomic DNA samples were analysed by qPCR using primers P1, P2, P3 and P4. The combination of P1 with P2 results in amplification only in *CEN4** cells, while the use of P3 and P4 produces amplification exclusively in *cen4-* cells. **C:** *CEN4* excision efficiency calculated at different time points after addition of β-estradiol.

1.4.5 Centromere-regulated transcription

The centromere is identified as a critical locus that instructs chromosome condensation, which limits whole-chromosome gene expression in *cis*. Inhibiting chromatin condensation by centromere excision disturbs communication between genes and their associated signals, emphasizing the significance of chromatin state in transcriptional regulation (Kruitwagen et al., 2018; Ramos Alonso et al., 2023).

The effect of centromere excision on gene expression is not revealed directly after excision, but rather after the cells have undergone mitosis (mitotic chromosome condensation) and stepped into the next interphase (**Figure 7**, bottom square). The same results were obtained by arresting cells in G1 with alpha-factor, in prometaphase using nocodazole or in S phase with hydroxyurea. Then, performing the centromere excision assay and releasing the cells into the

cell cycle. The loss of mitotic chromosome condensation significantly influences transcriptional activation within 90 minutes after completing mitosis, and this effect persists.

ChIPseq comparing *CEN4* and *cen4-* between all chromosomes show that markers of transcriptional activation; H4K12ac, H4K16ac, H3K4me3, RNA Pol II, CTD-S5p, CTD-S2p and RNAseq are all at much higher levels in the affected chromosome IV (in *cis*), relative to other chromosomes (in *trans*) after centromere excision. It has no topological effect, meaning these signals are evenly located through chromosome IV regardless of centromere location. This translates to centromere-less chromatin being more open, which increases random expression, triggering both erratic transcription and stress response from centromeric chromosomes (**Figure 7**). Failure of a chromosome to condense in mitosis leads to uncontrolled recruitment of transcription machinery to excessively relaxed chromatin, resulting in unregulated transcription of the entire chromosome in the next interphase, preventing transcriptional homeostasis by other means than merely silencing chromatin by physically excluding transcription factors. As the centromere is crucial for the segregation of sister chromatids, loss of the entire chromosome eventually results in loss of viability on all *cen4-* strains. It is therefore difficult to distinguish all the different effects from each other. However, it was found that the increase in transcription is not due to an excess of DNA templates caused by polyploidy.

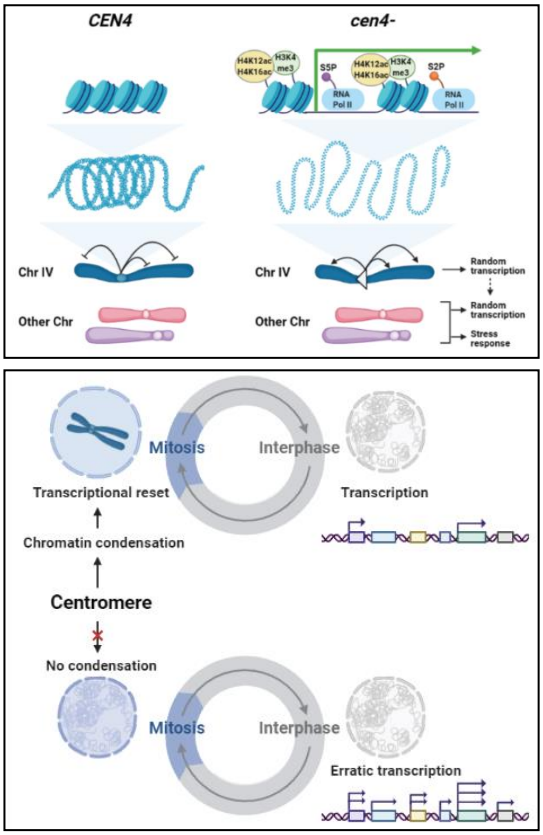

Figure 7. Mitotic chromosome condensation resets chromatin to safeguard transcriptional homeostasis during interphase (Ramos Alonso et al., 2023). Upper square: Failure to condense chromosome IV results in increased histone acetylation, which is followed by increased H3K4 methylation at promoters and initiation of transcription by RNA polymerase II. **Bottom square**: Centromere-induced mitotic chromosome condensation resets the transcriptome to prevent transcriptional drifting during interphase.

In conclusion, proper transcriptional output levels during interphase are dependent on chromosome condensation. Therefore, mitotic chromosome condensation, facilitated by centromeres, plays a crucial role in maintaining transcriptional homeostasis.

1.5 Aim of the study

After recent findings that centromeres license the mitotic condensation of yeast chromosome arms in *cis*, many of the upstream and downstream factors involved are still unknown. This study aims to characterize up- or downstream factors of centromere-dependent gene expression and mitotic chromosome condensation.

In the first part of this study, the intention was to create deletion mutant strains for 9 chosen genes of interest;

DOT1, HAT1, RPD3, RTT109, SAS2, SAS3, SET1, SET2 and *SNF2.*

These deletion mutants, together with a 10th mutant for *HST2* (already in Chymkowitch lab) could later be analysed by qPCR to compare differences in gene expression of chromosome IV genes before- and after *CEN4* excision.

2 Materials and methods

This chapter describes the materials and methods used in this study (**Figure 8**). Starting with yeast techniques and culture, followed by methods for the construction of deletion strains for the chosen genes of interest. Finished by methods to compare gene expression between wildtype and mutant strains before- and after centromere excision (**Chapter 1.4.4 Centromere excision assay** & **2.15 Centromere excision assay**). Appendixes B-E includes lists of materials, plasmids, *S. cerevisiae*, and *E. coli* strains, recipes, and software. Autoclaved and sterile materials were used in all culturing protocols to avoid contamination.

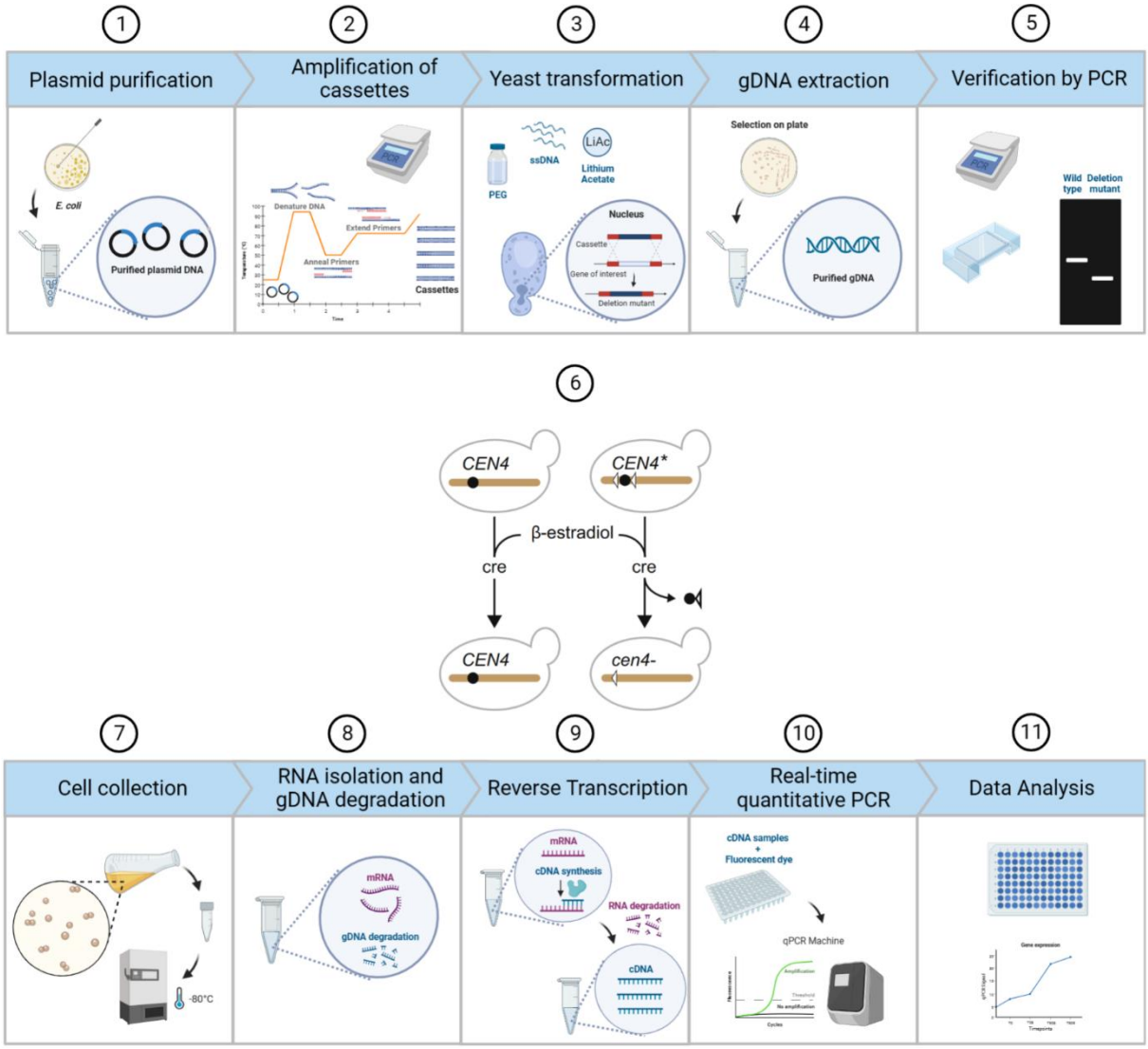

Figure 8. An overview of the workflow between various methods used in this master's thesis. The upper panel (1-5) shows methods used for strain construction, followed by the centromere excision (6) (Kruitwagen et al., 2018; Ramos Alonso et al., 2023). The lower panel (7-11) shows methods used for gene expression analysis (made using BioRender).

2.1 Yeast techniques and culture

2.1.1 Saccharomyces Cerevisiae strain

The experiments in this project were carried out using *S. cerevisiae* strains with S288c genetic background. The strain is used in the systematic sequencing project, the reference sequence stored in *Saccharomyces* Genome Database (SGD).

2.1.2 Yeast growth conditions

In this study, cultures of *S. cerevisiae* were either grown in YPD or CSM-His media with or without agar (**Appendix D**) in sterile, aerobic conditions, in a 30°C incubator with or without shaking.

Growth on plates containing agar

Classical petri dishes with media containing agar were used. The cells were streaked in a zig-zag motion on the surface of the agar plates with the intention of diluting the cell load and isolating single colonies of the yeast strain.

Liquid cultures

Single colonies were picked and incubated in a 200 rpm shaker in sterile vials containing liquid media occupying no more than 1/5 of the volume in the flask. The vials were placed at an angle to prevent precipitation and anaerobic conditions. Some methods use a liquid culture grown for 14-20 hours, which will be referred to as an overnight (O/N) culture.

2.1.1 Measuring cell culture density

A spectrophotometer (Eppendorf BioPhotometer) with OD_{600} settings was used for measuring yeast culture density. 1 ml sample was transferred to a cuvette and immediately measured to prevent incorrect measurements by cell precipitation. For maximum accuracy, the samples were diluted with mqH_2O so that OD_{600} of the sample was between 0.150 and 0.800. An OD_{600} of 0.5-1 corresponds to 1–2 x 10^7 yeast cells/ml for *S. cerevisiae*.

2.1.2 Storage of yeast strains

After 2 days of growth, plates were placed in at 4°C for short-term storage up to 2 months.

For long-term storage, a stock of yeast cells can be frozen in liquid YPD containing 20% glycerol at -80°C. This keeps the cells in a dormant phase for several years. The glycerol protects the cells by slowing the freezing time and prevents the formation of ice crystals that can damage the cell.

To prepare a stock solution, centrifuge an O/N culture at 4000 rpm for 1 min. and discard all but 1.5 ml of YPD. Add 500 µl 60% glycerol. Transfer the mixture to a cryotube and immediately freeze at -80°C. Cells can be plated directly from the frozen stock solution to an agar plate with a sterile inoculator.

2.2 Purification of plasmids from transformed bacteria

The plasmids used in this study were purified from host *E. coli* DH5a (Appendix C) in LB culture by using the kit Nucleospin® Plasmid (NoLid) from Macherey-Nagel™ following the manufacturer's instruction. The E. coli LB culture is first pelleted and resuspended in buffer (A1). The cells are then lysed in a lysis buffer (A2) before they are neutralized in buffer (A3). The sample is centrifuged to separate the supernatant containing plasmid DNA from cell debris and dissolved proteins. The supernatant with plasmid DNA is bound to the Nucleospin silica column under high-ionic conditions. Afterwards, any remaining contaminants along with the salt is washed away with buffer AW and A4. The plasmid DNA is then eluted with buffer AE.

Protocol for Nucleospin® Plasmid / Plasmid (NoLid)

1. 5 ml of a saturated E. coli culture was pelleted by centrifugation at 13 000 rpm for 30 sec. The supernatant was removed.

2. The cell pellet was completely resuspended in 250 µl Buffer A1 by vortexing

Attention: Check Buffer A2 for precipitated SDS prior to use. If a white precipitate is visible, warm the buffer for several minutes at 30–40 °C until any precipitate is dissolved. Mix thoroughly and cool buffer down to room temperature (18–25 °C).

3. 250 µl Buffer A2 was added and mixed gently by inverting the tube 6–8 times. The sample was not vortexed to avoid the shearing of genomic DNA. Incubated at RT for 5 min.

4. 350 µl Buffer A3 was added and mixed thoroughly by inverting the tube until the blue samples turned colourless.

5. The lysate was clarified by centrifugation at 13 000 rpm for 10 min. at RT.

6. 700 µl of the supernatant was loaded in the provided NucleoSpin® Plasmid Column and placed in a collection tube.

7. The sample was centrifuged at 13 000 rpm for 30 sec.

8. The remaining sample was loaded into the column and step 7 was repeated.

9. The silica membrane was washed by adding 500 µl Buffer AW and centrifuged at 13 000 rpm for 30 sec.

10. 600 µl Buffer A4 was loaded, and the sample was centrifuged 13 000 rpm for 1 min.

11. The sample was dried by placing the column into a new 2 ml collection tube and centrifuged at 13 000 rpm for 1 min. to remove Buffer A4 completely.

12. The DNA was eluted by placing the column into a new 1.5 ml Eppendorf (not provided). 50 µl Buffer AE was loaded directly to the membrane and incubated at RT for 1 min. before the sample was centrifuged at 13 000 rpm for 1 min.

The plasmid was stored in a -20°C freezer.

2.3 PCR

In this study, PCR was used to amplify the "cassette" used in homologous recombination by transformation, and later for genotyping possible mutants. The BIOTAQ™ kit from Meridian Bioscience™ was used for all PCR experiments. See Appendix B: Oligonucleotides for forward/reverse primers.

Polymerase chain reaction (PCR) is used to amplify a selected region of DNA into multiple copies so there is enough to be either analysed or used in downstream applications. PCR requires sequence-specific forward/reverse primers, a heat-stable DNA polymerase, a mix of the four deoxynucleotides (dNTPs) and buffers to keep the pH stable and improve primer annealing conditions. PCR works in a three-step process.

1. Denaturation: Double-stranded DNA is separated into single-stranded DNA.
2. Annealing: Primers and the DNA polymerase enzyme bind to DNA.
3. Elongation: DNA polymerase enzyme adds deoxynucleotides (dNTPs) in the 3'-end of the primer, complementary to the template DNA being used.

These three steps are repeated usually 30-40 times, and with each replication the amount of the target DNA doubles. The kit also contains MgCl2 equivalent to make it 3mM in the final reaction. The reaction mix was prepared and loaded in the thermocycler with reaction settings based on recommendations from the kit (**Table 2**). The expected fragment lengths were calculated in SnapGene® Viewer 6.0.5 and verified by separating the PCR products on an agarose gel.

Table 2. Overview of products and volumes used in a 50 µl PCR reaction. * 1 minute for plasmid, 3 minutes for gDNA. ** ~1 min/Kb. ***DMSO together with 46°C annealing temperature was used to amplify the *hph*-cassette.

50 µl PCR Reaction Mix		**PCR Conditions**		
		Temperature	*Length*	
10x NH_4 Reaction Buffer	5 µl			
50 mM $MgCl_2$ Solution	3 µl	94°C	*1-3 min.	
100mM dNTP Mix	0.5 ng			
DNA Template	100 µl	94°C	30 sec.	
10 µM F Primer	2.5 µl	***50 or 46°C	30 sec.	35 cycles
10 µM R Primer	2.5 µl	72°C	**2 min.	
BIOTAQ DNA Polymerase	1 µl			
***DMSO to 5%	2.5 µl	72°C	10 min.	
Water (mqH_2O)	Up to 50 µl	4°C	∞	
Total	**50 µl**			

2.4 Agarose gel electrophoresis

The purpose of agarose gel electrophoresis is to separate fragments of DNA by size using an electric field. The negatively charged phosphate backbone of DNA causes it to migrate towards the positive anode. The smaller DNA fragments move faster through the agarose gel matrix than the larger fragments. Tris-acetate-EDTA (TAE) is used as an electrophoresis buffer in addition to making the agarose gel. The ions in the buffer carry the electrical current and stabilize the pH, and EDTA inactivates any present DNA nucleases by chelating magnesium ions. To enable visualization of the DNA fragments, SYBR™ Safe DNA Gel Stain is added to the agarose gel. Due to its absorbance spectrum, the DNA with the intercalated SYBR™ Safe can be visualized with blue or ultraviolet (UV) light. GeneRuler™ DNA Ladder Mix (**Figure 9**) was used as a reference to estimate the size of unidentified PCR products.

Procedure for agarose gels

1. For a 1% agarose gel, 0.8 grams of agarose was added to 80 ml of 1X TAE buffer (diluted from 50X stock) in a 250 ml chemical storage bottle.
2. The bottle was closed loosely, and the powder was dissolved by heating in a microwave until the solution was clear with no precipitates.
3. The solution was cooled down to approximately 60°C and 8 µl SYBR™ Safe DNA Gel Stain was added to the solution to a final concentration of 0.1 µl/ml.
4. The solution was poured in a cassette and a gel comb was placed in it to form the wells.
5. The gel was left to solidify for 20 min. at RT or in a 4°C refrigerator.
6. 6X TriTrack DNA Loading Dye was added to the DNA sample.

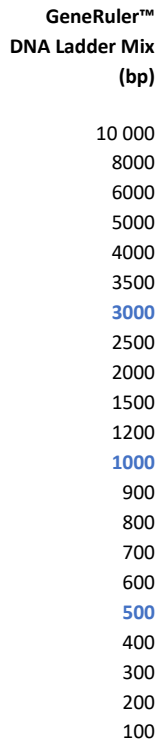

Figure 9. GeneRuler fragment sizes (bp). Fragments with a higher concentration are marked with blue

7. The gel comb was removed, and the gel was placed in an electrophoresis chamber filled with 1x TAE buffer.

8. The DNA samples and a DNA marker were loaded into the wells.

9. The gel was left to run for 40-60 min. at 100 V.

10. The DNA fragments in the gel were visualized with UV light.

2.5 Nucleic acid integrity

In this study, a nanodrop spectrophotometer was used to assess the concentration and quality of purified nucleic acids (Plasmids, PCR products, gDNA and RNA). This spectrophotometer measures the concentration and purity of the sample based on their absorbance characteristics; the amount of light (photons) that passes through a sample at different wavelengths.. The device measure absorbance at 230nm, 260nm, and 280nm.

Beer-Lambert Law; $A = \varepsilon bc$
A = absorbance
b = path length
c = analyte concentration
ε = extinction coefficient (for DNA, ε = 50 µg/ml, for RNA, ε = 40 µg/ml).

Quantification of nucleic acids

Measurements made at 260nm are used to determine the concentration of nucleic acid present in the sample as both purines and pyrimidines have peak absorbances at this wavelength. Beer-Lambert law predicts a linear correlation between absorbance and concentration.

Quality control of nucleic acids

At 280nm, aromatic amino acid side chains and phenol groups of organic compounds are mainly responsible for the absorbance. The ratio of 260/280nm absorbance should be around 1.8 for DNA and 2.1 for RNA. A lower ratio suggests protein contamination in the nucleic acid sample. Absorbance at 230nm indicates a presence of salts, phenol or peptide bonds and

a ratio of the absorbance at 260/230nm should be over 1.8 or close to 2.0. A lower ratio suggests above mentioned contaminants.

Nanodrop

The analysis was performed using 1 µl of the sample in a NanoDrop® 2000 UV-Vis Spectrophotometer according to the manufacturer's instructions.

2.6 PCR Amplification of histidine- and hygromycin cassettes

Gene deletion starts with the amplification of selection cassettes from the plasmid pFA6a-His3MX6 and pFA6a-hphMX6 (Janke et al., 2004) (**Figure 10**, plasmids in Appendix **C**, and primers in Appendix **B**).

pFA6a-His3MX6 contains an auxotrophic selective marker for the amino acid histidine, and pFA6a-hphMX6 contains an antibiotic resistance gene rendering cells resistant to hygromycin. The plasmids were used as templates to obtain a histidine- or hygromycin cassette respectively by PCR and will hereby be referred to as *HIS3*-cassette or *hph*-cassette. In the plasmids, the TEF promoter/terminator flanking the ORF makes up the selection genes *HIS3* and *hph*. The 60 bp long primers were designed so 20 bp would attach 53 bp upstream-, and 30 bp downstream from *HIS3MX6* or *hphMX6*, and the remaining 40 bp would create overhangs specific to the genes of interest for later transformation. The primers were designed in such a way that they would not bind to any other genomic sequence.

Fragment calculations

His3MX6 (TEF promoter/terminator + *HIS5* from *S. pombe*) = 1201 bp
Forward + Reverse primer = 60 bp + 60 bp
Upstream and downstream primer attachment sites from *His3MX6*= 53 bp + 30 bp
Expected length of *HIS3*-cassette: 1201+60+60+53+30 = 1404 bp

hphMX6 (TEF promoter/terminator + *HygR* from *E. coli*) = 1576 bp
Forward + Reverse primer = 60 bp + 60 bp
Upstream and downstream bp of primer attachment sites from *hphMX6* = 53 bp + 30 bp
Expected length of *hph*-cassette: 1576+60+60+53+30 = 1779 bp

The cassette was amplified through a PCR reaction. Recommended conditions from Meridian Bioscience™ were used accordingly (**Table 2).** The PCR products were verified with agarose gel electrophoresis.

For later transformation, the PCR products (cassettes) need to be purified and concentrated.

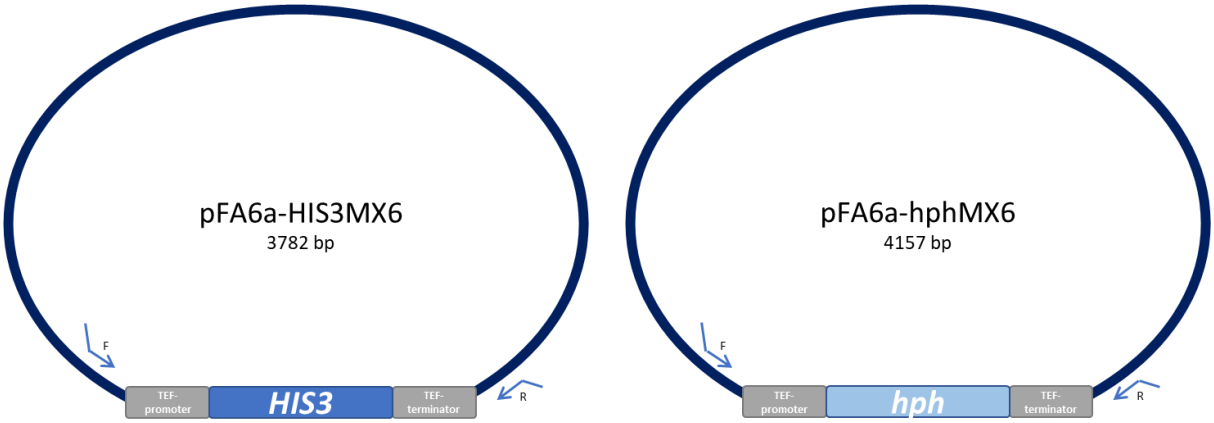

Figure 10. Primer localization for cassette amplification in pFA6a-HIS3MX6 (blue, left) and pFA6a-hphMX6 (light blue, right). F-primer attachment sites is 53 bp upstream from the TEF-promoter. R-primer attachment site is 30 bp downstream from the TEF-terminator. The primers are 60 bp long, where 20 bp correspond to the plasmid, and 40 bp overhangs correspond to flanking regions of mentioned genes of interest.

Protocol for purification and concentration of PCR products

1. Added 0.1x volume of 3M NaOAc with 2.5x volume of 96% EtOH.

2. The tubes were vortexed and placed in -20°C for ~1 h.

3. The precipitates were centrifuged at 13 000 rpm for 15 min, then washed with 70% EtOH and centrifuged at 13 000 rpm for 5 min.

4. The DNA pellet was dried either at room temperature or in a 50°C Thermomixer for no more than 10 min. to avoid degradation and hardening of the DNA pellet.

5. The pellet was resuspended in 10 µl sterile mqH_2O.

2.7 Gene deletion by homologous recombination

The HO pathway (**Chapter 1.2.5 DNA Damage Response (DDR)**) during homologous recombination (HR) is a crucial mechanism for DNA single- and double-strand break (SSB and DSB) repair, as well as replication fork collapse rescue (Eckert-Boulet et al., 2011). The

process involves several key steps involving proteins from the *RAD52* epistasis group. This study utilizes the HR-machinery for transformation.

Firstly an initiating event, typically a DSB is recognized by a complex of proteins called MRX (Mre11-Rad50-Xrs2). MRX recruits a nuclease, Sae2, to the break site, which creates ssDNA overhangs at the ends of the DSB. These ssDNA tails are then coated by an ssDNA-binding protein RPA (Replication Protein A), which prevents ssDNA from being degraded and facilitates the recruitment of downstream HR proteins. Secondly, Rad51 is loaded onto the RPA-coated ssDNA by the mediator protein Rad52. Rad51 is the key protein that searches for homologous DNA sequences to initiate strand invasion. Here, it searches for a homologous sequence, usually provided by the sister chromatid, generating a displacement loop (D-loop) structure. Thirdly, the invading strand is extended using the homologous DNA sequence as a template. This results in the formation of a Holliday junction, which is a temporary intermediate structure that can be resolved in different ways, depending on the specific HR pathway. Finally, the Holliday junction can be resolved by nucleases, resulting in either crossover or non-crossover events which are tightly regulated, especially during meiosis.

In this study, (**Figure 11**) the HR template product is made by PCR amplification of a *HIS3*- and *hph*-cassette from plasmids (see **Chapter 2.6**, **Appendix C**, **Figure 10**). The gene-specific cassette products is then used to transform (**Chapter 2.8 Yeast transformation**) the *CEN4** strain by homologous recombination to yield deletion mutants. The transformants can then be grown on selection media, and isolated gDNA from

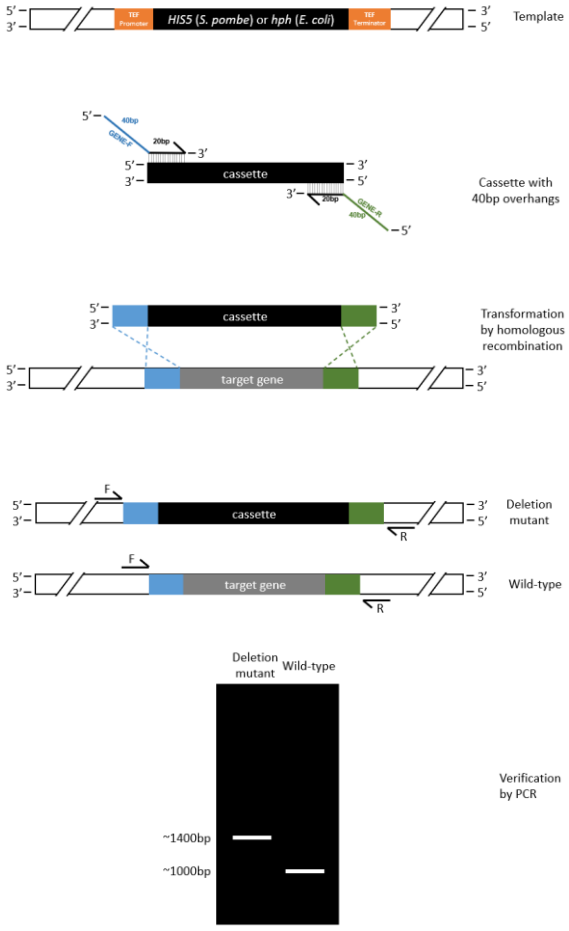

Figure 11. Gene deletion by homologous recombination. The cassette is made by using a plasmid as template. The resulting cassette has a 40 bp sequence that corresponds to the sequence flanking the target genes (genes of interest). The cassettes can be used to transform yeast by the homologous recombination machinery, and genotype can be verified by PCR. Bottom figure is an example of a gel showing how fragment size is comparable between mutant (1400 bp) and wild-type (1000 bp).

the colonies can be used for PCR to compare calculated fragment lengths between wild-type and deletion mutants.

2.8 Yeast transformation

In this study, successful transformation requires that the cassette DNA has been transported inside the yeast cell genome by the HR machinery (**Figure 11**). Transformation of *S. cerevisiae CEN4** strain was done by a combination of lithium acetate (LiAc), single-stranded carrier DNA (ssDNA) and polyethylene glycol (PEG).

Only PEG and carrier DNA is essential for transformation, but LiAc increases its efficiency. It might do so through lithium's chaotropic abilities by disrupting the network of hydrogen bonding between water molecules and weakening the hydrophobic effect of the cell membrane. Lithium cations also neutralize the negative charges on DNA used for transformation. PEG increases the cell wall's permeability (Kawai et al., 2009).

The ssDNA in this study is from salmon sperm and is first denatured by heating at 95°C and then kept on ice to prevent the strands from re-ligation. The ssDNA may protect the transforming DNA (cassette) in three ways. First, the ssDNA interacts with the defence on the cell wall to fill some of the interacting surfaces before the cassette is added. Second, ssDNA saturates DNase with substrate and as a result, the cassette more often locates to the nucleus without degradation. Third, it may induce repair by the homologous recombination machinery (Fu et al., 2008).

Protocol for transformation using LiAc, ssDNA and PEG.
For each gene, a flask of at least 5 times the volume of YPD was inoculated with an O/N culture to an OD_{600} of 0.4 and incubated 5 hours (2 replication times) at 30°C in a 200 rpm orbital shaker.

1. A stock of 1 mg/ml single-stranded carrier DNA (ssDNA) was denatured by 5 min. heating at 95°C, then rapidly cooled on ice.

2. 5-10 OD_{600} of yeast cells* were collected for each transformation by centrifugation at 4000 rpm for 1 min.

3. The supernatant was removed, and cells were washed with 5 ml sterile ddH_2O.

4. Cells were then centrifuged 4000 rpm for 2 min, supernatant was removed, and the cell pellet was resuspended in 1 ml of 1x TE and moved to a 1.5 ml Eppendorf tube.

5. The tubes were then centrifuged 10 000 rpm for 30 sec.

6. The supernatant was removed, and the pellet was resuspended in 200 µl 0.1M LiAc/1x TE solution.

7. 25 µl ssDNA was added together with 100 ng of the transforming DNA cassette and then vortexed.

8. Add 1.2 ml 40% PEG 3350/0.1M LiAc/1x TE solution was mixed, then vortexed.

9. The culture was incubated at 30°C for 30 min.

10. A thermal shock of 42°C was applied to the culture (water bath) for 20 min, then snap-cooled on ice for 1 min.

11. Cells were collected by centrifugation at 10 000 rpm for 1 min, then washed with 1 ml sterile ddH_2O.

12. Yeast cells transformed by the *hph*-cassette were resuspended in 5 ml of fresh YPD and incubated in 30°C for 2 h in a 200 rpm orbital shaker to regain viability.

13. Cells were then plated with an L-shaped spreader on either CSM-his plates or hygromycin 200 µg/ml plates depending on the selective marker.

14. The cells were incubated at 30°C for 2 days.

*10 OD_{600} of yeast cells for transformation by *HIS3*-cassette, 5 OD_{600} of yeast cells for transformation by *hph*-cassette.

2.9 gDNA extraction with phenol

Purification of genomic DNA (gDNA) requires extracting it from the cell, and discarding the proteins. In this study, the procedure is performed by mechanical disruption of the cell walls using glass beads and vigorous shaking in a buffer containing Triton™ X-100 as a detergent and Sodium dodecyl sulphate (SDS) to lyse the cells and solubilize proteins and lipids.

Ethylenediaminetetraacetic acid (EDTA) is a chelator that acts as a scavenger for metal ions in solution and is added to remove magnesium ions (Mg^{2+}). Mg^{2+} is an essential co-factor for DNases, therefore removal of Mg^{2+} inactivates DNases, preventing DNA degradation. Phenol-chloroform is used for breaking down superfluous cell materials and separating proteins from nucleic acids. This creates a cell lysate in which all components of the cells have been broken down, and gDNA can be extracted from this lysate. Since DNA is water soluble, the cell lysate can be centrifuged, and the aqueous layer can be moved to another tube with a pipette and can further be precipitated and washed to remove salts and other contaminants.

Protocol for gDNA extraction with phenol.

1. Cells from ~10 ml O/N culture were collected by centrifugation at 4000 rpm for 2 min. and washed with sterile distilled water (1 drop from each possible mutant were plated again to store the strain).

2. The cell pellet was then resuspended in 200 µl lysis buffer (Triton X-100 2%, SDS 1%, NaCl 100mM, Tris-HCl pH 8.0 10mM) and transferred into a screw-cap tube containing ~300 µl sterile glass beads and 200 µl phenol:chloroform:isoamyl alcohol (25:24:1) saturated with 10mM Tris-HCl pH 8.0 and 1 mM EDTA.

3. The cells were vigorously shaken in a 4°C cold room for 10 min.

4. Added 200 µl 1x TE buffer to each tube and centrifuged at 12 000 rpm for 5 min.

5. The aqueous layer was transferred to a fresh 1.5 ml Eppendorf tube and the nucleic acids were precipitated with 1 ml 96% EtOH.

6. The tubes were centrifuged at 12 000 rpm for 5 min, the supernatant was removed, and the DNA pellet was resuspended in 1x TE buffer.

7. 30 µl 1 mg/ml RNAse A was added, and the solution was incubated at 37°C for 2 h or O/N.

8. the DNA was precipitated by adding 10 µl 4M Ammonium Acetate and 1 ml 96% EtOH.

9. Centrifuged at 12 000 rpm for 5 min, then washed with 96% EtOH, and second wash with 70% EtOH to remove salts.

10. The DNA pellet was finally resuspended in either 200 µl 1x TE buffer or mqH_2O.

The concentrations and integrity of nucleic acids in the gDNA samples were analysed using a Nanodrop.

2.10 Verification of possible transformants

A PCR-based approach was used to validate gene deletion mutants. Recommended conditions from Meridian Bioscience™ were used accordingly (**Table 2**

Table 2**)** but scaled down to 20 µl reactions. Agarose gel electrophoresis was used to visualize fragment lengths.

The primer combinations were selected to anneal to a sequence either inside- or outside of the cassettes (**Figure 15,** results part). Ideally using the primers flanking the gene to compare expected fragment size between mutant or wild-type (**Figure 11**).

2.11 Cell collection

The collected volume contained approximately the same OD_{600} (cell count), and depended on the experiment (**Chapter 3.2 A qPCR-based screen to identify chromatin regulators involved in centromere-regulated transcription in synchronized cells**).

Cells were collected from liquid YPD media by centrifuging 4000 rpm for 1 min, the YPD was removed by pouring. The pellet was resuspended in 700 µl mqH_2O and moved to a 1.5 ml Eppendorf. Samples were centrifuged again at 13 000 rpm for 1 min, the H_2O was removed with a vacuum aspirator and the remaining cells were immediately snap-frozen at -80°C. The flask sizes were adjusted so that the remaining cell culture would not take up more than 1/5 of the volume in the flask.

2.12 Light microscopy

Light microscopy on-site (Motic AE21 and Leitz HM-LUX) was used to inspect the cells at different time points to control the cell cycle and possible contamination. The *S. cerevisiae* cell is slightly oval, and budding is identified as a cell having a smaller cell ("bud") appear and grow outwards from the bud neck. Interphase cells are single and usually separated from other cells. S phase cells are budding, with the appearance of two cells visually stuck together as cell doublets. In early S phase, one of the cells is visually bigger than the other, and during late S phase the cell size is more similar. Visually, it is not possible to distinguish late S with G2/M phase by microscopy. Asynchronous cell culture has the presence of single cells, budding cells and multiple cells stuck together during and after mitosis.

One droplet (~10 µl) of cell culture was added to a glass slide, covered with a cover slip, and put in a 4°C refrigerator until inspection. Light microscopy images of the samples with 40x magnification were taken by a mobile phone camera (Huawei p30 Pro), microscope setting: phase contrast 3.

2.13 Flow Cytometry

In this study, flow cytometry is used for the purpose of verifying the cell cycle for each collection time point, and hereby verify if the cells have been properly arrested. Sytox green is used to stain DNA in the yeast cells. Several detectors are carefully placed around the stream. When cells passage in a single file in front of the laser, the fluorescently labelled cell components are excited by the laser and emits light at a longer wavelength, the detectors therefore pick up a combination of scattered and fluorescent light. One of these detectors is in line with the light beam and is used to measure Forward Scatter or FSC which detects size and shape. Another detector is placed perpendicular to the stream and is used to measure Side Scatter (SSC) which detects intracellular structures.

The flow cytometer detects, counts, and groups events based on the amount of DNA in each cell. Cells in G1 would contain 1N genome and cells in G2/M would contain 2N genome. As the genome is replicated in S phase, each cell would contain between 1-2N genomes. The

fluorescence will have different peaks in the population data sheet depending on the overall cell cycle stage.

Protocol for Flow Cytometry samples

1. A stock of 0.5M sodium citrate buffer was diluted to a final concentration of 50mM and filtered in a cornig 0.5 µM filter.

2. ~0.25 OD_{600} yeast cells were pelleted and resuspended in 300 µl mqH_2O.

3. The samples were transferred to 15 ml tubes and 700 µl 96% EtOH was added slowly while vortexing before incubation for 1 h at RT.

4. Samples was centrifuged 4000 rpm for 1 min, then resuspended in 250 µl sodium citrate buffer containing 250 µg/ml RNAse A and 1 mg/ml proteinase K before incubation at 37°C O/N.

5. Samples were then centrifuged at 4000 rpm for 1 min, resuspended in 1 ml sodium citrate buffer and transferred to Falcon® 12 X 75 polystyrene tubes.

6. Samples were sonicated 30% for 3 sec.

7. Sytox green were added to a final concentration of 1 µM and incubated for 1 h at RT, then 4°C for up to a week.

8. Samples were analysed by Flow Cytometry at 488nm excitation, collected at 523nm.

2.14 S phase arrest with hydroxyurea

Hydroxyurea (HU) works by inhibiting the activity of RNR which is required for the synthesis of DNA. HU reduces the availability of deoxynucleotides in the cell, which in turn leads to the accumulation of replication forks during S phase DNA replication. The cell then activates a DNA damage checkpoint, which prevents the cell from progressing through the cell cycle until the DNA damage is repaired (Alvino Gina et al., 2007).

To arrest the cells, hydroxyurea is added to a final concentration of 200 mM in liquid YPD. Because the culture is asynchronous, some of the cells are already in S phase while

hydroxyurea is added, 2.5 hours of waiting time ensures that all free dNTPs have been used and that all the cells have reached S phase and are properly synchronized.

2.15 Centromere excision assay

All strains in this study (**Appendix C**) express Cre recombinase fused to an estradiol binding domain (Cre-EBD). The constructed strain with lox recombination sites flanking the centromere of chromosome IV has the genotype *lox-CEN4-lox::KanMX* and is referred to as *CEN4**. The centromere can be excised from chromosome IV by adding β-estradiol in the mutant strain *CEN4**, becoming *cen4-* after excision (**Chapter 1.4.4 Centromere excision assay** & **Figure 6**).

Centromere excision was done by adding β-estradiol from a 1000x concentrated stock dissolved in ethanol, to a final concentration of 1 µM. A waiting time of 1.5 h ensures that most (97.41%, **Figure 6 C**) of the *CEN4** strains have their centromere removed.

2.16 RNA extraction

Total RNA is transcribed from gDNA (and mitochondrial DNA) and generally refers to a sample containing: Ribosomal, transfer and messenger RNA (rRNA, tRNA and mRNA) and does not include microRNA (miRNA) or smaller non-coding RNAs (ncRNA). In this study, mRNA is extracted from cell lysates to provide cDNA for further analysis by RT qPCR. The protocol seen below includes columns, buffers and RNase-free tubes supplied with the Qiagen RNeasy Mini Kit, with the column capturing RNA by silica membrane technology.

The cell lysate is obtained by mechanical disruption of the cell walls using glass beads and vigorous shaking in a buffer containing β-mercaptoethanol (β-ME) and guanidine thiocyanate. β-ME protects the RNA against degradation by providing a reducing environment that denatures the four disulphide bridges formed between the eight cysteine residues of RNase A. Guanidine thiocyanate has chaotropic activity that makes proteins denature readily, cellular structures disintegrate, and nucleoproteins dissociate from nucleic acids when secondary structure of the protein is lost. The combination of a reducing agent and a chaotropic agent causes the RNAse to unfold and completely lose its activity. Lysates are centrifuged, and only the aqueous solution is used in subsequent steps while the cellular debris pellet remains. The

supernatant is then applied to a silica column to bind total RNA, followed by washing and elution with RNase free buffer or water.

Protocol for RNA extraction with RNeasy Mini Kit from Qiagen

2×10^6 - 5×10^7 yeast cells can be processed. 30–100 µg RNA is expected from 4×10^7 cells.

Important points before starting.
- Buffer RLT may have formed a precipitate upon storage. If necessary, redissolve by warming, then place at RT.
- All steps of the procedure were performed at RT
- β-ME must be added to Buffer RLT before use; 10 µl β-ME per 1 ml Buffer RLT. Buffer RLT containing β-ME can be stored at room temperature for up to 1 month.
- Buffer RPE is supplied as a concentrate. Before using for the first time, 4 volumes of ethanol (96–100%) were added as indicated on the bottle to obtain a working solution.

1. 600 µl Buffer RLT was added to resuspend the frozen cell pellets and the solution was immediately transferred to an autoclaved screw-cap-tube already containing 300 µl of acid-washed glass beads.

2. The cells were vigorously shaken by a cell disruptor in a 4°C cold room for 15 min.

3. The lysate was transferred to a new microcentrifuge tube (not supplied).

4. Samples were centrifuged at 13 000 rpm for 2 min and the supernatant was transferred to a new microcentrifuge tube (not supplied). Only the supernatant was used in subsequent steps.

5. 1x volume of 70% ethanol was added to the homogenized lysate and mixed well by pipetting.

6. The sample, including any precipitate that may have formed was transferred to an RNeasy spin column placed in a 2 ml collection tube (supplied). Centrifuged at 13 000 rpm for 15 sec. The flow-through was discarded and the collection tube was reused in step 7, 8 and 9.

7. 700 µl Buffer RW1 was added to the RNeasy spin column. Centrifuged at 13 000 rpm for 15 sec to wash the spin column membrane. The RNeasy spin column was removed carefully from the collection tube so that the column did not contact the flow-through. The collection tube was emptied completely.

8. 500 µl Buffer RPE was added to the RNeasy spin column. Centrifuged at 13 000 rpm for 15 sec to wash the spin column membrane. The collection tube was emptied completely.

9. 500 µl Buffer RPE was added to the RNeasy spin column. Centrifuged at 13 000 rpm for 2 min. to wash the spin column membrane. The long centrifugation dried the spin column membrane, ensuring that no ethanol was carried over during RNA elution. Note: After centrifugation, the RNeasy spin column was carefully removed from the collection tube so that the column did not contact the flow-through. Otherwise, carryover of ethanol occurs.

10. The RNeasy spin column was placed in a new 2 ml collection tube (supplied), and the old collection tube with the flow-through was discarded. Centrifuged at 13 000 rpm for 1 min.

11. Placed the RNeasy spin column in a new RNAse free 1.5 ml collection tube (supplied). 30 µl RNAse-free water was added directly to the spin column membrane. Centrifuged at 13 000 rpm for 1 min. to elute the RNA.

The samples were immediately analysed with Nanodrop, then directly proceeded with reverse transcription afterwards to avoid freezing/thawing cycles.

2.17 Reverse transcription and gDNA removal

This process converts all mRNA to cDNA while maintaining the differences between the levels of the mRNA for all the genes. The QuantiTect® Reverse Transcription Kit (Qiagen) was used to perform reverse transcription (RT). This kit allows for reverse transcribing up to 1 µg of RNA into cDNA using random primers (RT Primer mix) that are necessary for binding of reverse transcriptase to the mRNA. After binding, reverse transcriptase will start adding nucleotides complementary to the mRNA. The RT Buffer ensures proper environment for the reaction.

It is important to ensure that there is no gDNA contamination as the template strand in gDNA will be identical to the cDNA synthesized by RT. Treatment of the samples with DNase (in the gDNA Wipeout buffer) is recommended for removing contaminating gDNA before doing reverse transcription.

Protocol for QuantiTect® Reverse Transcription Kit (Qiagen)

1. gDNA wipe-out buffer, Quantiscript RT Buffer, RT Primer mix and RNAse-free water was thawed in RT, vortexed, spun down and immediately stored on ice.
2. The gDNA elimination reaction were prepared on ice according to Table 3.
3. The samples were incubated at 42°C for 5 min, then placed immediately back on ice.
4. A Master Mix for the RT reaction was prepared on ice according to Table 3 and added to each gDNA elimination reaction before vortexing.
5. The samples were incubated at 42°C for 20 min, then at 95°C for 3 min. to inactivate the reverse transcriptase before placing them back on ice.

Table 3. Left side show reaction components for gDNA elimination, and right show reaction components for RT reaction.

gDNA Elimination reaction		Reverse Transcription reaction	
7x gDNA Wipeout Buffer	2 µl	Reverse transcriptase	1 µl
RNase-free water	up to 14 µl	5x RT Buffer	4 µl
Template RNA	500 ng	RT Primer Mix	1 µl
		Entire gDNA elimination reaction	14 µl
Total	**14 µl**	**Total**	**20 µl**

The cDNA was stored in a -20°C freezer.

2.18 Real-time quantitative PCR (qPCR)

For this real-time quantitative PCR (qPCR) experiment, HOT FIREPol® EvaGreen® is used as a fluorescent dye to detect amplification of the DNA target at each PCR cycle (**Figure 12**).

EvaGreen® bound to DNA is excited by illumination at 490nm wavelength, this produces fluorescence at 530nm to release the extra energy which is measured by a fluorescence detector (Mao et al., 2007). The released fluorescence is linear to the amount of dsDNA formed, so this process detects the differences between the levels of the cDNA, and hereby expression for the genes of interest. The fluorescence is converted to a threshold cycle (CT) value, which is the number of PCR cycles it takes for the software to distinguish at which cycle the fluorescence is above background noise.

Both software and instrument Lightcycler®96 1.1 from Roche was used to analyse the data. A relative quantification method was used with *MNN2* as a reference gene. A serial dilution of an undiluted sample of cDNA was made to create a standard curve used to find the relative amount of cDNA for each primer set. Then the expression of different genes was compared to the reference gene, which was shown to have the same expression levels between *CEN4* and *CEN4** strains (**Figure 28,** (Ramos Alonso et al., 2023)).

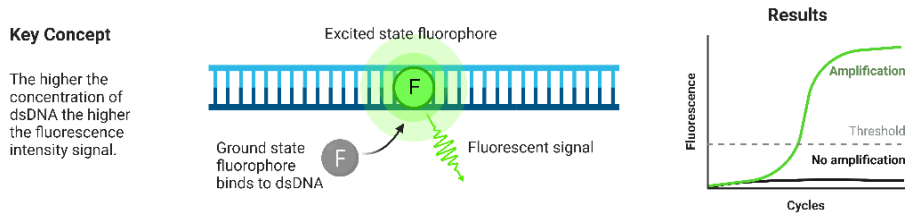

Figure 12. Key concept of Real Time quantitative PCR (qPCR). A fluorescent dye is added to the PCR reaction. Unbound (ground state) fluorophore (grey) is not fluorescent but becomes excited when bound to dsDNA (green). The fluorescence is detected at each amplification cycle and is converted to a CT value. (made using BioRender)

Two technical replicates were analysed for each sample.

Protocol HOT FIREPol® EvaGreen® qPCR Supermix (Solis Biodyne)

1. The program “LightCycler96” was used to setup qPCR conditions and for arranging the samples and standards to the plates. The program file was saved to a folder named “experiments” directly on a USB drive for detection by the LightCycler qPCR machine.

2. A 1/20 dilution was made for each sample of cDNAs.

3. A standard mix from all cDNA samples were combined in a separate tube to make a standard dilution.

4. A $\frac{1}{5}$ $\frac{1}{10}$ $\frac{1}{50}$ $\frac{1}{100}$ $\frac{1}{500}$ $\frac{1}{1000}$ standard dilution series were made from the standard cDNA mix.

5. A Master Mix was prepared according to **Table 4** and a CombiTip were used to fill the wells of a 96 well qPCR plate.

6. The appropriate cDNA/primers were added to each reaction.

7. The plates were covered with a cover slip.

8. The plates were centrifuged ~ 1 minute, and the plates were loaded into the LightCycler qPCR machine to start qPCR analysis with settings from **Table 4.**

9. After completion of the reaction, the results were exported to an excel file.

10. The values of the genes of interest were normalised to the values of the reference gene and compared between strains.

Table 4. Left side shows reaction components, and right side shows conditions for qPCR. See Appendix B for primers.

10µl qPCR Reaction Mix		**qPCR Conditions**		
		Temperature	*Length*	
		95°C	720 sec	
10 µM F Primer	0.2 µl			
10 µM R Primer	0.2 µl	95°C	15 sec	
EvaGreen® qPCR Supermix	2 µl	58°C	20 sec	40 cycles
cDNA in 1/20 dilution	2 µl	72°C	20 sec	
Water (mqH_2O)	5.6 µl			
		95°C	10 sec	
		65°C	60 sec	
		97°C	∞	
Total	**10 µl**			

2.19 Spot assay

Spot assays (spot tests) are used in the field to study growth differences comparing genotypes, media, and environmental stress factors. In this study, an equal number of cells from control and deletion mutant strains were spotted on YPD plates with or without 0.1mM β-estradiol. The spot assay was done with a 6x serial dilution (1:10) for each strain.

Protocol for yeast Spot Assay.

1. For each strain, a flask of at least 5 times the volume of YPD were inoculated with an O/N culture to an OD_{600} of 0.3 and incubated ~3-5 hours (2 replication times) at 30°C in a 200 rpm orbital shaker.

2. The cells were washed by centrifuging at 4000 rpm for 1 min. and resuspended in sterile H_2O.

3. An OD_{600} of 0.1 or 0.5 was then used to make a 6x dilution series (1:10) in 6x8 cell culture plate.

4. A 48 (6x8) pin replicator was then used to spot the cells on dry plates with even droplets.

5. Plates were incubated in a 30°C incubator and pictures were taken on day 1, 2 and 3.

3 Results

The results from this thesis are presented in two parts;

1. Construction of deletion mutant strains.

2. Assessment of deletion mutant impacts on gene expression before- and after *CEN4* excision.

3.1 Construction of deletion mutant strains

To characterize factors acting downstream of the centromere at mitosis entry in the process of chromosome condensation (or a parallel pathway) to regulate gene expression beyond mitosis, I constructed deletion mutant strains derived from *CEN4** cells (**Appendix C**, **Chapter 2.15 Centromere excision assay** & **1.4.4 Centromere excision assay)**, for the genes of interest mentioned in the introduction and methods part. Successful construction of deletion mutant strains requires successful replacement of the gene of interest with the cassette DNA inside the yeast cell genome by the homologous recombination machinery (**Chapter 2.7 Gene deletion by homologous recombination** and **Figure 11**). The inserted *HIS3MX6* and *hphMX6* cassettes (*HIS3*-cassette or *hph*-cassette) will confer auxotrophy for the cells' production of histidine or resistance to the antibiotic hygromycin respectively. gDNA from colonies picked from selection plates are verified by PCR (**2.10 Verification of possible transformants & Figure 11**) to select positive deletion mutants.

3.1.1 Amplification of the cassettes by PCR

The cassettes were amplified by PCR (**Table 2),** using two different purified plasmids as templates (**Appendix C**) with primer pairs from **Appendix B**. The resulting products were run on an agarose gel and visualized by UV light. The results are shown together with a simple schematic of the plasmid and primer annealing sites in **Figure 13**.

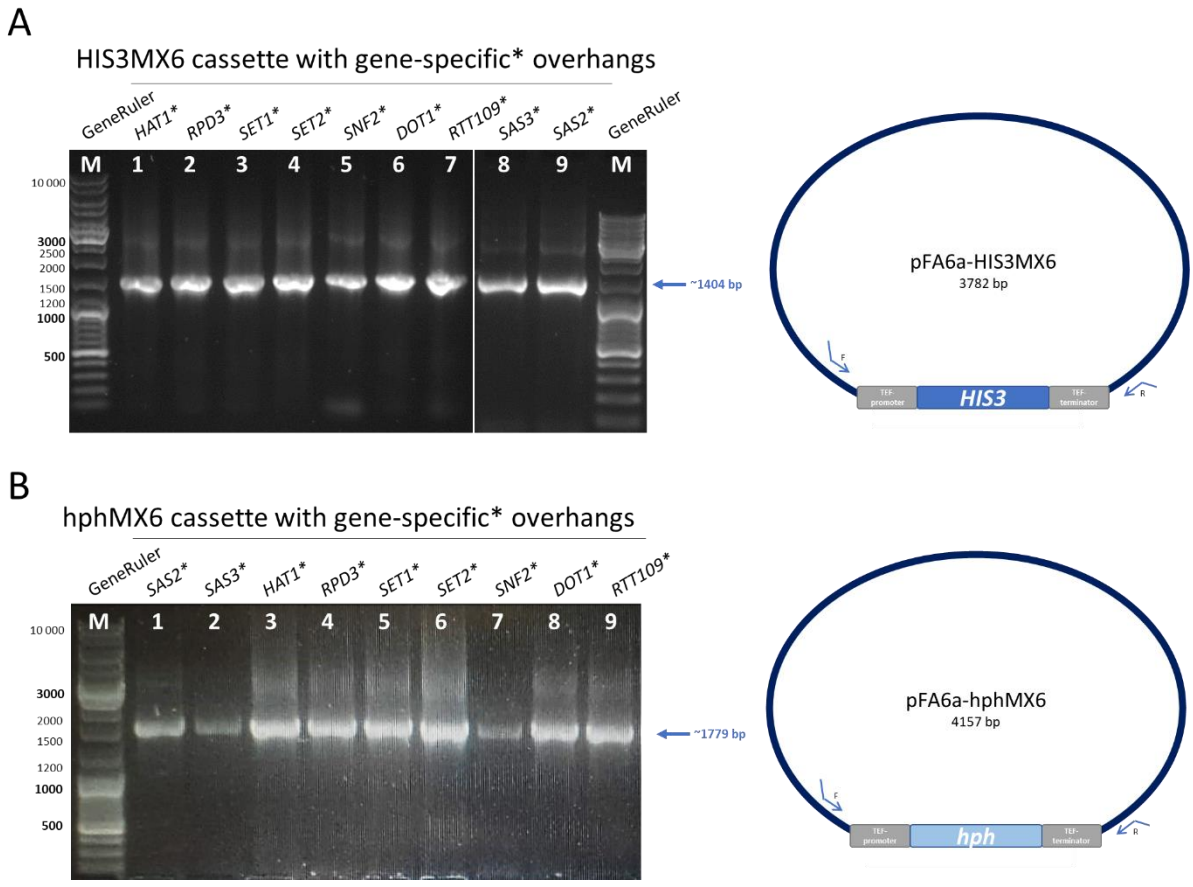

Figure 13. Cassettes were obtained for homologous recombination. Two different purified plasmids (**Appendix C**) was used as template to amplify **A:** *HIS3MX6* and **B**: *hphMX6* cassettes using PCR conditions according to **Table 2** and primer pairs from **Appendix B**. **Left**: The products were run on a 1% agarose gel at 90V for 1 hour and visualized by UV light. Blue arrows show the expected fragment lengths 1404 bp for *HIS3MX6* cassette (**A**) and 1779 bp for the *hphMX6* cassette (**B**). **Right**: Simple schematic of plasmid and primer ("F" and "R") annealing sites and 40 bp gene-specific* overhangs that flanks the gene of interest.

The expected fragment lengths for the *HIS3*-cassettes are 1404 bp, and the expected fragment length for the *hph*-cassettes are 1779 bp. Calculations are shown in **Chapter 2.6 PCR Amplification of histidine- and hygromycin cassettes**. The results show successful amplification of both cassettes as the bands have the correct fragment size (**Figure 13 A & B).** The *hph*-cassettes with flanking regions specific for *SAS2*, *SAS3* and *SNF2* had lower band intensity compared to the others, and can be seen comparing lane 1, 2 and 7 in **Figure 13 B** but amplification was still successful.

3.1.2 Transformed *CEN4** strains

Successful transformation requires that the cassette DNA (**Figure 13)** has been transported inside the yeast cell genome by the homologous recombination

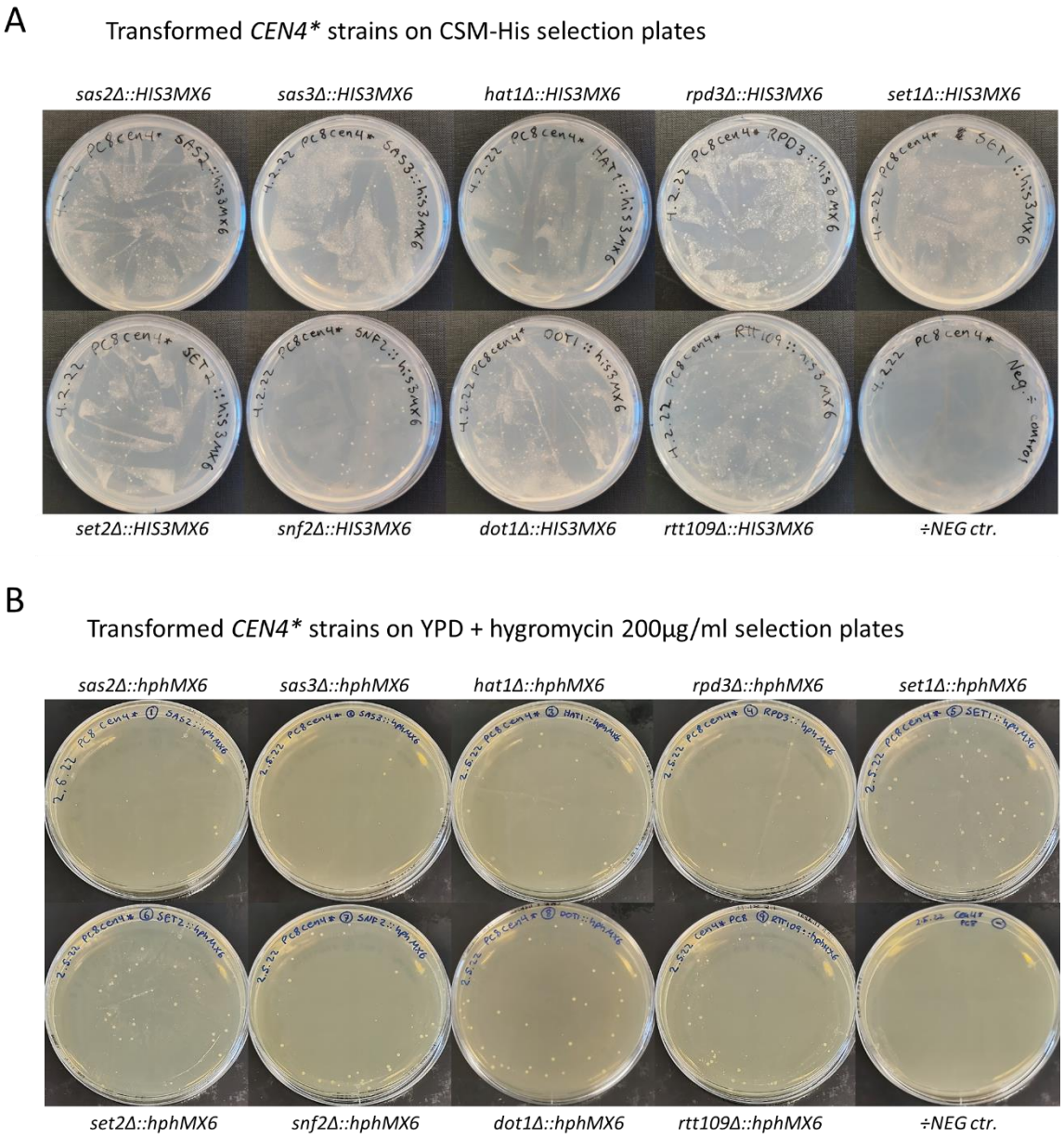

Figure 14. Transformed *CEN4 strains growing on selection plates.** Deletion strains plated on **A**: CSM-His media plates for cells transformed with the *HIS3*-cassette or **B**: YPD+hygromycin 200 µg/ml plates for cells transformed with the *hph*-cassette. Bottom left plate is untransformed *CEN4** strain as negative control (÷NEG ctr.). The plates were incubated at 30°C and the photos were taken after 2 days of growth.

machinery. The strain *CEN4** (**Appendix C**) was transformed according to PEG, LiAc, ssDNA method described in **Chapter 2.8 Yeast transformation**, yielding possible *CEN4** deletion mutants shown in **Figure 14**. To select positive transformants, cells are grown on selection plates containing CSM-His media or YPD+200 µg/ml hygromycin to ensure that only the cells with integrated cassettes can grow. Untransformed *CEN4** was used as negative control. Both transformation experiments had growth in all plates except for the negative control plates (bottom left plates in **Figure 14 A & B)**, indicating successful integration of all the cassettes.

3.1.3 Verification of *SET1*, *SET2*, *DOT1*, *RPD3*, *RTT109* and *SAS3* deletion mutant strains

Successful homologous recombination and thus gene deletion requires that the cassette DNA has been recombined at the right genomic location, i.e. the targeted gene.

A total of 28 colonies were picked from the CSM-His plates, and 79 colonies were picked from YPD + hygromycin plates for gDNA isolation **(Chapter 2.9 gDNA extraction with phenol)**. Nanodrop results indicating gDNA integrity for later genotyping is shown in **Table 7** in **3.3 Supplemental results**. A PCR-based approach was used to ensure that cassettes were inserted in the correct location (**2.10 Verification of possible transformants & Figure 11**), deleting the gene of interest from the yeast genome. To verify the genotype of possible deletion mutants, different primer pairs (**Figure 15**) were used on isolated gDNA (**Table 7**) from possible mutants (**Figure 14**) in a PCR reaction (**Table 2).** The products were then visualized on an agarose gel by UV light, and fragments were compared to calculated fragment sizes (**Table 5**) for each primer pair (**Figure 15**) to verify if the cassette had replaced the gene of interest. The primers (**Appendix B**) were designed to anneal upstream or downstream from the gene ORF (**Figure 15**, number 1 and 5), inside the TEF promoter/terminator associated with the cassette, or inside the *HIS3* or *hph* gene respectively (**Figure 15**, 2-4 and 6 and 7). Primer pair 1 and 5 was used with untransformed *CEN4** gDNA as WT control.

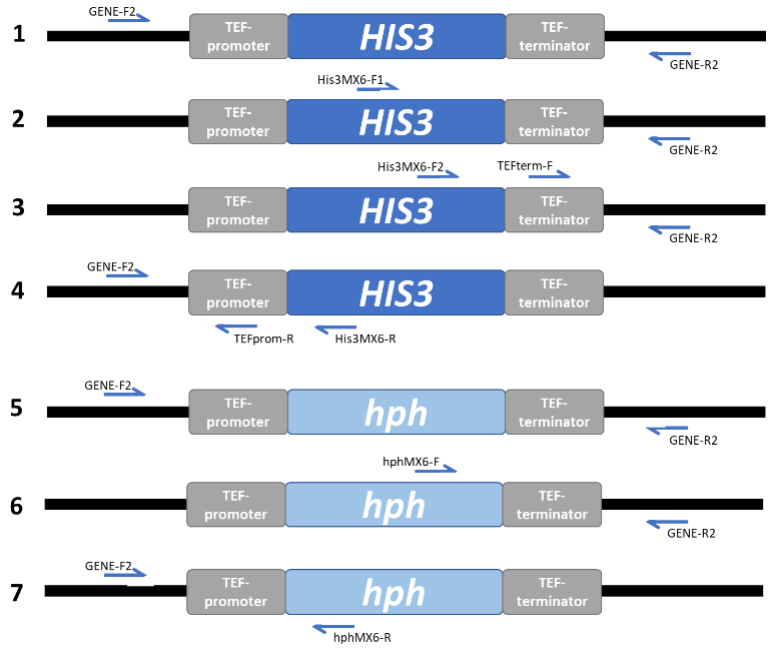

Figure 15. Schematic of primer pairs used for genotyping (added to results part for easy reference). Primer pair 1-4 is used for *HIS3MX6* (blue) cassette, and primer pair 5-7 is used for *hphMX6* cassette (light blue) (primers from Appendix B). See **Table 5** for calculated fragment lengths. The primer ID "GENE" refers to the gene-specific sequences and varies for each transformant. Blue arrows indicate location and direction of the primers.

Table 5. Expected fragment lengths (in bp) with different primer pairs from Figure 15. Red numbers indicate fragment size too similar to WT to be distinguishable on an agarose gel.

Primer pairs 1, 5

Primer combination	WT	::*HIS3*-cassette	::*hph*-cassette
SAS2-F2 + SAS2-R2	1558	1865	2240
SAS3-F2 + SAS3-R2	3052	1880	2255
HAT1-F2 + HAT1-R2	1705	1904	2279
RPD3-F2 + RPD3-R2	1915	1937	2312
SET1-F2 + SET1-R2	3809	1890	2265
SET2-F2 + SET2-R2	2657	1779	2154
SNF2-F2 + SNF2-R2	5376	1588	1963
DOT1-F2 + DOT1-R2	2111	1678	2061
RTT109-F2 + RTT109-R2	1661	1674	2049

Primer pairs 2, 3, 6

Primer ID	His3MX6-F1	His3MX6-F2	TermTEF-F	hphMX6-F
SAS2-R2	869	639	463	650
SAS3-R2	804	574	398	585
HAT1-R2	685	455	279	466
RPD3-R2	881	651	475	662
SET1-R2	862	632	456	643
SET2-R2	707	477	301	488
SNF2-R2	632	402	226	413
DOT1-R2	804	574	398	585
RTT109-R2	764	534	358	545

Primer pairs 4, 7

Primer ID	His3MX6-R	TEFprom-R	hphMX6-R
SAS2-F2	720	360	682
SAS3-F2	800	440	762
HAT1-F2	943	583	905
RPD3-F2	780	420	742
SET1-F2	752	392	714
SET2-F2	796	436	758
SNF2-F2	680	320	642
DOT1-F2	606	246	568
RTT109-F2	634	274	596

The resulting gels are shown in **Figure 16, Figure** 17**, Figure** 18 andFigure 19**,** where only bands corresponding to calculated fragment sizes are indicated with a blue arrow.

A mutant was validated if the correct fragment size was observed comparing deletion mutant to WT *(CEN4** gDNA*)* with primer pair 1 or 5 (**Figure 18** and **Figure** 19**,** no successful validation) or if either primer pair 2/3 as well as 4, or both 6 and 7 produced expected fragment lengths for deletion mutants. For example, in **Figure 16**, for *set1Δ::HIS3MX6* #2, gDNA with primer pair 3 produced expected fragment of 632 bp in lane 9, and gDNA with primer pair 4 produced expected fragment of 752 bp in lane 2. This approach was used to validate all deletion mutants in **Table 6**.

Table 6. Summary of validated deletion mutants from Figure 16 and Figure 17.

Results	Genotype	ID
Figure 16 A	*MATa set1::HIS3MX6 lox-CEN4-lox:KanMX GDP-creEBD78:LEU2 his3Δ1 leu2Δ0 ura3Δ0 met15Δ0*	yPC55 *CEN4* set1Δ::HIS3* #2
Figure 16 A	*MATa set2::HIS3MX6 lox-CEN4-lox:KanMX GDP-creEBD78:LEU2 his3Δ1 leu2Δ0 ura3Δ0 met15Δ0*	yPC56 *CEN4* set2Δ::HIS3* #1
Figure 17 C	*MATa sas3::hphMX6 lox-CEN4-lox:KanMX GDP-creEBD78:LEU2 his3Δ1 leu2Δ0 ura3Δ0 met15Δ0*	yPC58 *CEN4* sas3Δ::hphMX6* #3
Figure 17 A	*MATa rpd3::hphMX6 lox-CEN4-lox:KanMX GDP-creEBD78:LEU2 his3Δ1 leu2Δ0 ura3Δ0 met15Δ0*	yPC59 *CEN4* rpd3Δ::hphMX6* #5
Figure 16 B	*MATa set1::hphMX6 lox-CEN4-lox:KanMX GDP-creEBD78:LEU2 his3Δ1 leu2Δ0 ura3Δ0 met15Δ0*	yPC60 *CEN4* set1Δ::hphMX6* #7
Figure 16 B	*MATa set2::hphMX6 lox-CEN4-lox:KanMX GDP-creEBD78:LEU2 his3Δ1 leu2Δ0 ura3Δ0 met15Δ0*	yPC61 *CEN4* set2Δ::hphMX6* #6
Figure 16 B	*MATa set2::hphMX6 lox-CEN4-lox:KanMX GDP-creEBD78:LEU2 his3Δ1 leu2Δ0 ura3Δ0 met15Δ0*	yPC62 *CEN4* set2Δ::hphMX6* #9
Figure 16 C	*MATa dot1::hphMX6 lox-CEN4-lox:KanMX GDP-creEBD78:LEU2 his3Δ1 leu2Δ0 ura3Δ0 met15Δ0*	yPC63 *CEN4* dot1Δ::hphMX6* #5
Figure 16 C	*MATa dot1::hphMX6 lox-CEN4-lox:KanMX GDP-creEBD78:LEU2 his3Δ1 leu2Δ0 ura3Δ0 met15Δ0*	yPC64 *CEN4* dot1Δ::hphMX6* #7
Figure 17 B	*MATa rtt109::hphMX6 lox-CEN4-lox:KanMX GDP-creEBD78:LEU2 his3Δ1 leu2Δ0 ura3Δ0 met15Δ0*	yPC65 *CEN4* rtt109Δ::hphMX6* #8

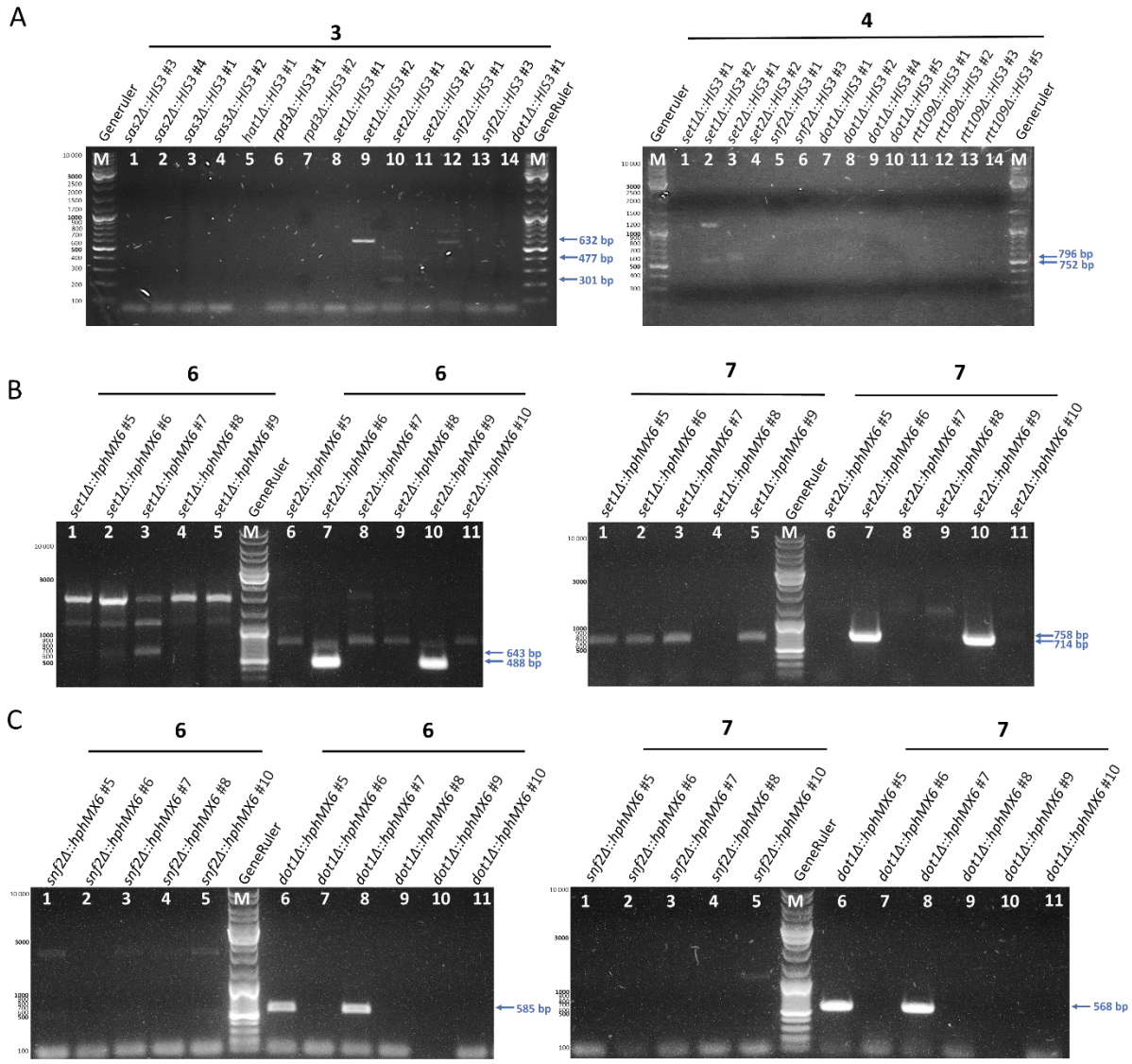

Figure 16. Verifying Set1, Set2 and Dot1 methyltransferase deletion mutants by PCR. gDNA from transformants indicated above lanes were used as template in a PCR reaction. Number above the gel indicate primer combinations from **Figure 15**. Gels were visualized by UV-light and lanes are numbered from left to right with white numbers or "M" for marker/ladder. Fragments corresponding to expected fragment sizes (**Table 5**) are indicated with a blue arrow with the calculated number on the right side of the gel. Ladder fragment lengths in bp (**Figure 9**) shown on the left with bold numbers indicating a stronger signal.
A: Verification of *set1Δ::HIS3MX6* #2 and *set2Δ#1::HIS3MX6* #1. 2% Agarose gel, run on 90V for 1 h 45 min. **Left**: primer pair 3. **Lane 9**: expected size 632 bp. **Lane 10**: expected size 477 bp and 301 bp. **Right**: primer pair 4. **Lane 2**: expected size 752 bp and **Lane 3**: expected size 796 bp.
B: Verification of *set1*Δ*::hphMX6* #7, *set2*Δ*::hphMX6* #6 and *set2*Δ*::hphMX6* #9. Both gels are 1% Agarose, run on 100V for 1 h. **Left**: primer pair 6. **Lane 3**: expected size 643 bp and **Lane 7 & 10**: expected size 488 bp. **Right**: primer pair 7. **Lane 1, 2, 3 & 5**: expected size 714 bp and **Lane 7 & 10**: expected size 758 bp.
C: Verification of *dot1*Δ*::hphMX6* #5 and *dot1*Δ*::hphMX6* #7. Both gels are 1% Agarose, run on 100V for 1 h 10 min. **Right**: primer pair 6. **Lane 6 & 8:** expected size 585 bp. **Left**: primer pair 7. **Lane 6 & 8**: expected size 568 bp.

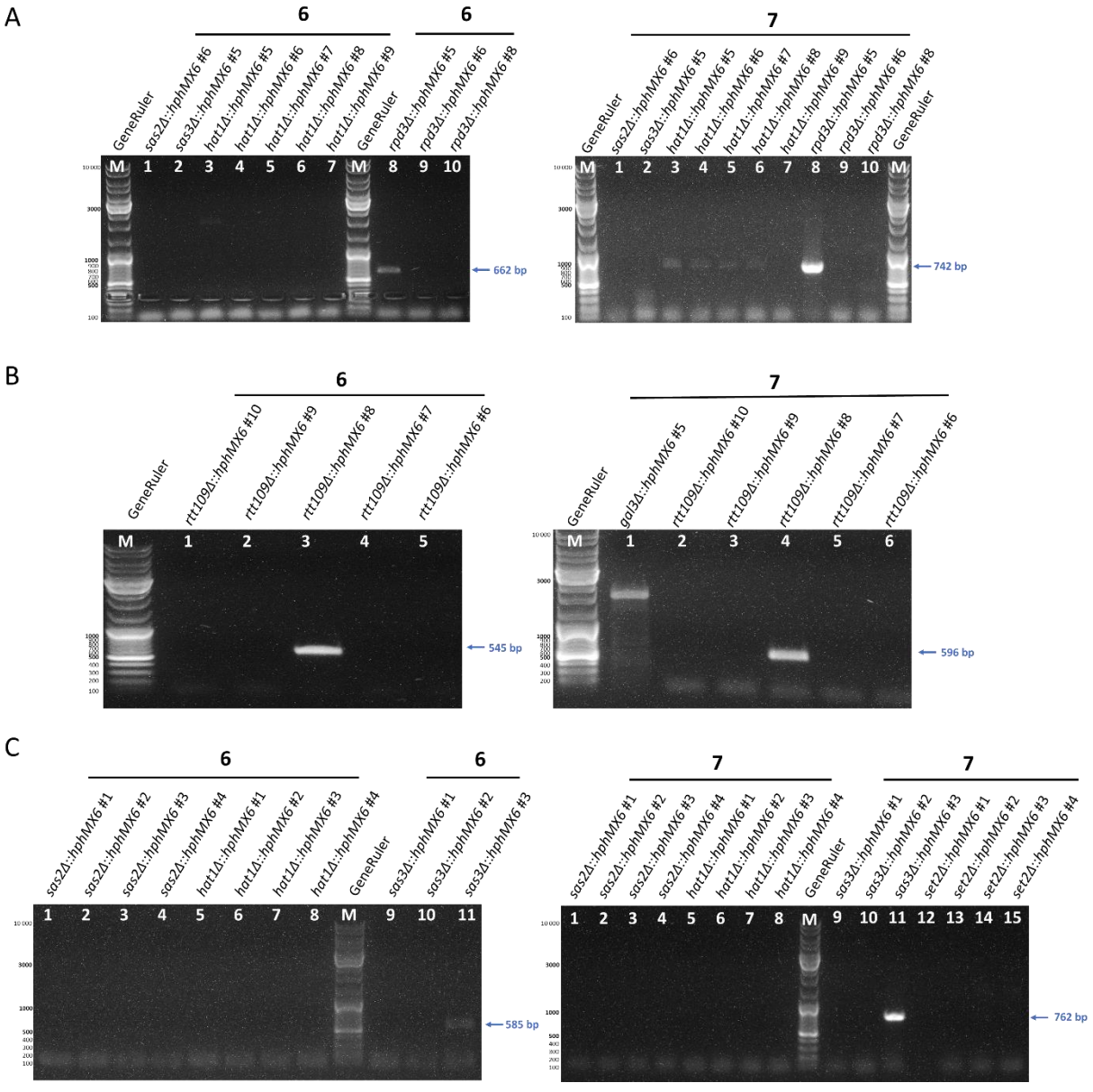

Figure 17. Verifying Rpd3, Rtt109 acetyltransferase and Sas3 deacetylase deletion mutants by PCR. gDNA from transformants indicated above lanes were used as template in a PCR reaction. Number above the gel indicate primer combinations from **Figure 15**. Gels were visualized by UV-light and lanes are numbered from left to right with white numbers or "M" for marker/ladder. Fragments corresponding to expected fragment sizes (**Table 5**) are indicated with a blue arrow with the calculated number on the right side of the gel. Ladder fragment lengths in bp (**Figure 9**) shown on the left with bold numbers indicating a stronger signal. All gels are 1% Agarose, run on 90V for ~1 h.
A: Verification of *rpd3Δ::hphMX6* #5. **Left**: primer pair 6. **Lane 8**: expected size 662 bp. **Right**: primer pair 7. **Lane 8:** expected size 742 bp
B: Verification of *rtt109*Δ*::hphMX6* #8 . **Left**: primer pair 6. **Lane 3**: expected size 545 bp. **Right**: primer pair 7. **Lane 4:** expected size 596 bp. gDNA from a *gal3*Δ strain was also included on this gel but is unrelated to this study (Another project from Chymkowitch lab).
C: Verification of *sas3*Δ*::hphMX6* #3. **Left**: primer pair 6. **Lane 11**: expected size 585 bp. **Right**: primer pair 7. **Lane 11**: expected size 762 bp.

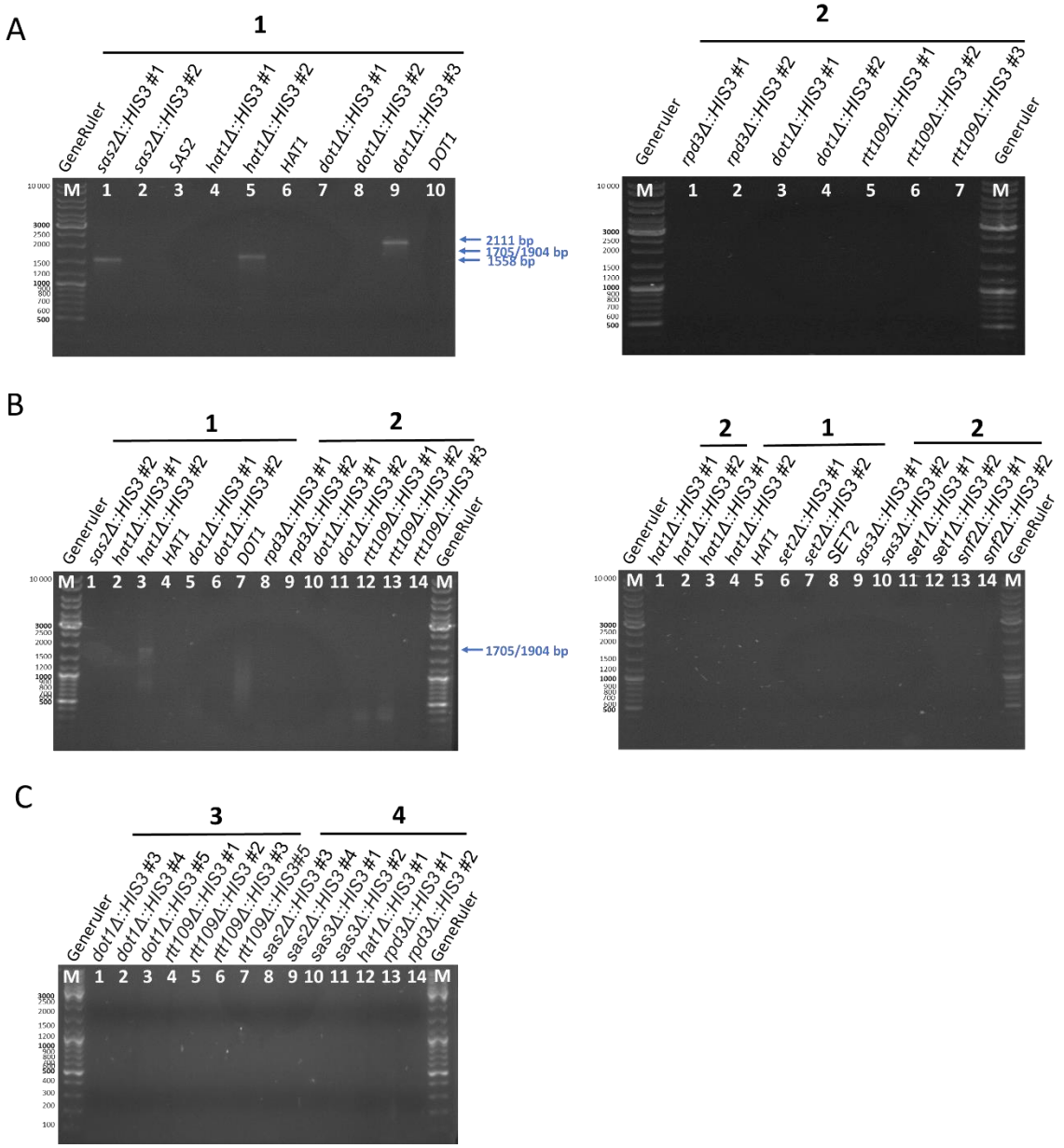

Figure 18. Gels leading to unsuccessful verification of deletion mutants transformed by *HIS3*-cassette. gDNA from transformants indicated above lanes were used as template in a PCR reaction. Number above the gel indicate primer combinations from **Figure 15**. Gels were visualized by UV-light and lanes are numbered from left to right with white numbers or "M" for marker/ladder. Fragments corresponding to expected fragment sizes (**Table 5**) are indicated with a blue arrow with the calculated number on the right side of the gel. Ladder fragment lengths in bp (**Figure 9**) shown on the left with bold numbers indicating a stronger signal.
A: Left: 1% Agarose, run on 90V for ~1 h 30 min. **Lane 1** seems to correspond with *SAS2* exp. 1558 bp. **Lane 5** fragment could correspond with both exp sizes, 1705 bp for *HAT1* and 1904 bp for mutant. **Lane 9** fragment corresponds with *DOT1* exp. 2111 bp. **Right:** 1% Agarose, run on 100V for ~1 h 20 min. No bands.
B: Left: 1% Agarose, run on 100V for ~ 1 h 30min. **Lane 3** fragment could correspond with both exp sizes, 1705 bp for *HAT1* and 1904 bp for mutant. **Lane 7** shows unspecific binding. **Lane 12 & 13** fragments do not correspond to expected size of 764 bp. **Right:** 1% Agarose, run on 100V for ~1 h 30 min. No bands.
C: 2% Agarose, run on 90V for ~ 1 h 45 min. No bands

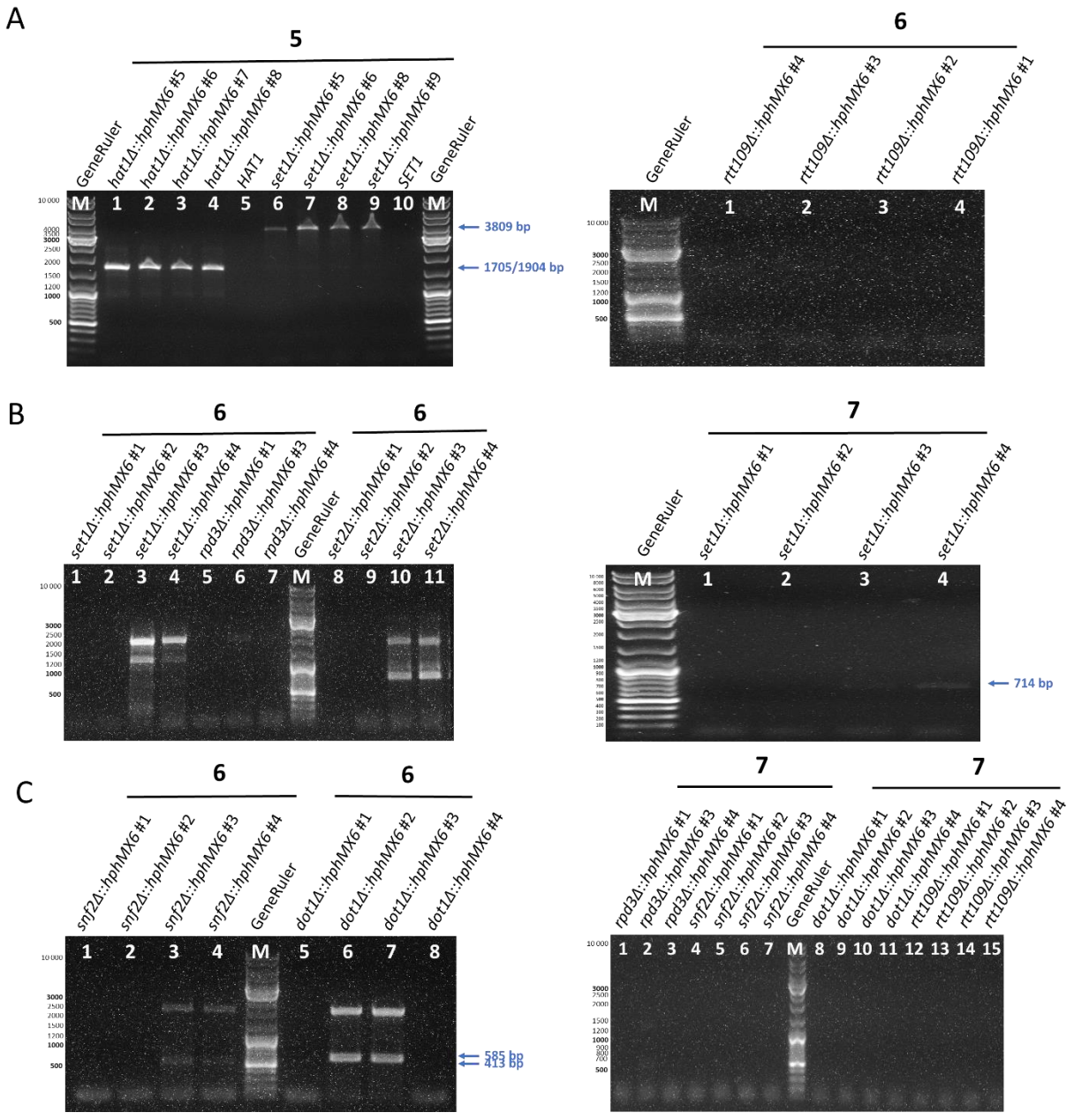

Figure 19. Gels leading to unsuccessful verification of deletion mutants transformed by *hph*-cassette. gDNA from transformants indicated above lanes were used as template. Number above the gel indicate primer combinations from **Figure 15**. Gels were visualized by UV-light and lanes are numbered from left to right with white numbers or "M" for marker/ladder. Fragments corresponding to expected fragment sizes (**Table 5**) are indicated with a blue arrow with the calculated number on the right side of the gel. Ladder fragment lengths in bp (**Figure 9**) shown on the left with bold numbers indicating a stronger signal.
A: Left: 1% Agarose, run on 90V for ~1 h 10 min. **Lane 1-4** fragment could correspond with both exp sizes, 1705 bp for *HAT1* and 1904 bp for mutant. **Lane 6-9** fragments correspond with *SET1* exp. 3809 bp. **Right**: 1% Agarose, run on 100V for ~1 h. No bands
B: Left: 1% Agarose gel, run on 100V for ~ 1 h 20 min. **Lane 3 – 4 & 10 - 11** fragments do not correspond with any expected sizes. **Right**: 1% Agarose gel, run on 90V for ~ 1 h 30 min. **Lane 4** fragment correspond to expected size of 714 bp.
C: Both gels are 1% Agarose, run on 90V for ~ 1 h 30min. **Left: Lane 3 & 4** lower fragment correspond to expected size of 413 bp. **Lane 6 & 7** lower fragment correspond to expected size of 585 bp. **Right**: No bands.

3.1.1 Spot assay

A spot assay was done according to **Chapter 2.19 Spot assay** to verify that the mutants still have intact Cre-recombinase activity, but also to see if the genotype could somehow rescue the fitness of the *CEN4* strain. The assay was done comparing *CEN4, CEN4** and the verified deletion mutants with the *HIS3*-cassette in **Figure 20 A**. In **Figure** 20 **B & C** *CEN4, CEN4** was compared to the deletion mutants containing the *hph*-cassette. Only one mutant for each strain chosen for the proceeding centromere excision during S phase arrest screening experiments (**Chapter 3.2 A qPCR-based screen to identify chromatin regulators involved in centromere-regulated transcription in synchronized cells**) were tested. The strains are grown on plates containing YPD, YPD + EtOH (for transformants containing the *HIS3*-cassette) and YPD+β-estradiol.

From the results, all strains have normal growth in YPD and YPD + EtOH plates. All mutants express *cen4-* phenotype in the YPD+β-estradiol plates except for *cen4- set2*Δ mutants, where yPC61 *set2*Δ*::hphMX6* has the same phenotype as *CEN4*, and yPC56 *set2Δ::HIS3* has the same phenotype as *cen4-*.

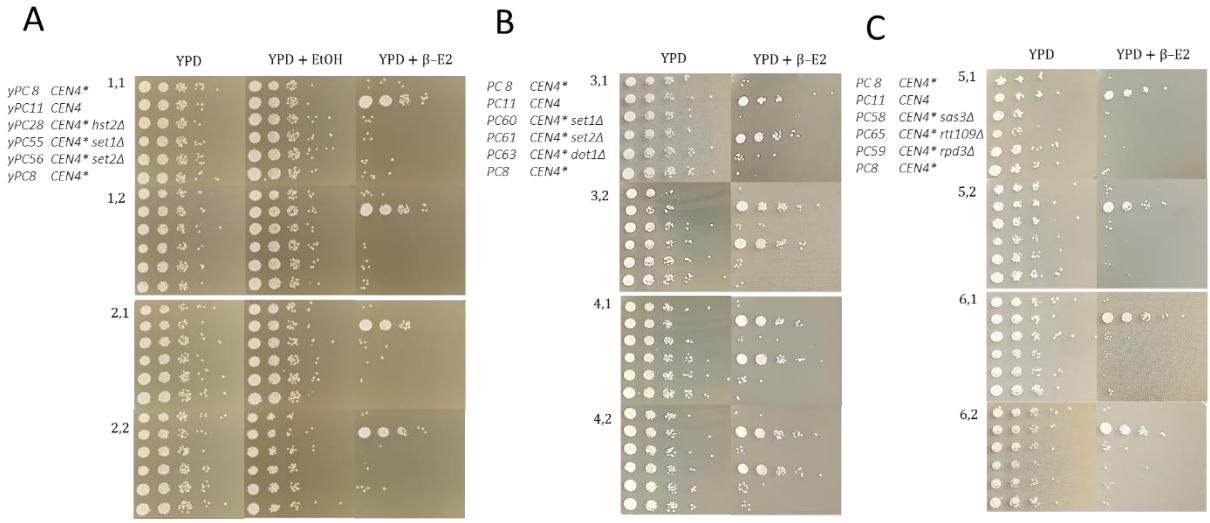

Figure 20. Comparison of yeast cell growth upon β-E2 treatment. Spotted 2 x 2 biological and technical replicates in a 6 times 10x serial dilution starting with an OD_{600}=0.1 in **A** and with OD_{600}=0.5 in **B/C**. Cells were grown on YPD plates (control), YPD+EtOH (additional control in **A**) and YPD+0.1 µg/ml β-E2 (centromere excision). Strains are mentioned once on the upper left plate and follows the same pattern vertically. As for numbering, the left number indicates biological replicate and right number indicates technical replicate. The plates were incubated at 30°C and the photos were taken on day 2 of growth.

3.2 A qPCR-based screen to identify chromatin regulators involved in centromere-regulated transcription in synchronized cells

The centromere's role in licensing chromatin condensation at mitosis entry is essential for maintaining transcriptional homeostasis in cis during interphase, but the mechanism behind this remains largely unknown (Ramos Alonso et al., 2023). Other than the HDAC Hst2, what are the downstream factors from the centromere involved in chromatin- and gene regulation?

To identify the downstream factors of the centromere in this mechanism, we synchronized cells prior to G2/M phase entry using HU. Afterward, we released these cells into the cell cycle, with or without excising the centromere on chromosome IV, and monitored the expression of relevant genes using qPCR at various time points in one of each deletion mutant genotype (**Table 6**).

Experimental setup

(**Figure 21**) Experiments were done in a similar manner, but in a combination of different time points (stated in each experiment). A liquid culture starting at 0.2 OD_{600} was incubated according to **Chapter 2.1.2** and collected (**Chapter 2.11**) at time point t_{log} yielding asynchronized and exponentially growing cells. Remaining cells are synchronized in S phase with HU (**Chapter 2.14**) and collected at t_S before adding 1 µM β-estradiol for centromere excision from chromosome IV, where *CEN4** cells become *cen4-* after excision (**Chapter 2.15**), and cells were collected at $t_{S+β-E2}$. Remaining cells were washed two times by centrifuging the cells 4000 rpm for 1 minute and resuspended with 1x volume of YPD. Cells were collected at 90, 120 or 150 minutes; t_{90R}, t_{120R} or t_{150R} after release from S phase.

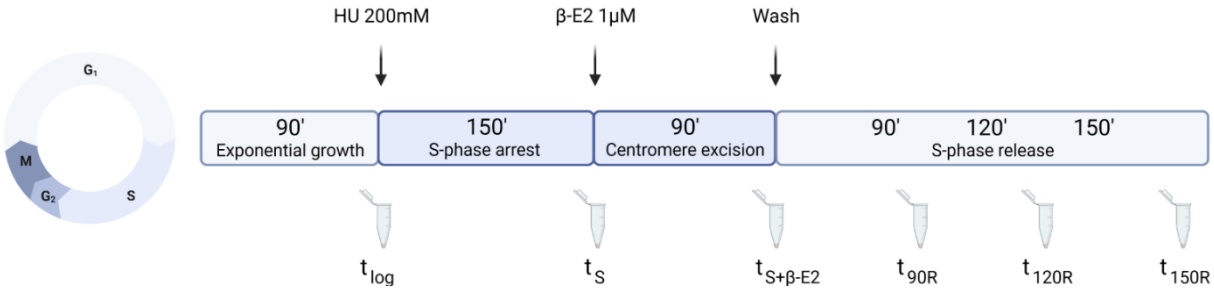

Figure 21. Experimental overview and summary of time points used for cell collection in this thesis. Simple schematic of the cell cycle is shown to the left. Numbers inside boxes indicate time from left to right in minutes. Text above boxes indicate treatments to the cells during the experiment. Time points for cell collection are indicated below and includes t_{log}, t_S, $t_{S+β-E2}$, t_{90R}, t_{120R} and t_{150R}.

Samples were collected at each time point for microscopy (**Chapter 2.12**) to look at phenotype and detect contamination, and for flow cytometry (**Chapter 2.13**) for cell cycle analysis. Two or three biological replicates (stated in each experiment) were collected for RNA extraction (**Chapter 2.16**) at each time point. RNA is extracted from the collected cells for the purpose of doing reverse transcription and gDNA removal (**Chapter 2.17**) to yield complementary DNA (cDNA) to the given RNA. The cDNA was then analysed by RT-qPCR **(Chapter 2.18)** to quantify the expression of six genes from chromosome IV in *CEN4*, *CEN4** and the deletion mutants derived from the *CEN4** strain (**Table 6**). The qPCR results shown are relative to the reference gene *MNN2* because expression levels were similar between *CEN4* and *CEN4** strains (**Figure 28** in **3.3 Supplemental results**), and normalized to t_S.

3.2.1 Centromere-regulated gene expression in *cen4- hst2Δ*

Two biological replicates of the *CEN4* strain (three replicates initially), and three biological replicates of the *CEN4** and *CEN4* hst2Δ* strains were collected for RNA extraction. Results from flow cytometry, microscopy and qPCR from **Figure 22** are from cells collected at time points t_{log}, t_S, $t_{S+\beta\text{-}E2}$, t_{90R} and t_{120R} (**Figure 22 A)**.

Flow cytometry results (**Figure 22 B)** for *CEN4** and *CEN4* hst2Δ* strains show asynchronous cells at t_{log} where the 1n left peak shows cells in G1 phase, the right peak shows 2n cells in G2/M phase and the signal from between the peaks belong to cells replicating its genome in S phase. There is a deviant profile for *CEN4 at* t_{log}. Time points t_S and $t_{S+\beta\text{-}E2}$ show cells arrested in S phase by an absence of the two peaks, and presence of a wider peak located in between. Cells collected at $t_{S+\beta\text{-}E2}$ are arrested in later S phase, identified by the slight skew of the S phase peak towards the right side. *CEN4* cells collected at t_{90R} are mostly in G2/M phase, while at t_{120R} more cells have entered G1. *cen4-* cells, however, show a delay in the cell cycle after β-estradiol treatment and have more cells in G1- and S phase in t_{90R}, and more cells in G2/M phase at t_{120R} compared to *CEN4*.

Microscope results (**Figure 22 C)** validate flow cytometry by also showing asynchronous cells across strains at t_{log}, identified visually by the presence of single cells, budding cells and multiple cells stuck together during and after mitosis, with a contamination of an unknown bacteria in one of the *CEN4* cultures (leading to one of the three initial replicates being discarded). Time point t_S and $t_{S+\beta\text{-}E2}$ show phenotypic S phase arrested cells which includes

budding, and the appearance of two cells visually stuck together with a higher cell count in $t_{S+\beta\text{-}E2}$. The phenotype of cells collected at t_{90R} and t_{120R} also has a phenotype of S phase cells with more budding at t_{90R} compared to t_{120R} and more cell adhesion in t_{120R} compared to t_{90R}. Visually, it is not possible to distinguish late S- with G2/M phase by microscopy.

Results from qPCR (**Figure 22 D)** show relative gene expression of the six different genes from chromosome IV normalized to t_S in *CEN4*, *CEN4** and *CEN4* hst2Δ* strains. The results display varying differences in expression between strains at all time points except t_{120R} when *cen4-* has the highest expression of the strains in all genes except for *YCF1* after displaying lower or same expression levels compared to *CEN4* at t_{90R} except for in *PHO2*. Looking at *cen4- hst2Δ* expression, it is higher than *cen4-* for all genes, but lower than *CEN4* except for in *BUG1* at $t_{S+\beta\text{-}E2}$. However, it is lower than *CEN4* at t_{120R} for all genes. These results show that *CEN4** excision leads to increased transcription in chromosome IV genes in *cen4-* and a decrease in *cen4- hst2Δ* at 120 minutes after S phase release compared to *CEN4*.

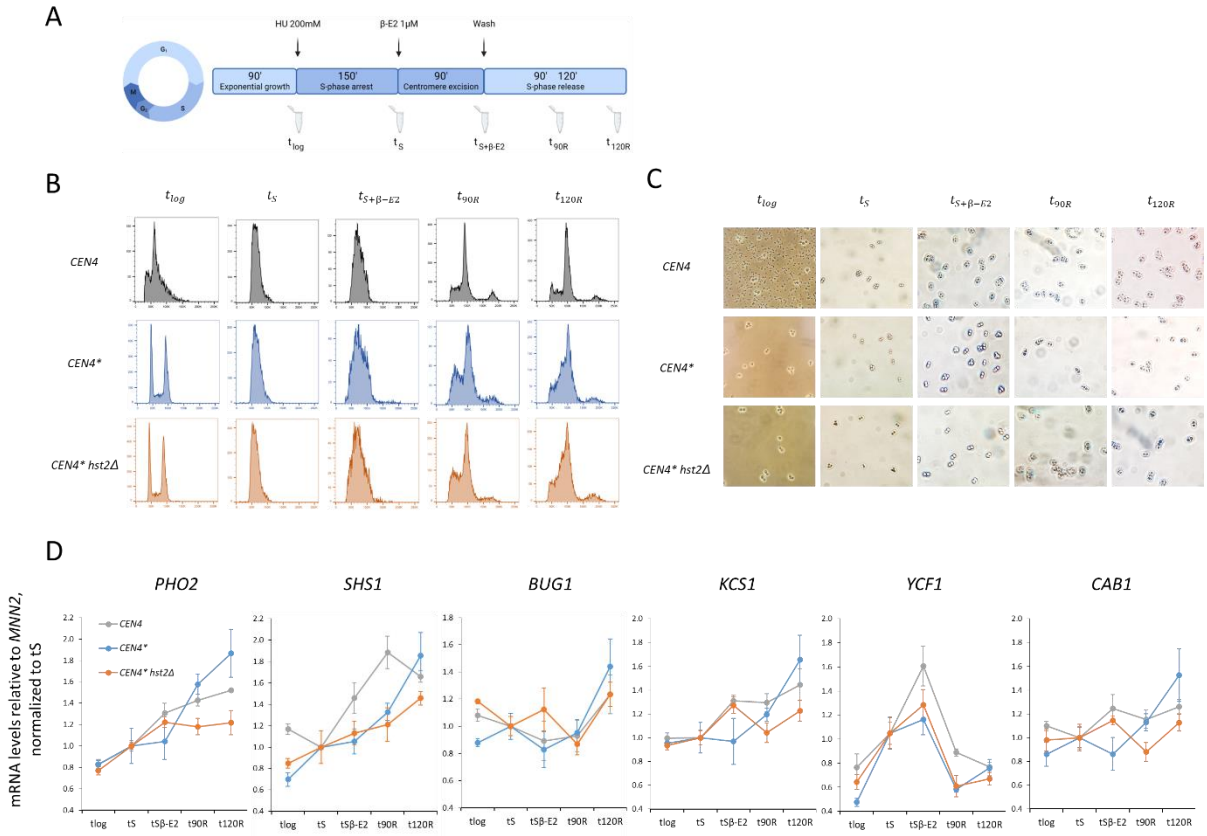

Figure 22. Centromere excision leads to increased gene expression in *cen4-* and decreased gene expression in *cen4- hst2Δ* at 120 min after release from S phase compared to *CEN4*.
A: Simple schematic of the *CEN4** excision during S phase arrest experiment introducing five cell collection time points.
B: Cell cycle analysis by flow cytometry was performed on one sample for each time point and strain; *CEN4* (grey), *CEN4** (blue) and *CEN4* hst2Δ* (orange). Time points indicated on top and strain indicated on the left. *cen4-* strains are lagging behind in cell cycle progression.
C: Light microscopy pictures from the same samples and indications as **B.**
D: RT-qPCR analysis of the expression of six selected genes from chromosome IV at different time points before- and after centromere excision during S phase arrest and release. Gene expression levels are shown relative to *MNN2* and normalized to time point tS. The results from *CEN4** strains are calculated from three replicates, while the results from *CEN4* was calculated with two replicates.

3.2.2 Centromere-regulated gene expression in *cen4- rpd3Δ* and *cen4- dot1Δ* strains

Results from flow cytometry, microscopy and qPCR for each time point is shown in **Figure 23**. Two biological replicates from each of the strains *CEN4*, *CEN4**, *CEN4* rpd3Δ* and *CEN4* dot1Δ* were collected for RNA extraction at time points t_S, $t_{S+\beta\text{-}E2}$ and t_{150R} (**Figure 23 A)**, and RNA integrity results accompanying this experiment can be found in **Table 8** in **3.3 Supplemental results**.

Flow cytometry results (**Figure 23 B)** show cells arrested in S phase cells at t_S, by the presence of a single peak. Cells collected at $t_{S+\beta\text{-}E2}$ has a wider peak skewed towards the right indicating arrest further into S phase. Cells collected at t_{150R} show cells in all cell cycle stages except for *CEN4* rpd3Δ* which has cells mostly in late S phase or G2/M, ahead of the other *cen4-* strains still having the G1 peak. All *cen4-* strains show delayed cell cycle compared to *CEN4*.

Microscope results (**Figure 23 C)** validate flow cytometry results by also showing that all cells across strains at t_S and $t_{S+\beta\text{-}E2}$ express the S phase phenotype. cells, budding cells and multiple cells stuck together during and after mitosis. The phenotype of cells collected at t_{150R} are also similar to the S phase arrested cells, showing no single cells. However there are many clusters of three cells, and many showing signs of early budding (easily visible for *CEN4* and *cen4- rpd3Δ).* All strains also show signs of HU damage, forming abnormal and elongated cell shapes.

Results from qPCR (**Figure 23 D)** show relative gene expression of the six different genes from chromosome IV normalized to t_S in *CEN4*, *CEN4**, *CEN4* rpd3Δ* and *CEN4* dot1Δ* strains. The results for each mutant is separated (upper and lower panel), while control strain results are shown in both panels. Difference in *YCF1* expression is undistinguishable between all strains. Comparing the rest of the genes between *CEN4* to *cen4-* from t_S to $t_{S+\beta\text{-}E2,}$ both display a decrease in transcription, and even more so in *cen4-*. However, when comparing the same strains at t_{150R} there is a high increase in gene expression in the *cen4-* strain. Comparing both mutants to the control strains, they have an overall similar pattern to each other with a considerably higher gene expression in $t_{S+\beta\text{-}E2}$ for the genes *PHO2 (*mostly in *cen4- dot1Δ), SHS1, BUG1* and *KCS1*, and at t_{150R} in *PHO2* and *BUG1*, or a similar expression to *cen4-* in *SHS1, KCS1* and *CAB1*.

In summary, these results show that *CEN4* excision leads to increased transcription in *cen4-*, *cen4- rpd3Δ* and *cen4- dot1Δ*, in five out of six chromosome IV genes compared to *CEN4* at 150 minutes after S phase release. And both mutants display a considerably higher gene expression in four out of six genes even before releasing the cells into mitosis compared to the control strains.

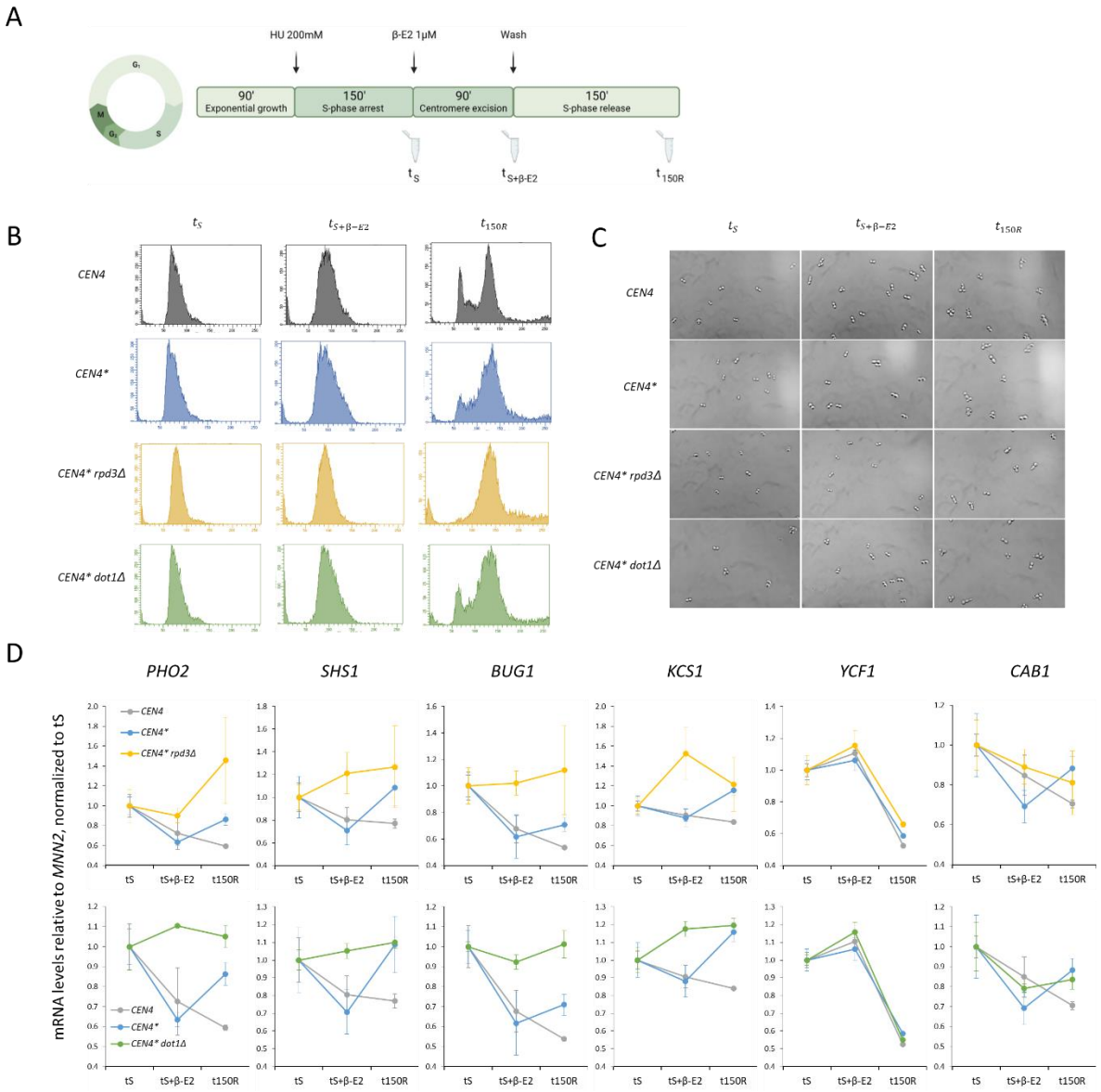

Figure 23. Centromere excision leads to increased gene expression in *cen4- rpd3Δ*, *cen4- dot1Δ* and *cen4-* at 150 min after release from S phase.

A: Simple schematic of the *CEN4** excision during S phase arrest experiment, introducing three cell collection time points. This experiment had two biological replicates for each strain.

B: Cell cycle analysis by flow cytometry was performed on one sample for each time point and strain; *CEN4* (grey), *CEN4** (blue), *CEN4* rpd3Δ* (yellow) and *CEN4* dot1Δ* (green). Time points indicated on top and strain indicated on the left.

C: Light microscopy pictures from the same samples and indications as **B.**

D: RT-qPCR analysis of the expression of six selected genes from chromosome IV at different time points before- and after centromere excision during S phase arrest and release. Gene expression levels are shown relative to *MNN2* and normalized to time point tS. Upper panel shows control strains with mutant *CEN4* rpd3Δ* (yellow) and lower panel shows control strains with *CEN4* dot1Δ* (green).

3.2.1 Centromere-regulated gene expression in *cen4- set1Δ* and *cen4- set2Δ* strains

Results from flow cytometry, microscopy and qPCR for each time point is shown in **Figure 24**. Two biological replicates from each of the strains *CEN4, CEN4*, CEN4* set1Δ* and *CEN4* set2Δ* were collected for RNA extraction at time points t_S, $t_{S+\beta\text{-}E2}$ and t_{150R} (**Figure 24 A)**, and RNA integrity results accompanying this experiment can be found in **Table 9** in **3.3 Supplemental results**.

Flow cytometry results (**Figure 24 B)** show cells arrested in S phase cells at t_S, by the presence of a single peak. Cells collected at $t_{S+\beta\text{-}E2}$ has a wider peak skewed towards the right indicating arrest further into S phase. Cells collected at t_{150R} show cells in all cell cycle stages, where *cen4- set2Δ* shows a similar phenotype to *CEN4,* and *cen4- set1Δ* to *cen4-* having a delay in cell cycle.

Microscope results (**Figure 24 C)** validate flow cytometry results by also showing that most cells across strains at t_S and $t_{S+\beta\text{-}E2}$ express the S phase phenotype. The phenotype of cells collected at t_{150R} are also similar to the S phase arrested cells,. However there are many clusters of three cells, with many cells showing signs of early budding. Strains also show signs of HU damage, especially visible for *cen4- set2Δ* .

Results from qPCR (**Figure 24 D)** show relative gene expression of the six different genes from chromosome IV normalized to t_S in *CEN4*, *CEN4**, *CEN4* set1Δ* and *CEN4* set2Δ* strains. The results for each mutant is separated (upper and lower panel), while control strain results are shown in both panels. Comparing gene expression between *CEN4* and *cen4-* at $t_{S+\beta\text{-}E2}$, *CEN4* display an increase the gene expression of chromosome IV genes in four of six genes, but at t_{150R}, there is a high increase in gene expression in the *cen4-* strain across all genes. For *cen4- set1Δ,* gene expression is similar to *cen4-* at t_{150R} in three genes, and even higher than *cen4-* in the remaining three genes. The opposite is the case for the *cen4- set2Δ* mutant, which at t_{150R} display a strong resemblance to *CEN4* gene expression.

In summary, these results show that *CEN4** excision leads to increased transcription in *cen4-* across all tested genes after release from S phase, with *cen4- set1Δ* displaying an even higher expression in half of the genes compared to *cen4-*. Also, *cen4- set2Δ* is able to rescue both the cell cycle- and gene expression phenotype of *CEN4.*

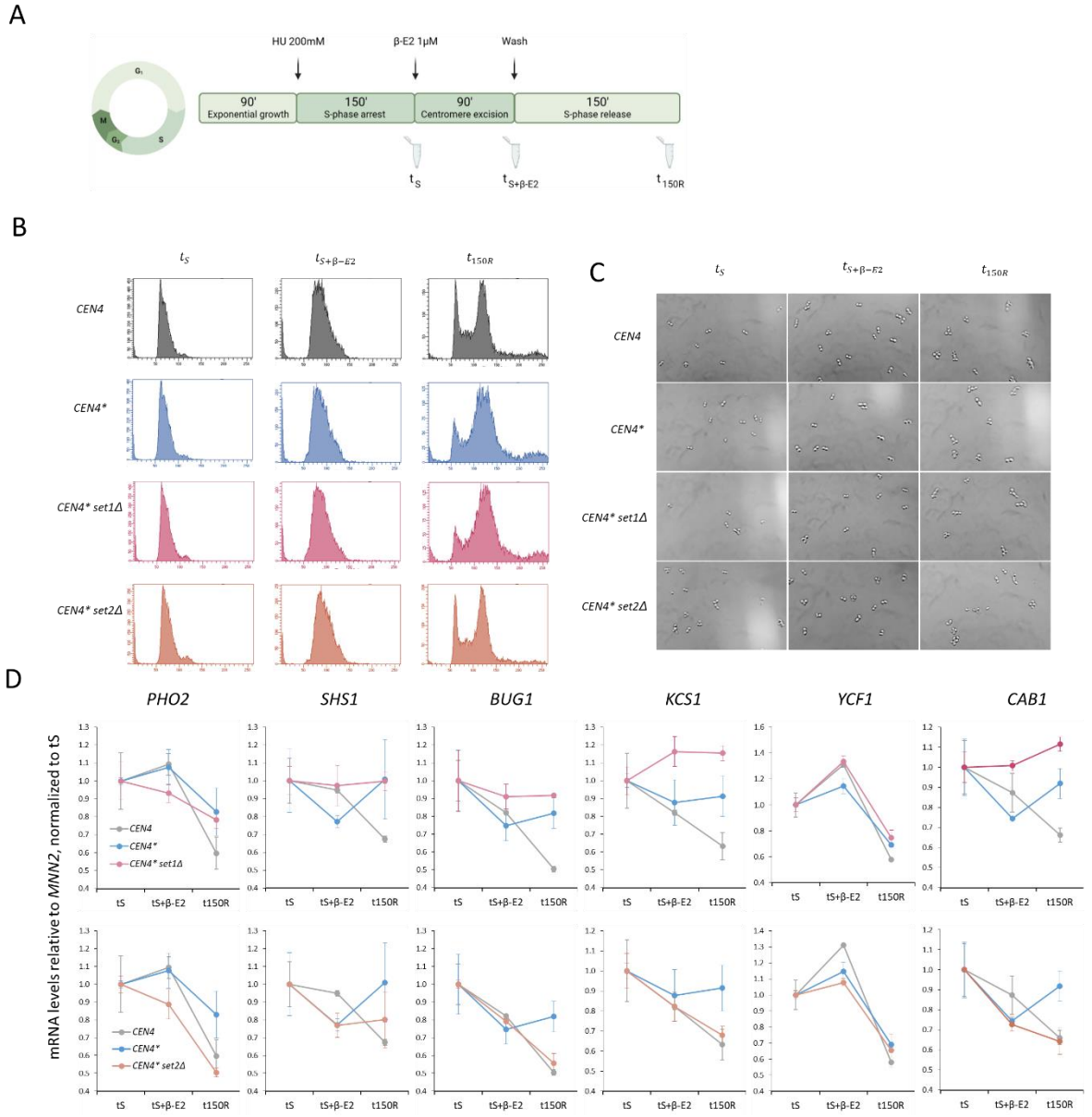

Figure 24. Centromere excision leads to increased gene expression in *cen4-* and *cen4- set1Δ*, while *cen4-set2Δ* is rescuing the phenotype of *CEN4*.

A: Simple schematic of the *CEN4** excision during S phase arrest experiment, introducing three cell collection time points. This experiment had two biological replicates for each strain.

B: Cell cycle analysis by flow cytometry was performed on one sample for each time point and strain; *CEN4* (grey), *CEN4** (blue), *CEN4* set1Δ* (pink) and *CEN4* set2Δ* (dark orange). Time points indicated on top and strain indicated on the left.

C: Light microscopy pictures from the same samples and indications as **B.**

D: RT-qPCR analysis of the expression of six selected genes from chromosome IV at different time points before- and after centromere excision during S phase arrest and release. Gene expression levels are shown relative to *MNN2* and normalized to time point tS. Upper panel shows control strains with mutant *CEN4* set1Δ* (pink) and lower panel shows control strains with *CEN4* set2Δ* (dark orange).

3.2.1 Centromere-regulated gene expression in *cen4- sas3Δ* and *cen4- rtt109Δ* strains

Results from flow cytometry, microscopy and qPCR for each time point is shown in **Figure 25**. Two biological replicates from each of the strains *CEN4, CEN4*, CEN4* sas3Δ* and *CEN4* rtt109Δ* were collected for RNA extraction at time points t_S, $t_{S+\beta\text{-}E2}$ and t_{150R} (**Figure 25 A)**, and RNA integrity results accompanying this experiment can be found in **Table 10** in **3.3 Supplemental results**.

Flow cytometry results (**Figure 25 B)** show cells arrested in S phase cells at t_S, by the presence of a single peak. Cells collected at $t_{S+\beta\text{-}E2}$ has a wider peak skewed towards the right indicating arrest further into S phase. Cells collected at t_{150R} show cells in all cell cycle stages, but *cen4-* cells display a delay in cell cycle progression compared to *CEN4* with *cen4- rtt109Δ* showing an even higher delay than the other two *cen4-* strains.

Microscope results (**Figure 25 C)** validate flow cytometry results by also showing that most cells across strains at t_S and $t_{S+\beta\text{-}E2}$ express the S phase phenotype. The phenotype of cells collected at t_{150R} are also similar to the S phase arrested cells,. However there are many clusters of four cells, with many showing signs of early budding. Strains also show signs of HU damage, especially visible in *cen4- sas3Δ* .

Results from qPCR (**Figure 25 D)** show relative gene expression of the six different genes from chromosome IV normalized to t_S in *CEN4*, *CEN4**, *CEN4* sas3Δ* and *CEN4* rtt109Δ* strains. The results for each mutant is separated (upper and lower panel), while control strain results are shown in both panels. Comparing gene expression between *CEN4* and *cen4-* at $t_{S+\beta\text{-}E2}$, *cen4-* display the same level or higher expression than *CEN4* after centromere excision in S phase. At t_{150R}, gene expression is higher in *cen4-* for all six genes. For the *cen4- sas3Δ* mutant, gene expression levels varies compared to control strains, but displays a phenotype similar to *cen4-* at t_{150R} in *PHO2, BUG1, KCS1* and *CAB1*. In the mutant *cen4- rtt109Δ* however, gene expression levels are far higher than control strains in both $t_{S+\beta\text{-}E2}$ (except *YCF1),* and t_{150R} compared to *cen4-*.

These results show that *CEN4** excision leads to increased transcription in *cen4- sas3Δ* in five of six chromosome IV genes, and across all genes in *cen4-* and *cen4- rtt109Δ* at 150 minutes after S phase release compared to *CEN4. cen4- rtt109Δ* display considerably higher gene expression than *cen4-* cells in five out of six genes.

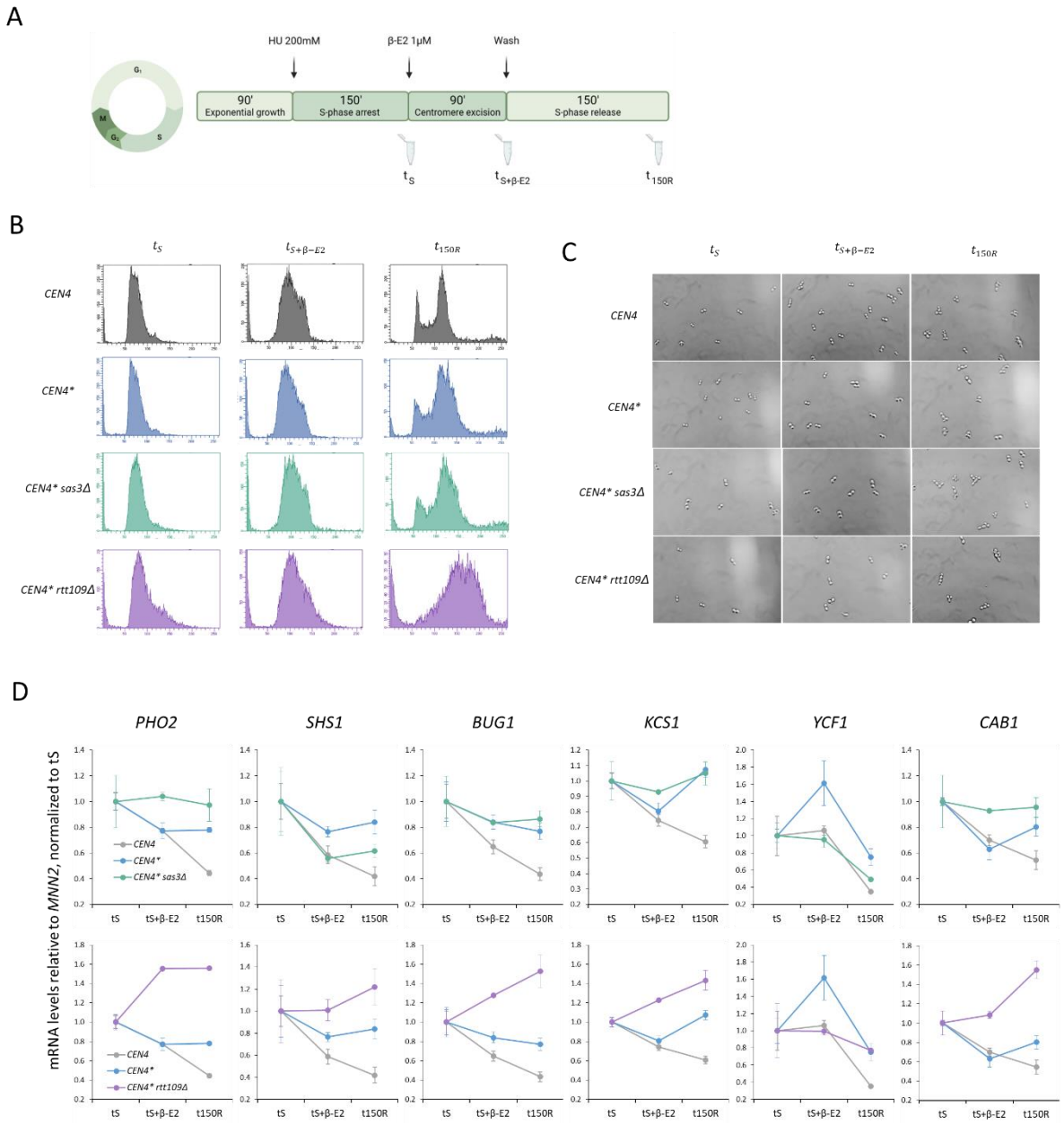

Figure 25. Centromere excision leads to increased gene expression in *cen4-* and *cen4- sas3*Δ at 150 min after release from S phase compared to *CEN4*. While *cen4- rtt109*Δ shows increased expression and cell cycle lagging. A: Simple schematic of the *CEN4** excision during S phase arrest experiment, introducing three cell collection time points. This experiment had two biological replicates for each strain.
B: Cell cycle analysis by flow cytometry was performed on one sample for each time point and strain; *CEN4* (grey), *CEN4** (blue), *CEN4* sas3Δ* (turquoise) and *CEN4* rtt109Δ* (purple). Time points indicated on top and strain indicated on the left.
C: Light microscopy pictures from the same samples and indications as **B.**
D: RT-qPCR analysis of the expression of six genes from chromosome IV at different time points before- and after centromere excision during S phase arrest and release. Gene expression levels are shown relative to *MNN2* and normalized to time point tS. Upper panel shows control strains with mutant *CEN4* sas3Δ* (turquoise) and lower panel shows control strains with *CEN4* rtt109Δ* (purple).

3.2.2 Overall results for centromere-regulated gene expression in obtained *cen4-* deletion mutants

To more easily being able to compare differences between *CEN4** strains to *CEN4* qPCR results was normalized to *CEN4* gene expression instead of to time point t_S (**Figure 22, 23, 24, 25**), and a heatmap with the results was created displaying a similar expression to *CEN4* in white, lower expression in blue and a higher expression than *CEN4* in red. The heatmap is shown in **Figure 26**.

When comparing *CEN4** with *CEN4*, the results show a moderately higher expression level for *CEN4** in t_S except for *YCF1* in the experiment with *CEN4* sas3Δ* and *CEN4* rtt109Δ*. Also in this experiment, *cen4-* expression levels were higher than *CEN4* at $t_{S+\beta\text{-}E2}$ while being lower or similar to *CEN4* in experiments with other mutants. After 150 minutes release from S phase at t_{150R}, expression was much higher than *CEN4* after centromere excision in all experiments.

When looking at overall expression levels in the *CEN4** deletion mutants at t_S, levels are decreased compared to *CEN4* in all

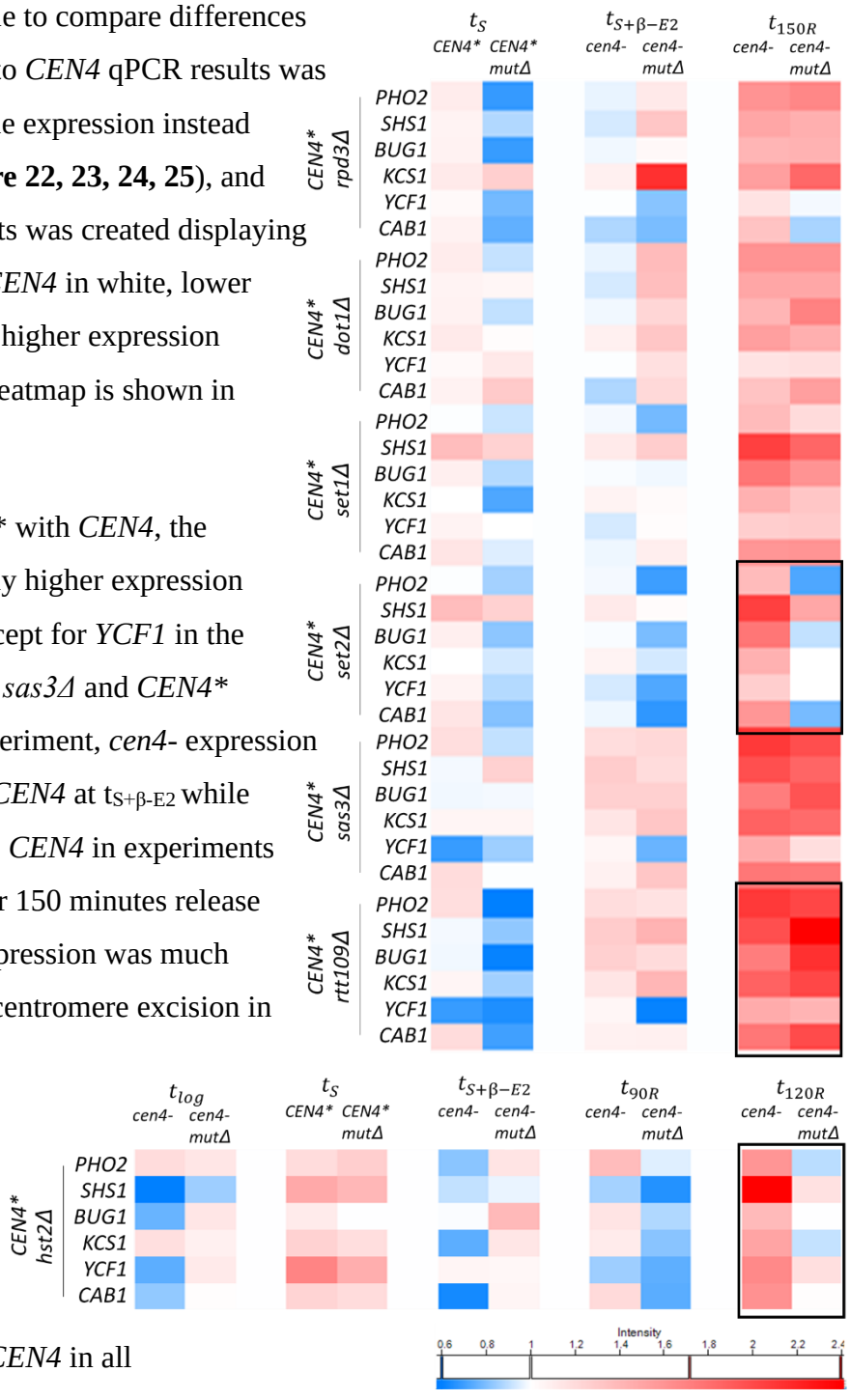

Figure 26. Heatmap with an overview of all RT-qPCR results relative to *MNN2* and normalized to *CEN4* strain.
Each column refers to a time point indicated on top, with *CEN4** expression on the left, and *CEN4* "mutΔ"* deletion mutant expression on the right. Specific mutants are shown on the left side next to the six genes analysed from chromosome IV. Data for *CEN4* hst2Δ* is shown on the bottom and has additional time points. A white color indicates the same expression as *CEN4* while a blue color indicate lower expression, and red indicate a higher expression. The colors shown is according to bottom intensity reference band and shows gene expression converted from a numeral ratio where 1 equals *CEN4* expression.

mutants except for *CEN4* dot1Δ* which has an overall more similar level as *CEN4*, and *CEN4* hst2Δ* which is similar to *CEN4**. After *CEN4** excision at $t_{S+\beta\text{-}E2}$, the expression levels are higher than both *CEN4* and *cen4-* in *cen4- rpd3Δ*, *cen4- dot1Δ*, *cen4- hst2Δ* and *cen4- set1Δ*, higher than *CEN4* in *cen4- sas3Δ* and *cen4- rtt109Δ*, but lower than *CEN4* in *cen4- set2Δ*. After 150 minutes release from S phase at t_{150R}, the four mutants *cen4- rpd3Δ*, *cen4- dot1Δ*, *cen4- set1Δ* and *cen4- sas3Δ* have a similar expression level to *cen4-* while *cen4- rtt109Δ* has a higher expression. In contrast, *cen4- hst2Δ* has similar gene expression to *CEN4* (120 minutes after release) and *cen4- set2Δ* has a lower expression level in chromosome IV genes compared to *CEN4*.

In conclusion, among all the deletion mutants tested, the deletion of *SET2*, as well as *HST2* was able to reverse the aberrant increase in interphase gene expression caused by the lack of mitotic chromatin condensation resulting from the deletion of *CEN4** before mitosis entry.

3.3 Supplemental results

Table 7. Nanodrop data from gDNA extraction of possible deletion mutants (Figure 14)
Verified mutants indicated in bold.

Strain	ng/µl	A260 (Abs)	A280 (Abs)	260/280	260/230	Sample Type
sas2Δ::HIS3MX6 #1	200.6	4.011	2.179	1.84	1.12	DNA
sas2Δ::HIS3MX6 #2	11.0	0.219	0.174	1.26	0.14	DNA
sas2Δ::HIS3MX6 #3	502.0	10.040	5.083	1.98	1.79	DNA
sas2Δ::HIS3MX6 #4	157.9	3.157	1.662	1.90	1.14	DNA
sas3Δ::HIS3MX6 #1	235.0	4.701	3.696	1.27	0.77	DNA
sas3Δ::HIS3MX6 #2	197.4	3.948	2.195	1.80	0.98	DNA
hat1Δ::HIS3MX6 #1	40.5	0.811	0.480	1.69	0.48	DNA
hat1Δ::HIS3MX6 #2	337.1	6.741	3.663	1.84	1.34	DNA
rpd3Δ::HIS3MX6 #1	258.8	5.176	2.837	1.82	1.18	DNA
rpd3Δ::HIS3MX6 #2	225.7	4.515	2.449	1.84	1.24	DNA
set1Δ::HIS3MX6 #1	517.0	10.339	5.533	1.87	1.52	DNA
***set1Δ::HIS3MX6* #2**	**644.5**	**12.889**	**6.773**	**1.90**	**1.54**	**DNA**
***set2Δ::HIS3MX6* #1**	**407.4**	**8.148**	**4.428**	**1.84**	**1.32**	**DNA**
set2Δ::HIS3MX6 #2	423.5	8.470	4.567	1.85	1.42	DNA
snf2Δ::HIS3MX6 #1	512.5	10.249	5.663	1.81	1.26	DNA
snf2Δ::HIS3MX6 #2	11.0	0.219	0.157	1.39	0.16	DNA
snf2Δ::HIS3MX6 #3	267.3	5.347	2.729	1.96	1.53	DNA

dot1Δ::HIS3MX6 #1	253.7	5.074	2.787	1.82	1.10	DNA
dot1Δ::HIS3MX6 #2	150.2	3.003	1.679	1.79	0.92	DNA
dot1Δ::HIS3MX6 #3	488.1	9.762	5.280	1.85	1.39	DNA
dot1Δ::HIS3MX6 #4	368.2	7.364	3.814	1.93	1.56	DNA
dot1Δ::HIS3MX6 #5	225.4	4.507	2.309	1.95	1.60	DNA
rtt109Δ::HIS3MX6 #1	314.4	6.289	3.490	1.80	1.07	DNA
rtt109Δ::HIS3MX6 #2	574.4	11.488	6.174	1.86	1.61	DNA
rtt109Δ::HIS3MX6 #3	162.5	3.250	1.854	1.75	0.81	DNA
rtt109Δ::HIS3MX6 #4	21.5	0.431	0.257	1.67	0.25	DNA
rtt109Δ::HIS3MX6 #5	248.2	4.964	2.565	1.94	1.47	DNA
sas2Δ::hphMX6 #1	1816.5	36.330	18.866	1.93	1.85	DNA
sas2Δ::hphMX6 #2	2372.9	47.458	24.331	1.95	1.93	DNA
sas2Δ::hphMX6 #3	2776.3	55.526	27.794	2.00	2.53	DNA
sas2Δ::hphMX6 #4	2586.7	51.735	25.736	2.01	2.48	DNA
sas2Δ::hphMX6 #6	3429.6	68.592	33.944	2.02	2.46	DNA
sas3Δ::hphMX6 #1	1035.9	20.719	11.286	1.84	1.58	DNA
sas3Δ::hphMX6 #2	2757.2	55.144	28.170	1.96	2.00	DNA
***sas3Δ::hphMX6* #3**	**469.5**	**9.390**	**4.896**	**1.92**	**2.21**	**DNA**
sas3Δ::hphMX6 #5	354.1	7.083	3.678	1.93	1.79	DNA
hat1Δ::hphMX6 #1	2478.6	49.572	25.423	1.95	1.99	DNA
hat1Δ::hphMX6 #2	2723.1	54.461	27.792	1.96	2.00	DNA
hat1Δ::hphMX6 #3	649.0	12.979	6.674	1.94	2.00	DNA
hat1Δ::hphMX6 #4	452.3	9.047	4.707	1.92	2.28	DNA
hat1Δ::hphMX6 #5	4903.6	98.072	48.103	2.04	2.49	DNA
hat1Δ::hphMX6 #6	5071.8	101.436	49.612	2.04	2.51	DNA
hat1Δ::hphMX6 #7	4395.7	87.915	43.212	2.03	2.49	DNA
hat1Δ::hphMX6 #8	4369.5	87.389	42.976	2.03	2.49	DNA
hat1Δ::hphMX6 #9	77.6	1.553	0.919	1.69	0.82	DNA
rpd3Δ::hphMX6 #1	2836.7	56.733	28.832	1.97	2.03	DNA
rpd3Δ::hphMX6 #3	2104.7	42.094	21.016	2.00	2.48	DNA
rpd3Δ::hphMX6 #4	1648.7	32.973	16.565	1.99	2.44	DNA
***rpd3Δ::hphMX6* #5**	**5100.2**	**102.003**	**49.965**	**2.04**	**2.50**	**DNA**
rpd3Δ::hphMX6 #6	4118.5	82.370	40.396	2.04	2.54	DNA
rpd3Δ::hphMX6 #8	5202.5	104.05	51.092	2.04	2.49	DNA
set1Δ::hphMX6 #1	1722.2	34.444	17.379	1.98	1.94	DNA
set1Δ::hphMX6 #2	2579.0	51.579	26.261	1.96	2.04	DNA
set1Δ::hphMX6 #3	1364.1	27.283	13.884	1.96	2.57	DNA
set1Δ::hphMX6 #4	3477.6	69.552	34.620	2.01	2.54	DNA
set1Δ::hphMX6 #5	5297.7	105.955	51.868	2.04	2.49	DNA
set1Δ::hphMX6 #6	5547.6	110.952	54.555	2.03	2.52	DNA
***set1Δ::hphMX6* #7**	**6217.7**	**124.355**	**61.061**	**2.04**	**2.48**	**DNA**
set1Δ::hphMX6 #8	5595.3	111.905	54.818	2.04	2.51	DNA
set1Δ::hphMX6 #9	6048.9	120.977	59.087	2.05	2.51	DNA
set2Δ::hphMX6 #1	84.1	1.681	1.109	1.52	0.52	DNA

set2Δ::hphMX6 #2	2677.1	53.542	27.299	1.96	1.99	DNA
set2Δ::hphMX6 #3	2582.2	51.644	25.943	1.99	2.49	DNA
set2Δ::hphMX6 #4	1881.8	37.637	18.911	1.99	2.56	DNA
set2Δ::hphMX6 #5	6148.9	122.978	60.501	2.03	2.50	DNA
***set2Δ::hphMX6* #6**	**4723.7**	**94.474**	**46.338**	**2.04**	**2.51**	**DNA**
set2Δ::hphMX6 #7	4597.3	91.945	45.097	2.04	2.56	DNA
set2Δ::hphMX6 #8	5228.8	104.577	51.016	2.05	2.54	DNA
***set2Δ::hphMX6* #9**	**4299.4**	**85.989**	**42.079**	**2.04**	**2.54**	**DNA**
set2Δ::hphMX6 #10	4733.8	94.676	46.214	2.05	2.55	DNA
snf2Δ::hphMX6 #1	3142.3	62.847	32.205	1.95	2.08	DNA
snf2Δ::hphMX6 #2	2282.4	45.649	23.716	1.92	1.90	DNA
snf2Δ::hphMX6 #3	891.2	17.825	9.181	1.94	2.35	DNA
snf2Δ::hphMX6 #4	1513.4	30.268	14.779	2.05	2.69	DNA
snf2Δ::hphMX6 #5	5454.9	109.097	53.874	2.03	2.49	DNA
snf2Δ::hphMX6 #6	10.2	0.203	0.115	1.76	0.61	DNA
snf2Δ::hphMX6 #7	5224.8	104.496	51.055	2.05	2.55	DNA
snf2Δ::hphMX6 #8	5426.8	108.535	53.198	2.04	2.55	DNA
snf2Δ::hphMX6 #10	2898.8	57.976	28.741	2.02	2.42	DNA
dot1Δ::hphMX6 #1	1513.4	30.268	15.875	1.91	1.65	DNA
dot1Δ::hphMX6 #2	2747.3	54.946	27.241	2.02	2.56	DNA
dot1Δ::hphMX6 #3	2025.5	40.509	20.270	2.00	2.51	DNA
dot1Δ::hphMX6 #4	75.4	1.509	0.878	1.72	1.06	DNA
***dot1Δ::hphMX6* #5**	**2943**.0	**58.861**	**29.097**	**2.02**	**2.39**	**DNA**
dot1Δ::hphMX6 #6	2031.8	40.636	20.115	2.02	2.50	DNA
***dot1Δ::hphMX6* #7**	**2611.9**	**52.238**	**25.954**	**2.01**	**2.39**	**DNA**
dot1Δ::hphMX6 #8	2435.7	48.715	24.257	2.01	2.37	DNA
dot1Δ::hphMX6 #9	27.3	0.547	0.294	1.86	1.19	DNA
dot1Δ::hphMX6 #10	1671.8	33.437	16.748	2.00	2.33	DNA
rtt109Δ::hphMX6 #1	2581.4	51.628	26.364	1.96	1.94	DNA
rtt109Δ::hphMX6 #2	2815.5	56.311	28.901	1.95	2.08	DNA
rtt109Δ::hphMX6 #3	2879.5	57.59	28.852	2.00	2.48	DNA
rtt109Δ::hphMX6 #4	3521.2	70.424	35.323	1.99	2.51	DNA
rtt109Δ::hphMX6 #6	241.5	4.831	2.523	1.92	1.91	DNA
rtt109Δ::hphMX6 #7	955.7	19.115	9.767	1.96	2.27	DNA
***rtt109Δ::hphMX6* #8**	**1872.1**	**37.441**	**18.647**	**2.01**	**2.27**	**DNA**
rtt109Δ::hphMX6 #9	2766.4	55.328	27.759	1.99	2.31	DNA
rtt109Δ::hphMX6 #10	2754.0	55.079	27.629	1.99	2.31	DNA

Table 8. Nanodrop data from RNA extraction belonging to Figure 23.

Time point	Strain	ng/µl	A260 (Abs)	A280 (Abs)	260/280	260/230	Sample Type
tS	*CEN4**	59.0	1.474	0.665	2.22	1.26	RNA
		102.5	2.561	1.182	2.17	2.30	RNA
	CEN4	55.3	1.383	0.642	2.16	1.73	RNA
		89.0	2.224	1.026	2.17	1.76	RNA
	CEN4 rpd3Δ*	41.2	1.029	0.471	2.19	0.21	RNA
		60.1	1.502	0.688	2.18	0.93	RNA
	CEN4 dot1Δ*	50.9	1.272	0.576	2.21	1.72	RNA
		57.4	1.435	0.666	2.16	0.50	RNA
tS + β-E2	*cen4-*	68.8	1.720	0.786	2.19	0.61	RNA
		124.9	3.122	1.421	2.20	0.30	RNA
	CEN4	87.7	2.193	1.003	2.19	2.28	RNA
		126.0	3.150	1.455	2.16	2.18	RNA
	cen4- rpd3Δ	83.3	2.083	1.003	2.08	2.20	RNA
		51.2	1.279	0.583	2.19	0.65	RNA
	cen4- dot1Δ	56.7	1.417	0.654	2.17	1.44	RNA
		55.5	1.388	0.644	2.16	2.01	RNA
t120R	*cen4-*	134.6	3.365	1.550	2.17	2.33	RNA
		115.4	2.886	1.344	2.15	1.92	RNA
	CEN4	83.3	2.083	0.970	2.15	1.48	RNA
		60.6	1.515	0.700	2.16	0.85	RNA
	cen4- rpd3Δ	63.5	1.587	0.724	2.19	0.59	RNA
		92.0	2.300	1.071	2.15	2.31	RNA
	cen4- dot1Δ	80.7	2.017	0.926	2.18	2.32	RNA
		97.5	2.437	1.125	2.17	2.40	RNA

Table 9. Nanodrop data from RNA extraction belong to Figure 24.

Time point	Strain	ng/µl	A260 (Abs)	A280 (Abs)	260/280	260/230	Sample Type
tS	*CEN4**	145.3	3.632	1.665	2.18	1.73	RNA
		125.2	3.129	1.443	2.17	1.43	RNA
	CEN4	100.1	2.502	1.147	2.18	1.80	RNA
		110.8	2.771	1.269	2.18	1.72	RNA
	CEN4 set1Δ*	101.7	2.542	1.180	2.15	1.39	RNA
		124.8	3.120	1.445	2.16	2.16	RNA
	CEN4 set2Δ*	126.1	3.153	1.436	2.20	1.95	RNA
		112.1	2.804	1.289	2.18	2.26	RNA
tS + β-E2	*cen4-*	152.1	3.802	1.734	2.19	1.38	RNA
		149.7	3.743	1.716	2.18	1.93	RNA
	CEN4	162.3	4.059	1.864	2.18	2.05	RNA
		252.8	6.319	2.896	2.18	2.23	RNA
	cen4- set1Δ	150.5	3.763	1.723	2.18	1.53	RNA
		129.4	3.236	1.476	2.19	0.55	RNA
	cen4- set2Δ	124.0	3.100	1.437	2.16	1.76	RNA
		124.9	3.124	1.439	2.17	1.86	RNA
t120R	*cen4-*	197.2	4.930	2.270	2.17	1.97	RNA
		143.3	3.584	1.657	2.16	1.72	RNA
	CEN4	113.3	2.831	1.301	2.18	1.73	RNA
		135.7	3.392	1.540	2.20	1.35	RNA
	cen4- set1Δ	141.7	3.543	1.634	2.17	2.16	RNA
		172.2	4.305	1.984	2.17	2.02	RNA
	cen4- set2Δ	80.5	2.013	0.935	2.15	1.57	RNA
		99.5	2.487	1.149	2.16	1.90	RNA

Table 10. Nanodrop data from RNA extraction belonging to Figure 25.

Time point	Strain	ng/µl	A260 (Abs)	A280 (Abs)	260/280	260/230	Sample Type
tS	*CEN4**	70.1	1.753	0.783	2.24	1.73	RNA
		86.8	2.170	0.978	2.22	0.97	RNA
	CEN4	89.4	2.235	0.996	2.24	0.43	RNA
		88.3	2.207	0.993	2.22	1.69	RNA
	CEN4 sas3Δ*	106.3	2.657	1.182	2.25	0.50	RNA
		145.7	3.642	1.655	2.20	2.04	RNA
	CEN4 rtt109Δ*	157.1	3.927	1.785	2.20	1.67	RNA
		156.0	3.900	1.757	2.22	2.02	RNA
tS + β-E2	*cen4-*	179.0	4.474	2.003	2.23	0.96	RNA
		146.9	3.674	1.630	2.25	1.08	RNA
	CEN4	156.3	3.906	1.781	2.19	2.30	RNA
		160.8	4.021	1.789	2.25	0.80	RNA
	cen4- sas3Δ	188.9	4.722	2.139	2.21	1.73	RNA
		225.0	5.625	2.544	2.21	1.67	RNA
	cen4- rtt109Δ	203.4	5.085	2.293	2.22	1.86	RNA
		187.3	4.683	2.105	2.22	1.58	RNA
t120R	*cen4-*	252.7	6.319	2.854	2.21	1.67	RNA
		205.3	5.132	2.318	2.21	2.33	RNA
	CEN4	127.8	3.195	1.441	2.22	1.87	RNA
		134.4	3.359	1.521	2.21	1.93	RNA
	cen4- sas3Δ	218.2	5.455	2.456	2.22	2.47	RNA
		210.1	5.253	2.382	2.21	1.62	RNA
	cen4- rtt109Δ	243.9	6.097	2.726	2.24	1.33	RNA
		192.0	4.801	2.176	2.21	2.46	RNA

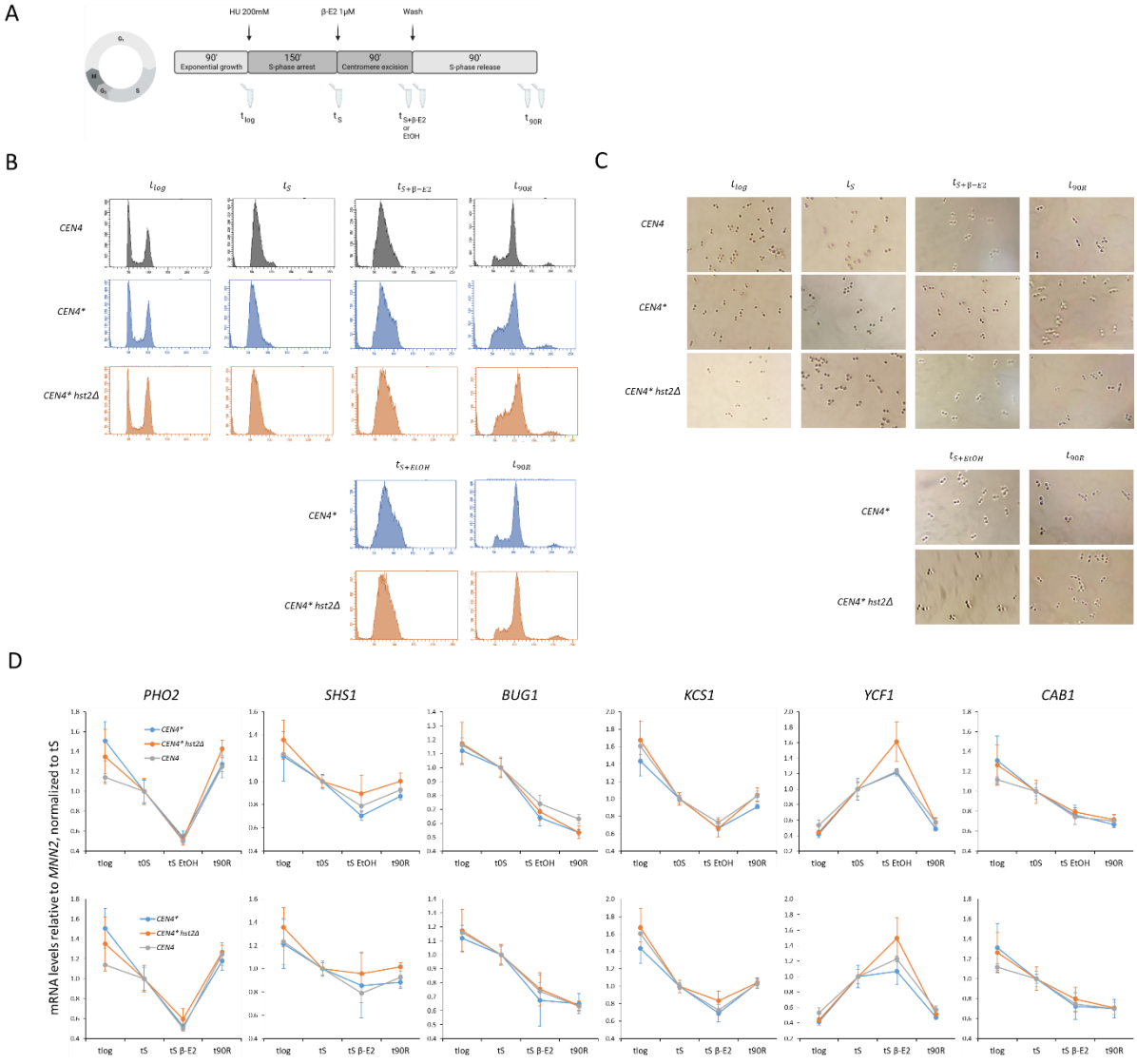

Figure 27. Centromere excision has no effect on gene expression at 90 min after release from S phase between *CEN4* and *CEN4 strains.**
A: Simple schematic of the *CEN4* excision during S phase arrest experiment introducing four cell collection time points. The cells were split after S phase arrest and EtOH was added to the CEN4* strains instead of β-estradiol as control. This experiment had three biological replicates for each strain.
B: Cell cycle analysis by flow cytometry for each time point and strain; *CEN4* (grey), *CEN4** (blue) and *CEN4* hst2Δ* (orange). Time points indicated on top and strain indicated on the left.
C: Light microscopy pictures from the same samples and indications as **B**.
D: RT-qPCR analysis of the expression of six selected genes from chromosome IV at different time points before- and after S phase arrest and release. The first two time points includes all cells, while upper panel shows data from the control experiment with ethanol, and lower panel show cells that were exposed to β-estradiol (centromere excision). Gene expression levels are shown relative to MNN2 and normalized to time point tS.

Three biological replicates of the strains *CEN4 CEN4** and *CEN4* hst2Δ* were collected for RNA extraction. Results from flow cytometry, microscopy and qPCR from **Figure 27** are from cells collected at time points t_{log}, t_S, $t_{S+\beta\text{-}E2}$ or t_{S+EtOH} and t_{90R} **(Figure 27 A)**. Flow

cytometry results (**Figure 27 B)** show asynchronous cells at t_{log} where the 1n left peak shows cells in G1 phase, the right peak shows 2n cells in G2/M phase and the signal from between the peaks belong to cells replicating its genome in S phase. Time points t_S, show cells arrested in S phase by an absence of the two peaks, and presence of a wider peak located in between. Cells collected at $t_{S+\beta\text{-}E2}$ and t_{S+EtOH} are arrested in later S phase, identified by the slight skew of the S phase peak towards the right side. Cells collected at t_{90R} show that most cells across strains are in S- and G2/M phase with a delay in *cen4-* strains compared to *CEN4*.

Microscope results (**Figure 27 C)** validate flow cytometry by also showing asynchronous cells across strains at $t_{log,}$ identified visually by the presence of single cells, budding cells and multiple cells stuck together during and after mitosis. Time point t_S, $t_{S+\beta\text{-}E2}$ and t_{S+EtOH} show phenotypic S phase arrested cells which includes budding, and the appearance of two cells visually stuck together which is more redundant at time points $t_{S+\beta\text{-}E2}$ and $t_{S+EtOH.}$ The phenotype of cells collected at t_{90R} are similar to the S phase arrested cells. Visually, it is not possible to distinguish late S- with G2/M phase by microscopy. Some cells also show signs of HU sensitivity, forming abnormal elongated cell shapes (**Figure 27 C,** *CEN4* at t_{90R}**).**

Results from qPCR (**Figure 27 D)** show relative gene expression of the six different genes from chromosome IV normalized to t_S in *CEN4*, *CEN4** and *CEN4* hst2Δ* strains. The results show small differences in expression between strains at $t_{log,}$ and a slight increase of expression in *CEN4* hst2Δ* at $t_{S+\beta\text{-}E2}$ and t_{S+EtOH} for the genes *SHS1* and *YCF1*, no significant differences of expression between strains, or treatments (upper vs lower panel) across time points. These results show that *CEN4* excision has no effect on chromosome IV gene expression at 90 minutes after S phase release.

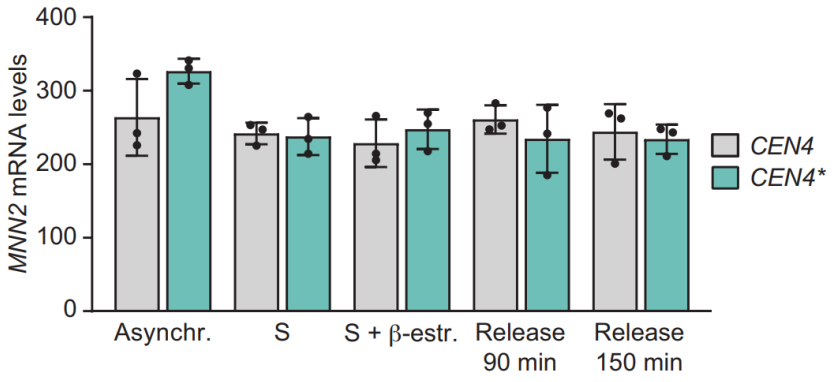

Figure 28 (Ramos Alonso et al., 2023). Expression of the control gene MNN2 during S phase and release experiments analyzed using RT-qPCR.

4 Discussion

This study aimed the identification of chromatin regulators involved in the maintenance of transcriptional homeostasis by centromeres and mitotic chromatin condensation in *Saccharomyces cerevisiae* by first; creating strains lacking genes of interest: *DOT1, HAT1, RPD3, RTT109, SAS2, SAS3, SET1, SET2* and *SNF2.* Second; using obtained deletion mutants, as well as *CEN4* hst2Δ* to test gene expression by qPCR before and after centromere excision. The results obtained are discussed below in detail.

4.1 Construction of deletion mutant strains

4.1.1 PCR cassette amplification efficiency

Initial PCR amplification of the *hph*-cassette intending to replace *SAS2, SAS3* and *SNF2* was not amplified (results not shown). After troubleshooting, 5% DMSO was added to the master mix (**Table 2)** during *hph*-cassette amplification and later genotyping. DMSO is known to relax supercoiled plasmids. It also aids in denaturing templates with high GC content. When DMSO was used, the annealing temperature was lowered as DMSO decreases the melting point of the primers. 10% DMSO can lower the melting point by 5-6°C and lead to more unspecific annealing (Obradovic et al., 2013). While the yield of the cassettes mentioned was lower, amplification was still successful and can be seen comparing lanes 1, 2 and 7 with other lanes in **Figure 13 B.**

4.1.2 Growth of transformed *CEN4** strains on selection plates

Transformation with the *HIS3*-cassette (**Figure 14 A**) yielded many colonies of various sizes, together with "streaks/smudges" looking like dead cells. Up to 5 big colonies were picked for gDNA isolation **(Table 7)** as they were considered most likely to have obtained the *HIS*3-cassette, although it may also be likely that a deletion mutant phenotype has a lower growth rate or viability than non-transformed cells. To get a cleaner plate with fewer colonies, the amount of *CEN4** cells was decreased from 10 to 5 OD_{600} for transformation with *hph*-cassette (**Figure 14 B**). This indeed provided a cleaner pate with fewer colonies, and up to 10 colonies were picked without discriminating by colony size, but rather limited by the number of colonies on each plate.

4.1.1 Unsuccessful verification of deletion mutants for *HAT1, SAS2* and *SNF2* by PCR

For verification of mutants, primer pairs 1 and 5 (**Figure 15**) were used in a PCR reaction with gDNA as a template from the possible mutants vs the untransformed *CEN4** as control, expecting being able to compare fragment sizes between transformed, and untransformed "WT" cells. However, *CEN4** gDNA was unsuccessfully amplified in all reactions and gDNA with mentioned primer pair was scarcely amplified overall (**Figure 18 & 19**). This may be due to long fragment lengths or gDNA fidelity. *SNF2*, a gene of 5112 bp is especially long and could explain difficulties in genotyping mutants with primer pairs 1 or 5 (gel not shown). Some genes were also approximately the same size as the cassette, thus preventing the distinction between wild-type and deletion strains (**Table 5,** red markings). For example, the calculated fragments for *CEN4* hat1Δ* (1705 bp)and *HAT1* (1904 bp) were too similar on the gel to distinguish compared to the ladder without a WT band (**Figure 19 A left**, lanes 1-4), preventing both positive and negative verification.

To circumvent these issues, different primer combinations were used, including primers binding inside the cassette, TEF promoter/terminators or flanking the gene (primer pair 2-4 and 6-7 from **Figure 15**). As these primers do not bind to *CEN4** gDNA template, it was not used as a control. There are multiple TEF promoters/terminators in the *S. cerevisiae* genome. However, unspecific amplifications should not produce mutant bands. Even so and for extra measure, mutants were only verified if either primer pair 2/3 and 4, or both 6 and 7 produced expected fragment lengths. This is why, again for the same populations of *CEN4* hat1Δ* in **Figure 17 A,** they were not verified as mutants since only templates with primer pair 7 produced calculated fragments in lane 3-6. *CEN4* snf2Δ* in **Figure 19 C** was not verified for the same reason. The gDNA template from *CEN4* sas2Δ* did not produce any bands (**Figure 16 A**,**Figure** 17 **A** and **C, Figure** 18 **B** and **C**) except for one band corresponding to WT in **Figure 18 A.**

In hindsight, it may have been better to use a lower concentration of template, as 100 ng template in a 50 µl reaction is in the upper recommended limit of 40-100 ng provided by Meridian Biosciences. One extra attempt to extract gDNA from *CEN4** could have yielded a higher fidelity template and possibly verified *CEN4* hat1Δ*.

In summary, deletion mutants for the genes *DOT1, RPD3, RTT109, SAS3, SET1* and *SET2* were obtained while deletion mutants for *HAT1, SAS2* and *SNF2* were not.

4.1.2 Growth assay shows conflicting results for *cen4- set2Δ*

Previous data from the Chymkowitch group shows that removal of *CEN4* (*CEN4** becoming *cen4-*) is detrimental to cell growth, and all *cen4-* cells eventually die. However, in **Figure 20 A** and **B** of this study, the growth results for two *cen4- set2Δ* mutants (yPC 56 and yPC 61) are contradictory as only one mutant rescues the phenotype of *CEN4*. This means that either, one; Cre-recombinase activity or expression was somehow lost in *CEN4* set2Δ::hphMX6* during transformation. Two; there was a contamination of *CEN4* in the *CEN4** culture used for transformation. Three; the samples were switched when doing the spot assay or genotyping. Lastly four; the insertion of the *hph-*, but not the *HIS3*-cassette rescues the fitness of *CEN4* control strain only in *set2Δ*. The latter would mean that the non-native *hph*-gene interferes with the pathway of chromosome condensation in mitosis through the lack of *SET2*, which is highly unlikely. It is possible that the *CEN4** culture used for transformation had contamination of *CEN4*, but a *CEN4* phenotype in other transformants on YPD+β-estradiol plates was not observed. The samples could have been switched during handling in the spot assay, but an earlier spot assay experiment shows the same result (not shown) and was redone because of bacterial contamination in the media. Flow cytometry as well as qPCR analysis (**Figure 24 B & D)** also shows a similar phenotype of *CEN4* set2Δ::hphMX6* to *CEN4*.

Only one deletion mutant for each genotype was chosen for the spot assays, which were done subsequently of the centromere-dependent gene expression experiments (**Chapter 3.2 A qPCR-based screen to identify chromatin regulators involved in centromere-regulated transcription in synchronized cells**). In hindsight, the spot assays should have been done in addition to the PCR-based approach (**Chapter 2.10 Verification of possible transformants**) as an extra verification step to ensure Cre-recombinase activity and mutant fidelity in advance of the centromere-dependent gene expression analysis experiments, as the fidelity of *CEN4* set2Δ::hphMX6* is currently not clear. Since the lab has two strains with this same genotype (yPC 61 & yPC 62 in **Table 6**), a spot assay with all mutants would provide clarity on this matter.

4.2 Centromere-regulated gene expression in synchronized cells

4.2.1 Experimental setup

As we are interested in the regulation of gene expression by the centromere and mitotic chromatin, and the cells need to undergo mitosis for the effects of centromere excision on gene expression to be observed (Ramos Alonso et al., 2023), it was decided to synchronize the cells before centromere excision to obtain results from cells at specific time points after *CEN4* excision. It was decided to arrest the cells as close as possible to when mitotic chromosome condensation occurs in anaphase. Nocodazole can be to arrest the cells in prometaphase, but it is not ideal since differences in gene expression would also be due to differences in mitotic entry between strains. Release from nocodazole arrest into the cell cycle is also proved more difficult than with hydroxyurea. As G2/M phase overlaps in *S. cerevisiae,* it was decided to use hydroxyurea to arrest the cells during S phase, then remove *CEN4* in obtained mutant vs control strains *CEN4* and *CEN4** to examine gene expression through mitosis.

Unexpectedly, results from a former experiment failed to show a difference in transcription between strains (**Figure 27, Chapter 3.3 Supplemental results)**. The cause was identified that 90 minutes were too short in the new lab environment for the effects of *CEN4* excision on gene expression to be detected (which caused the addition of time point t_{120R} in the experimental setup in **Figure 22)**. However, the experimental setup for identifying a relevant chromatin regulator is more promising since the setup includes additional control cultures where EtOH (as vehicle) is added instead of β-estradiol, thus preventing centromere excision from chromosome IV in *CEN4** strains. With this experimental setup, one could compare synchronized mutants with or without *CEN4* excision to obtain results more intently towards identifying promising chromatin regulators. The setups also included a time point for asynchronous cells, which shows the best baseline for transcription.

The reason these experimental setups were not utilized again was the construction of six different mutant strains (**Table 6**), which required a more effective setup where two mutants could be analyzed in parallel. A setup containing fewer time points and biological replicates was favored in a more screening-based approach with a prolonged waiting time of 150

minutes after S phase release (results in **Figure 23, Figure** 24 and **Figure** 25**).** The findings from this screening of mutants can aid in choosing the most promising chromatin regulators for a more extensive experimental setup to be done at a later stage.

4.2.2 t_S normalization

From litterature, all constructed deletion strains have proved to have smaller or bigger roles in DNA damage response except for Hst2 (Aricthota et al., 2022; Frigerio et al., 2023; Gershon & Kupiec, 2021; Zhang et al., 2013), which may have led to hydroxyurea disturbing gene expression in these mutants. Indeed, comparing overall data from t_S in **Figure 26** where gene expression of *CEN4** strains are normalized to *CEN4* instead of t_S, it seems like deletion mutant transcription is repressed compared to both *CEN4* and *CEN4**. Unexpectedly, *CEN4* excision seems to oppose this effect and lead to overall upregulation of transcription compared to arrested *cen4-* ($t_{S+\beta\text{-}E2}$) except for *set2Δ*. Since t_s was used as the transcriptional baseline, mutants may show a synthetic elevated gene expression in t_{150R} (**Figure 23 D, Figure** 24 **D** and **Figure** 25 **D**).

4.2.3 Promiscuous deacetylation by Rpd3

As mitotic condensation is a highly situation-dependent event, it is plausible to hypothesize that the event is triggered by a more residue-specific histone modulator. However, despite the relatively broad specificities, they do have distinct site preferences. For example, the HDACs Rpd3 and Hos2 are both required in vivo for deacetylation of H4 at sites K5, K8 and K12, but both also deacetylate other residues isolated from each other. This interplay in regard to mitotic chromosome condensation may be important and is worth investigating. However, promiscuous histone modulators are also often essential to the cell, making pure deletion strains not viable and would require more complex strain construction methods which is not appropriate for this thesis. Rpd3 has a role in transcriptional repression of actively transcribed genes during elongation, in transcriptional silencing, nucleosome assembly, and is also found at DSBs during DDR (Carrozza et al., 2005; Ehrentraut, 2010; Kishkevich et al., 2019; Tompa & Madhani, 2007; Zhou et al., 2009).

Unfortunately, results from qPCR data belonging to *cen4- rpd3Δ* (**Figure 23 D**) proved to have big differences in gene expression between the biological replicates compared to all the other mutants in all tested genes except for *YCF1*. When looking at RNA quality/quantity data

in **Table 8**, some of the samples have a low ratio for 260/230 absorption indicating contamination most likely from guanidine thiocyanate as it is used in high concentrations in the lysis buffer for RNA extraction. Multiple studies link Rpd3 to environmental stress response (McDaniel & Strahl, 2013; Ruiz-Roig et al., 2010), responding to such stress signals through a positive feedback-loop together with a combination of centromere excision and DNA damage caused by hydroxyurea could explain differences in the two cell cultures.

4.2.4 Cell cycle progression in *cen4-* cells

From previous work from the Chymkowitch group and this study, flow cytometry data from *cen4-* cells show a delay in cell cycle progression compared to WT in synchronized cells. This is most likely due to factors described earlier, such as aneuploidy, erratic transcription, and loss of transcriptional homeostasis in *cis* causing a stress response from chromosomes in *trans* (Kruitwagen et al., 2018; Ramos Alonso et al., 2023).

cen4- rpd3Δ & *cen4- set2Δ*

From literature, the mutants *rpd3Δ* as well as *set2Δ* cells undergo a more rapid S phase progression than WT because of earlier Cdc45 binding among others, while *rpd3Δ* also enter S phase more quickly (Kishkevich et al., 2019). Interestingly, flow cytometry for *cen4- rpd3Δ* cells supports the combined findings by showing a more rapid cell cycle progression than the other *cen4-* strains while still having a delay compared to *CEN4* seen in **Figure 23 B.** From literature, it is known that *set2Δ* cells have a 15 minute delay in the release from G1 into S phase, exiting S phase 15 minutes faster than WT while G2/M phase progression appears to be normal (Dronamraju et al., 2018). Flow cytometry results for *cen4- set2Δ* (**Figure 24 B**) have a minor difference showing a slightly lower peak in G1, but this could be both a delay or faster progression compared to WT and cannot be determined without analysing more time points.

cen4- rtt109Δ

The biggest difference in cell cycle progression can be seen in *cen4- rtt109Δ* (**Figure 25 B)** with the mutant showing a big delay, or arrest in G2/M phase. Rtt109 is highly important for the incorporation of newly synthesized histones during S phase, directionality of the replication fork and for turning off the DNA damage checkpoint following DNA repair (Chen

et al., 2008; Frenkel et al., 2021; Frigerio et al., 2023; Gershon & Kupiec, 2021). Cells lacking Rtt109 are incapable of reassembling chromatin following a DSB repair, which means that the DNA damage checkpoint remains active, causing the delay into G2/M. However, the peak is skewed excessively to the right, and far exceeds the G2/M phase peak in the other strains. This data suggest that the cells contain more than 2n genomes and could be explained by lacking of replication fork directionality and increased replication fork velocity leading to *rtt109Δ* cells having ~100% longer replicons (Frenkel et al., 2021).

4.2.5 *cen4- rtt109Δ* expression levels exceeds those of *cen4-*

As mentioned in above paragraph, Rtt109 is substantially important for the S phase progression. qPCR results shown in **Figure 25 D** shows gene expression exceeding *cen4-* at both time points $t_{S+\beta E2}$ and t_{150R} in all genes except for *YCF1*.

A possible explanation could be that first; *rtt109Δ* cells are found to produce 100% longer replicons. Normally, transcription levels remain stable due to replication-dependent factors that suppress transcription in replicated DNA. But in *rtt109Δ* lacking H3K56 acetylation, transcriptional homeostasis is lost due to an increase in DNA template (Bar-Ziv et al., 2020; Voichek et al., 2016; Voichek et al., 2018). Even though excess template is not the cause of elevated gene expression in *cen4-* cells (Ramos Alonso et al., 2023), the combined loss may lead to repressive signals being lost in *cen4- rtt109Δ*. Second; a delay in cell cycle progression could also explain the higher expression levels. Though it is hard to identify the cell cycle stage at t_{150R} in **Figure 25 B**, from literature describing *rtt109Δ* mutants, *cen4- rtt109Δ* is likely stuck at S phase interphase while both *cen4-* and *CEN4* proceeds. Meaning, more *cen4-* and *CEN4* cells are likely in interphase, so qPCR data are not from strains in the same cell cycle stage. Lastly, without an un-excised strain of *rtt109Δ* for comparison, the increased transcription could also be from a stress response due to hydroxyurea, which is known to cause strand-breaks in DNA especially during S phase. These effects might follow the cell when it proceeds in the cell cycle regardless of centromere function. Nonetheless, this mutant has shown the highest gene expression in comparison to *cen4-* (**Figure 25 D** & **Figure 26),** and should be examined further as a possible regulator of centromere-dependent gene expression.

4.2.6 Hst2 and Set2 mutants rescue the gene expression of *CEN4* cells

Hst2 mutants have a globally relaxed chromatin

The sirtuin Hst2 share a strong sequence identity with Sir2, and it is fascinating that it helps propagate the condensation signal from the centromere, while Sir2 helps propagating the condensation signal from telomeres. Contrary to Sir2, Hst2 is actively transported to- and localized in the cytoplasm but is recruited to the centromere during mitotic chromosome condensation, though the exact mechanism for nuclear transport remain unknown (Jain et al., 2021; Kruitwagen et al., 2018; Kruitwagen et al., 2015; Ramos Alonso et al., 2023). Contrary to the Rtt109 mutant, gene expression in *cen4- hst2Δ* (**Figure 22 D & Figure 26**) is lower than both *cen4-* and *CEN4* strains after *CEN4* excision and release from S phase.. However, since Hst2 facilitate chromosome condensation, all chromosomes fail to condense properly in *CEN4* hst2Δ*, meaning that chromosome IV is more open and accessible both before- and after centromere excision preventing differences in gene expression from *CEN4* hst2Δ,* becoming *cen4- hst2Δ* after excision. Though, recent findings from our group supports another explanation; that all free RNAPII mobilizes to global accessible chromatin, thus preventing excessive transcription in chromosome IV because of RNAPII shortage (Ramos Alonso et al., 2023). This might explain why we do not see the expected increase in gene expression in the *cen4- hst2Δ* mutant even though the mutant has an open and accessible chromatin.

Set2 might contribute to centromere-dependent gene expression independently of its canonical functions

Set2 is a transcriptional elongation factor responsible for H3K36 methylation, which is known to recruit the HDAC complex Rpd3S to chromatin to repress cryptic transcription initiation. Set2's significance during the cell cycle and mitosis is upheld by several facts. Firstly, it is a well-known regulator of genes associated with the cell cycle. Secondly, Set2 levels and the corresponding H3K36me3 deposition rise during G2/M phase and decrease during G1/S phase. Finally, Set2 is targeted for degradation by the APC/C/Cdc20 complex after mitosis (Dronamraju et al., 2018).Besides this, another study found that H3K36me also plays a distinct role in preventing the erroneous spread of silencing from heterochromatin into flanking euchromatin. The absence of Set2 causes a significant decrease in the expression of genes located within 20 kb of telomeres and is independent of Rpd3, the only known effector

of H3K36 methylation (Carrozza et al., 2005; Dronamraju et al., 2018; Tompa & Madhani, 2007).

Looking at transcription levels (qPCR results, **Figure 24 D** & heatmap **Figure 26**), the *cen4-set2Δ* mutant unexpectedly rescued *CEN4* transcription levels in all genes except for a partly rescue of *SHS1*. As for transcriptional silencing, there has been reported increased transcriptional silencing in *set2Δ* mutants. This corresponds to the observed decrease in gene expression in *cen4- set2Δ* compared to *cen4- (***Figure 24 D** & **Figure 26)**. However, the silencing is limited within ~20 Kb of telomeres, which is only about ~5% of the *S. cerevisiae* genome. This makes it unlikely to have such a big impact on gene repression alone, which means that if this hypothesis is true, another unknown centromere-dependent factor boosts the transcriptional silencing in *cen4- set2Δ* cells during mitosis.

Then, could the canonical function of repressing cryptic transcription be an explanation? Rpd3 is known to work downstream of Set2's signal. Another look at the results from *cen4-rpd3Δ* in **Figure 23 D,** overall expression does not seem to be significantly higher compared to *cen4-*, and the phenotype is not as distinct as for *cen4- set2Δ* even when having deacetylation targets on all four core histones. This makes it unlikely that they exist in the same signal pathway. It also seems contra intuitive that increased cryptic transcription levels, which leads to decreased transcriptional fidelity in publications, on the other hand aids in centromere-dependent transcriptional reset of interphase expression. Also, as up to 90% of genes are silenced in mitosis, there are simply not many ORFs for Set2/Rpd3 to silence. However, this causes a form of specificity to cryptic transcripts from these genes. Interestingly, studies have found that proper levels of centromeric noncoding RNA is required for centromere activity and is induced in S phase. Meaning that noncoding RNAs like cryptic transcripts also can improve centromere function at certain times (Ling & Yuen, 2019).

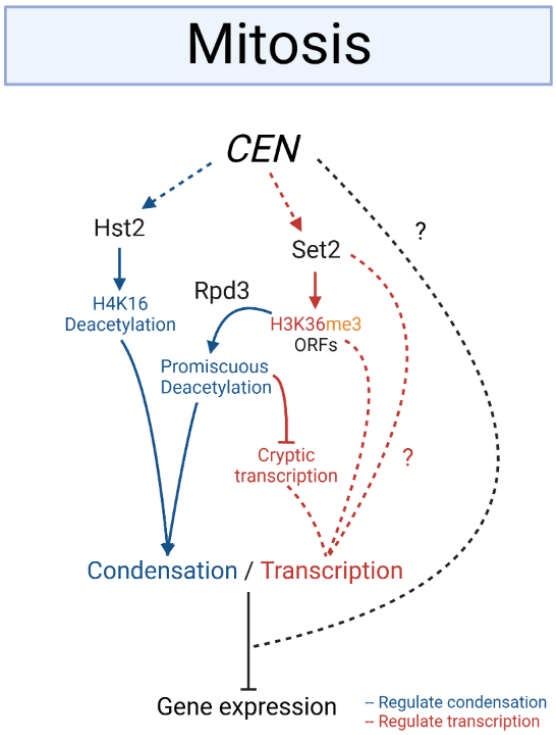

Figure 29. Scheme depicting interactions of chromatin modulators contributing to centromere-dependent gene expression. Parallel pathways of gene regulation by condensation (blue) and transcription (red). The centromere (*CEN*) recruits Hst2 which facilitate chromosome condensation and gene expression by its H4K16 deacetylation activity, and the centromere activates HMT Set2 which deposits marks on H3K36 on ORFs. H3K36me3 is either recognized by Rpd3 which aid in chromosome condensation via its promiscuous deacetylation activity, or Set2 regulates transcription dependently or independently of deposited chromatin marks.

In conclusion, the centromere may regulate transcription through several pathways **(Figure 29)**; the centromere recruits Hst2, which aids in chromosome condensation by deacetylating H4K16, propagating the signal to chromosome arms. It may also trigger a parallel pathway for the activation of Set2 on the CTD-tail of RNAPII, which tri-methylates H3K36. This marker is recognized by HDAC Rpd3's bromodomain, further leading to deacetylation and silencing of ORFs through condensation or repression of cryptic transcripts. However, both of these hypotheses seem unlikely since *cen4-rpd3Δ* does not express a distinct phenotype. In conclusion, gene expression may be regulated by Set2 dependently or independently of H3K36 methylation marks through a yet unknown factor.

5 Summary of findings and future perspectives

After recent findings from the Chymkowitch group that the centromere licenses the mitotic condensation of yeast chromosome arms in *cis*, and later that this condensation safeguards transcriptional homeostasis during interphase, many of the upstream and downstream factors remain unknown.

Focusing on histone acetylation and methylation, the first part of this project intended the creation of yeast strains lacking genes coding nine chromatin regulators of interest: *DOT1, HAT1, RPD3, RTT109, SAS2, SAS3, SET1, SET2* and *SNF2.* Employing the innate homologous recombination machinery in *S. cerevisiae*, I successfully transformed and created six deletion mutant strains equipped with loxP sites flanking the centromere of chromosome IV. Secondly, using the centromere excision assay as a tool, I carefully analysed chromosome IV gene expression in synchronized cells between *CEN4* and *cen4-* strains in a screening-based approach by qPCR to discover if any of my deletion mutants could be a factor in mitotic chromosome condensation and transcriptional homeostasis.

Indeed, the work from this thesis identified a possible role of histone methyltransferase Set2, which most likely aid the centromere in transcriptional homeostasis via a yet unknown factor. Though, Set2 may also regulate this directly dependently or independently by its H3K36 methyltransferase activity in another pathway. This thesis also identified the acetyltransferase Rtt109 and the deacetylase Hst2 as potential regulators of transcriptional homeostasis. However, there is a direct link between Rtt109 and Hst2 with replication and mitotic condensation of chromosomes, respectively. This will most likely render their investigation more complicated than the one of Set2

In the future, a similar but more extensive experiment with more biological replicates should be done with and without *CEN4* excision on deletion mutants for Set2, Hst2, Rtt109 and Rpd3 with asynchronous cells as a baseline for gene expression. Additional experiments investigating Set2 and Rpd3 could be ChIPseq of the H3K36me3 mark deposited by Set2, or

the protein Rpd3 in *CEN4* cells to see whether it increases at mitosis entry, or ChIPseq in *cen4-* cells expecting a failed recruitment of Set2, H3K36me3 and Rpd3S at mitosis.

These experiments could shed new light on the mechanisms maintaining transcriptional memory during mitosis and maintain transcriptional homeostasis at mitosis exit. Finally, future work will continue investigating how, a single locus, the centromere, regulates gene expression.

Appendix A: Abbreviations

Abbreviation	Definition
5mC DNA	5-methylcytosine DNA
APC/C	Anaphase-promoting complex/cyclosome
ADP	Adenosine diphosphate
ATP	Adenosine triphosphate
BAH	Bromo adjacent homology
CDKs	Cyclin-dependent kinases
CenH3	Centromeric histone H3
ChIPseq	Chromatin immunoprecipitation sequencing
COMPASS Complex	Complex of Proteins Associated with Set1
Cre-EBD	Cre recombinase-estradiol binding domain
CTD	Carboxy-terminal domain
DDR	DNA Damage Response
DMSO	Dimethyl sulfoxide
DNA	Deoxyribonucleic acid
dNTPs	Deoxyribonucleoside triphosphates
DSB	Double-strand break
dsDNA	Double-stranded DNA
FSC	Forward Scatter
gDNA	Genomic DNA
GTFs	General transcription factors
HATs	Histone acetyltransferases
HDACs	Histone deacetylases
HDMs	Histone demethylases
HMTs	Histone methyltransferases
HO Pathway	Homothallic switching endonuclease pathway
HPTMs	Histone post-translational modifications
HU	Hydroxyurea
MCC	Mitotic checkpoint complex
mRNA	Messenger RNA
ncRNA	Non-coding RNA
NFR	Nucleosome-free region
NHEJ	Non-homologous end joining
OAADPr	O-acetyl-ADP-ribose
OD	Optical density (spectrophotometer)
O/N culture	Overnight culture
ORF	Open reading frame
PCR	Polymerase Chain Reaction
PEG	Polyethylene glycol
PHD finger	Plant homeodomain finger
PIC	Preinitiation complex

qPCR	Quantitative polymerase chain reaction
RNA	Ribonucleic acid
RNAPII	RNA polymerase II
RNAseq	RNA sequencing
RNR	Ribonucleotide reductase
RT	Reverse Transcription
SAC	Spindle assembly checkpoint
SDS	Sodium Dodecyl Sulfate
SGD	Saccharomyces Genome Database
SPB	Spindle pole body
SSB	Single-strand break

Appendix B: Materials

Products	Producer	Cat. Number	Purpose
Agarose	VWR Life Science	35-1020, 21k104130	Gel electrophoresis
BioSpec Glass beads	Cole Parmer®	11079105	gDNA/RNA extraction
Ethanol (EtOH)	Provided by UiO	-	
Glycerol	Provided by UiO	21071516	Strain storage
Hydroxyurea	Sigma	H8627	S phase arrest
Proteinase K	Thermo Fisher	01147725, 01140450	Flow cytometry
RNAse A	Sigma	R5503-1G	gDNA/RNA extraction, Flow cytometry
Sodium Acetate (NaOAc)	Provided by UiO	-	Concentrate DNA
ssDNA (from salmon sperm)	Sigma	D7656	Transformation
SYBR™ Safe DNA Gel Stain	Invitrogen	S33102	Gel electrophoresis
Sytox green	Invitrogen	S7020	Flow cytometry
TriTrack DNA Loading Dye (6X)	Invitrogen	R1161	Gel electrophoresis
β-estradiol	Sigma	E8875	Centromere excision
β-Mercaptoethanol	Sigma	M3148	RNA extraction

Kits	Producer	Cat. No.	Purpose
BIOTAQ™ PCR kit	Meridian Bioscience™	PL313-B101870	PCR
HOT FIREPol® EvaGreen® qPCR Supermix	Solis Biodyne	08360640.2	qPCR
NucleoSpin Plasmid (NoLid), Mini kit	MACHEREY-NAGEL	740499.5	Plasmid purification
QuantiTect® Reverse Transcription Kit	Qiagen	205311	RT
RNeasy Mini Kit	Qiagen	74004	RNA extraction

Ingredients for Appendix D	Producer	Cat. No.	Purpose
0.5 M EDTA pH 8.0	Invitrogen	1757715	
Agar	VWR Life Science	18E2256629	
Ammonium acetate 4M	Provided by UiO	-	gDNA extraction
Complete supplement mixture (CSM) Drop-Out: -HIS (CSM-His media)	Formedium	DCS0079	
Glucose-Monohydrate	Merck	K33094542442	
LiAc 1 M	Provided by UiO	-	
NaCl 5 M	Provided by UiO	20082804	
PEG 3350 50%	Provided by UiO	-	
Peptone	Formedium Ltd.	PEP03	
SDS 20%	Thermo Fisher	00691367	

Sodium citrate 0.5 M	Provided by UiO	-	Flow Cytometry
TRIS 1 M pH 8.0	Provided by UiO	20060305	
Triton X-100	Sigma	STBJ7636	
Yeast extract powder	Formedium Ltd.	YEA03	
Yeast Nitrogen Base W/O Amino Acids	Sigma-Aldrich	Y0626-250g	

Buffers	Producer	Cat. No.	Purpose
Tris-Acetate-EDTA (TAE) X 50	Provided by UiO	21041411	Gel electrophoresis
0.1M LiAc/1x TE	Appendix D	-	Transformation
1X TE (Tris-HCl pH 8.0 10mM, EDTA 1mM)	Appendix D	-	Transformation, gDNA extraction
40% PEG 3350/0.1M LiAc/1x TE	Appendix D	-	Transformation
lysis buffer (Triton X-100 2%, SDS 1%, NaCl 100mM, Tris-HCl pH 8.0 10mM)	Appendix D		gDNA extraction
phenol:chloroform:isoamyl alcohol (25:24:1) saturated with (1x TE;) Tris-HCl pH 8.0 10mM and EDTA 1mM	Sigma	BCCG3703	gDNA extraction

Oligonucleotides*	Producer	Purpose
SAS2-F1 (-53)	CCTATTTTCTAGTTGCTTTTGTTTTCACTCGCAAAAAAA**CGGATCCCCGGGTTAATTAA**	For cassette construction Markings: *GENE-F/R (:± bp primer annealing sites from start/end of ORF) (**Bold** = sequence specific to plasmid)
SAS2-R1 (+30)	TGAAATACATATGCCATTAAGTTACATCCTGAATAGATTC**GAATTCGAGCTCGTTTAAAC**	
SAS3-F1 (-53)	TTCCTTCTTCATTAATTAGTCTCCGTATAATTTGCAGATA**CGGATCCCCGGGTTAATTAA**	
SAS3-R1 (+30)	TACATGTATATGCTTATATCCAATATATACCCATCGCCGC**GAATTCGAGCTCGTTTAAAC**	
HAT1-F1 (-53)	AAATTATGCTTAAGCTATAACTATAGTGAGAATCAAGAAT**CGGATCCCCGGGTTAATTAA**	
HAT1-R1 (+30)	GTTAAACAAATAAATATGTTATTATATATTTAATAAACAG**GAATTCGAGCTCGTTTAAAC**	
RPD3-F1 (-53)	CATACAAAACATTCGTGGCTACAACTCGATATCCGTGCAG**CGGATCCCCGGGTTAATTAA**	
RPD3-R1 (+30)	TCACATTATTTATATTCGTATATACTTCCAACTCTTTTTT**GAATTCGAGCTCGTTTAAAC**	
SET1-F1 (-53)	TATTTGTTGAATCTTTATAAGAGGTCTCTGCGTTTAGAGA**CGGATCCCCGGGTTAATTAA**	
SET1-R1 (+30)	TGTTAAATCAGGAAGCTCCAAACAAATCAATGTATCATCG**GAATTCGAGCTCGTTTAAAC**	
SET2-F1 (-53)	TCAAACCTTTCTCCTTTCCTGGTTGTTGTTTTACGTGATC**CGGATCCCCGGGTTAATTAA**	
SET2-R1 (+30)	GAAAACGTGAAACAAGCCCCAAATATGCATGTCTGGTTAA**GAATTCGAGCTCGTTTAAAC**	
SNF2-F1 (-53)	ACTTTCTGCTATTTTCACGACTTTCGATTAATTATCTGCC**CGGATCCCCGGGTTAATTAA**	

SNF2-R1 (+30)	CGTATAAACGAATAAGTACTTATATTGCTTTAGGA AGGTA**GAATTCGAGCTCGTTTAAAC**	
DOT1-F1 (-53)	CCAGTAATTGTGCGCTTTGGTTACATTTTGTTGTAC AGTA**CGGATCCCCGGGTTAATTAA**	
DOT1-R1 (+30)	TAGTTATTCATACTCATCGTTAAAAGCCGTTCAAAG TGCC**GAATTCGAGCTCGTTTAAAC**	
RTT109-F1 (-53)	GTAGAGTTAAAAGGTCAATTCAACCGGTCTTCAAT AAGAC**CGGATCCCCGGGTTAATTAA**	
RTT109-R1 (+30)	ATGCTACATACGTGTACTAAATAATAAATATCAATA TGTA**GAATTCGAGCTCGTTTAAAC**	
SAS2-F2(-213)	TTCGGAACACCCAATCATCA	Gene deletion check Markings: *GENE-F/R (:± bp primer annealing sites from start/end of ORF)
SAS2-R2(+328)	AGGTTTCCTTTATGCCCTTACC	
SAS3-F2(-293)	TAGTCAAACGTTCAGGCCAA	
SAS3-R2(+263)	GAGCAAGATGAACTTCCAGGTATAA	
HAT1-F2(-436)	GCTCGCTATTGTGTTTCTTGG	
HAT1-R2(+144)	CAACATAACGGCTTCAACCTTTG	
RPD3-F2(-273)	ATGAAGCGGTGAGAGCTAAT	
RPD3-R2(+340)	TCATTTACCCAGGCGTGATTAT	
SET1-F2(-245)	GAAGAGAAGCGTGAGGAGTG	
SET1-R2(+321)	GAATGCTGTCGGTAGCCTAAA	
SET2-F2(-289)	ACCGCTTAGAATACCTCACAC	
SET2-R2(+166)	AGCCCACTAATGCGGATATTT	
SNF2-F2(-173)	CTGAGGCGGTAGGACAATAAG	
SNF2-R2(+91)	CCAACTCGGTTAATGGGTACAA	
DOT1-F2(-99)	GGGCATCTCGTCGTCTTAAT	
DOT1-R2(+263)	CTCTGCCTCCTCCTTCAATTAT	
RTT109-F2(-127)	TTTCGTGTTCGCGTTGTAAG	
RTT109-R2(+223)	CCAACCTGAGCAGTAGAGTAAA	
His3MX6-F1 (-491)	GACGAAGCTCTTTCTAGAAGCG	
TermTEF-F (-85)	CGACATCATCTGCCCAGAT	
TEFprom-R (+74)	GGGCGACAGTCACATCAT	
His3MX6-R (+434)	CTCTTCAGGTAAGGGAGCT	
His3MX6-F2 (-261)	CGCGGCTACTAGTCTTACT	
hphMX6-R (+396)	CGATCAGAAACTTCTCGACAGAC	
hphMX6-F (-272)	GGGCGACAGTCACATCAT	
MNN2-F(:1103)	GGCTACGGCTCTTCTATCT	For qPCR Markings: *GENE-F/R (:bp, primer annealing sites from start of ORF, incl. primer length)
MNN2-R(:1197)	CTTATCACCTTCACCAGCAG	
KCS1-F (:2313)	CCTTGTGCACTGGATCTAAA	
KCS1-R (:2427)	GCCTAAACGCCTAGAAGTG	
CAB1-F (:425)	CATGGACTCAAAGGCTATCTAC	
CAB1-R (:533)	GAAGAACCGCCTACTCTACTA	
YCF1-F (:4389)	CATCGCGCATAGACTGAAC	
YCF1-R (:4486)	TAATAACTGGCCCGGAGAG	
SHS1-F (:1351)	CCAGAGCGTACCAAGTTAAG	
SHS1-R (:1457)	ACTGGGCCTCTAACTCTTC	
BUG1-F(:680)	CTGTCGATGACCTACAGGAT	

BUG1-R(:816)	CTTGCTGCCTTAGCTTCTG
PHO2-F(:1014)	GCTAACAGTCACCAGATCAC
PHO2-R(:1143)	GCGTCATTTACCTGTCTACC

Appendix C: Strains and plasmids

ID	Genotype	Source
E. coli		
pPC57 *(E.coli)*	*pFA6a-hphMX6 (AmpR)*	Jorrit Enserink Lab
Plasmids		
	pFA6a-His3MX6	Pierre Chymkowitch Lab (this project)
	pFA6a-hphMX6	Sandra Lopez-Aviles lab
S. cerevisiae		
yPC8 (CEN4 or cen4-)*	*MATa lox-CEN4-lox:KanMX GDP-creEBD78:LEU2 his3Δ1 leu2Δ0 ura3Δ0 met15Δ0*	Yves Barral Lab
yPC11 (CEN4)	*MATa ura3::GDP-creEBD78:LEU2 his3Δ1 leu2Δ0 ura3Δ0 met15Δ0*	
yPC28 (hst2Δ CEN4 or cen4-)*	*MATa hst2::KanMX lox-CEN4-lox:KanMX GDP-creEBD78:LEU2 his3Δ1 leu2Δ0 ura3Δ0 met15Δ0*	
yPC55 (set1Δ CEN4 or cen4-)*	*MATa set1::His3MX6 lox-CEN4-lox:KanMX GDP-creEBD78:LEU2 his3Δ1 leu2Δ0 ura3Δ0 met15Δ0*	Pierre Chymkowitch Lab (this project)
yPC56 (set2Δ CEN4 or cen4-)*	*MATa set2::His3MX6 lox-CEN4-lox:KanMX GDP-creEBD78:LEU2 his3Δ1 leu2Δ0 ura3Δ0 met15Δ0*	
yPC58 (sas3Δ CEN4 or cen4-)*	*MATa sas3::hphMX6 lox-CEN4-lox:KanMX GDP-creEBD78:LEU2 his3Δ1 leu2Δ0 ura3Δ0 met15Δ0*	
yPC59 (rpd3Δ CEN4 or cen4-)*	*MATa rpd3::hphMX6 lox-CEN4-lox:KanMX GDP-creEBD78:LEU2 his3Δ1 leu2Δ0 ura3Δ0 met15Δ0*	
yPC60 (set1Δ CEN4 or cen4-)*	*MATa set1::hphMX6 lox-CEN4-lox:KanMX GDP-creEBD78:LEU2 his3Δ1 leu2Δ0 ura3Δ0 met15Δ0*	
yPC61 (set2Δ CEN4 or cen4-)*	*MATa set2::hphMX6 lox-CEN4-lox:KanMX GDP-creEBD78:LEU2 his3Δ1 leu2Δ0 ura3Δ0 met15Δ0*	
yPC62 (set2Δ CEN4 or cen4-)*	*MATa set2::hphMX6 lox-CEN4-lox:KanMX GDP-creEBD78:LEU2 his3Δ1 leu2Δ0 ura3Δ0 met15Δ0*	
yPC63 (dot1Δ CEN4 or cen4-)*	*MATa dot1::hphMX6 lox-CEN4-lox:KanMX GDP-creEBD78:LEU2 his3Δ1 leu2Δ0 ura3Δ0 met15Δ0*	
yPC64 (dot1Δ CEN4 or cen4-)*	*MATa dot1::hphMX6 lox-CEN4-lox:KanMX GDP-creEBD78:LEU2 his3Δ1 leu2Δ0 ura3Δ0 met15Δ0*	
yPC65 (rtt109Δ CEN4 or cen4-)*	*MATa rtt109::hphMX6 lox-CEN4-lox:KanMX GDP-creEBD78:LEU2 his3Δ1 leu2Δ0 ura3Δ0 met15Δ0*	

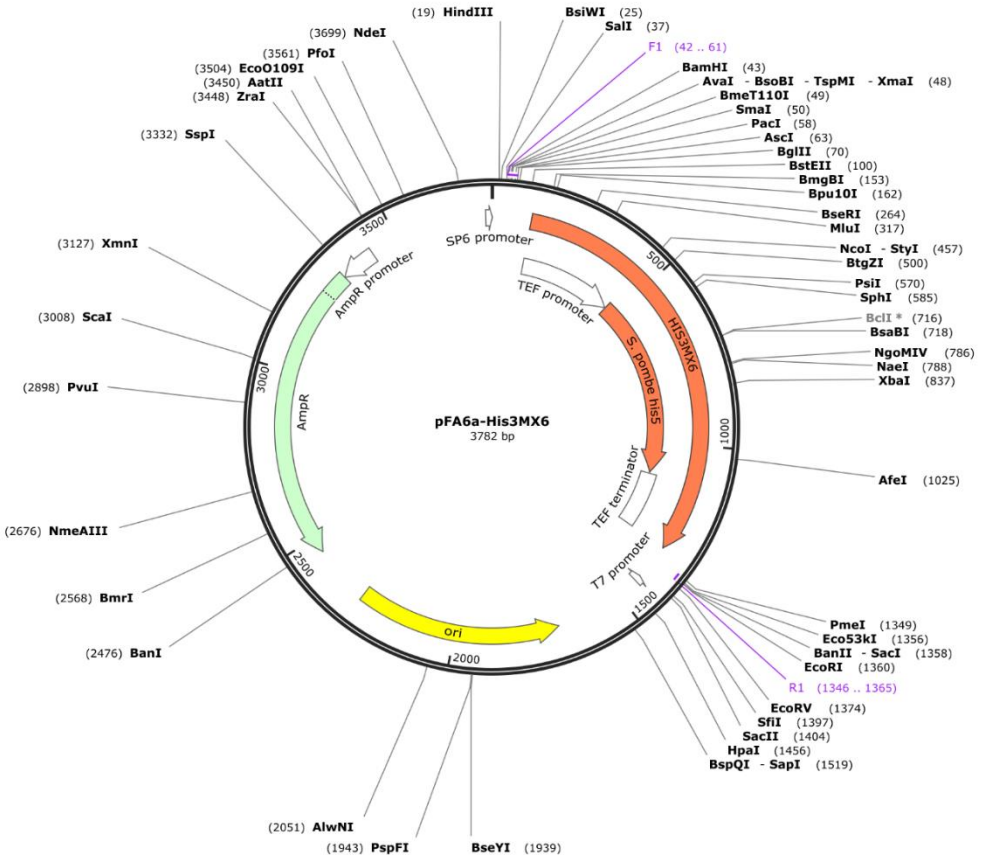

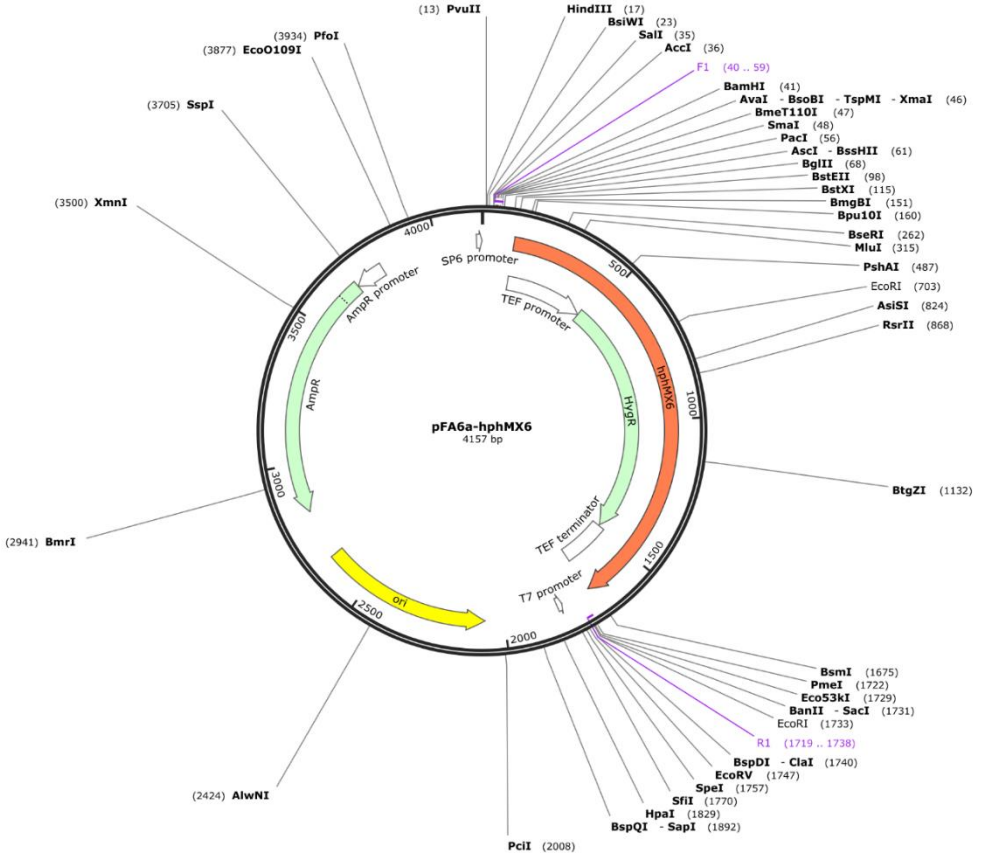

Appendix D: Recipes

10 mg/ml RNAse A stock solution

Ingredients		Final concentration	Procedure
5M NaCl 1M Tris-HCl (pH 8.0) Pancreatic RNAse A H_2O	30 µl 10 µl 100 mg Up to 10 ml	15 mM 10 mM 10 mg/ml	1. *Mix NaCl and Tris-Cl with H_2O* 2. *Dissolve pancreatic RNAse A in the solution* 3. *Dispense 1 ml aliquots into 1.5 ml Eppendorf tubes.* 4. *Store them at -20°C* 5. *If not completely dissolved, boil the required amount for 10 min.*
Total	**10 ml**		

1000X β-Estradiol

Ingredients		Final concentration	Procedure
β-Estradiol 100% EtOH	5.4476 mg Up to 10ml	2 mM	*β-Estradiol molecular weight is 272.38 g/mol.* *Carefully weigh and dissolve the ingredients. The solution is light sensitive, aliquot and keep at -20°C.*
Total	**10 ml**		

CSM-His media (± Agar)

Ingredients		Final concentration	Procedure
Yeast nitrogen base w/o aa	6.7 g	0.67%	*1. Dissolve powders in dH_2O and autoclave.* *2. Add sterile glucose before use.* **If using agar;* *1. Dissolve agar in 600 ml H_2O in a 1 L bottle with a magnetic spinner.* *2. Dissolve yeast nitrogen base and Drop-out in 300 ml H_2O and autoclave.* *3. While hot, add the mix to the agar solution together with glucose and stir with the magnetic spinner.* *4. Pour on to plates before the mixture cools down.*
CSM-His Drop-out	2 g	0.20%	
Agar*	23 g	2.30%	
20% Glucose	100 ml	2.00%	
dH_2O	900 ml		
Total	**1000 ml**		

YPD media (± Agar and Hygromycin)

Ingredients		Final concentration	Procedure
Yeast extract	10 g	1.0%	*1. Dissolve powders in dH_2O and autoclave.* *2. **If adding hygromycin, let the mixture cool until able to handle with your hands.* *3.Add sterile glucose before use.* **If using agar;* *1. Dissolve agar in 600 ml H_2O in a 1 L bottle with a magnetic spinner.* *2. Dissolve yeast extract and peptone in 300 ml H_2O and autoclave.* *3. While hot, add the mix to the agar solution together with glucose and stir with the magnetic spinner.* *4. Pour on to plates before the mixture cools excessively.*
Peptone (Casein digest)	20 g	2.0%	
Agar*	23 g	2.3%	
Hygromycin** (100 mg/ml)	2 ml	200 mg/L (379 µM)	
20% Glucose	100 ml	2.0 %	
dH_2O	900 ml		
Total	**1000 ml**		

10X TE

Ingredients		Final concentration	Procedure
1 M Tris-HCl pH 8.0	10 ml	100 mM 10 mM	*Mix all reagents and autoclave if necessary*
1 M EDTA	1 ml		
mqH_2O	Up to 100 ml		
Total	**100 ml**		

0.1M LiAc/1x TE

Ingredients		Final concentration	Procedure
1 M LiAc*	5 ml	0.1 M	*Use autoclaved materials and reagents. Mix all reagents under sterile conditions and vortex. Use for yeast transformation.*
10X TE*	5 ml	1X TE	
mqH_2O*	Up to 50 ml		
Total	**10 ml**		

*Sterile

40% PEG 3350/0.1M LiAc/1x TE

Ingredients		Final concentration	Procedure
1 M LiAc*	5 ml	0.1 M	Use autoclaved materials and reagents. Mix all reagents under sterile conditions and vortex. Use for yeast transformation.
10X TE*	5 ml	1X TE	
PEG 50%*	40 ml	40 %	
Total	**50 ml**		

*Sterile

Lysis buffer for gDNA extraction

Ingredients		Final concentration	**Procedure**
Triton X-100		2%	*Mix all reagents and vortex*
1 M Tris-HCl (pH 8.0)	5 ml	10 mM	
20 % SDS	0.5 ml	1%	
5 M NaCl	2 ml	100 mM	
H_2O	Up to 50 ml		
Total	**50 ml**		

Appendix E: Equipment and software

Equipment	Brand / model	Purpose
Big centrifuge (up to 50 ml)	VWR, Mega Star 1.6R, No. 521-1750	Cell collection, strain storage
Cell Disruptor	Scientific industries, Inc. Model No. SI-DD58, Disruptor Genie	gDNA and RNA isolation
Electrophoresis machine	Pharmacia Biotech	Agarose gel electrophoresis
Electrophoresis power supply	EPS 300 Power Supply, 300 V, 400 mA, 80 W Code no. 18-1123-97	Agarose gel electrophoresis
Flow Cytometer	LSRFortessa Cell Analyzer , BD Biosciences	Flow cytometry
Gel UV imaging	VWR GenoSmart2	Visualize Agarose gels
Incubator	Heraeus Kendro B6	Culturing
Incubator with orbital shaker	New Brunswich Scientific, Innova 4340	Culturing
Incubator with orbital shaker	Stuart Orbital Incubator S150	Culturing
Light microscopy	Leitz HM-LUX	Cell collection
Light microscopy	Motic AE21	Cell collection
Microcentrifuge	TOMY Micro One,	-
Small centrifuge (up to 2 ml)	-Eppendorf, 5415 D	-
Small centrifuge (up to 2 ml) w/temp. adjustment	-Eppendorf, 5415 R	-
Sonicator	Bioruptor Pico Sonicator, Diagenode	Flow cytometry
Spectrophotometer	Thermo Scientific™ Nanodrop 2000	Nucleotide integrity
Spectrophotometer	Eppendorf BioPhotometer	Measuring cell culture density
Thermoblock	Grant Boekel BBA	gDNA isolation, Transformation
Thermocycler (PCR)	Applied Biosystems by Life Technologies,	Amplification of cassettes and verification of mutants
Thermocycler (PCR)	2720 Thermal Cycler #4359659	Amplification of cassettes and verification of mutants
Thermomixer (24 stk)	Eppendorf Thermomixer C 5382	Reverse Transcription
Thermomixer (24 stk)	Thermomixer comfort No. 5355	Reverse Transcription
Vortexer	Scientific industries, Inc. Model No. SI-0256, Vortex-Genie2	-
-80°C freezer	Thermo Fisher Forma 700 series,	Storing RNA, cell collection
-80°C freezer	Panasonic MDF-S94-PE	Storing RNA, cell collection

Software	Brand	Purpose
BioRender	©BioRender	Create figures
FlowJo™ v.10	BD Biosciences	Flow cytometry analysis
Lightcycler®96 1.1	Roche	qPCR analysis
Word v.2208	Microsoft	Writing
Excel v.2208	Microsoft	Fragment calculations and qPCR analysis
PowerPoint v.2208	Microsoft	Create figures
NanoDrop 2000	Thermo Scientific™	Nucleotide integrity
SnapGene® Viewer 6.0.5	SnapGene®	Fragment calculations

References

Ai, X., & Parthun, M. R. (2004). The Nuclear Hat1p/Hat2p Complex. *Molecular Cell*, *14*(2), 195-205. https://doi.org/10.1016/s1097-2765(04)00184-4

Allan, J., Hartman, P. G., Crane-Robinson, C., & Aviles, F. X. (1980). The structure of histone H1 and its location in chromatin. *Nature*, *288*(5792), 675-679. https://doi.org/10.1038/288675a0

Allard, S., Utley, R. T., Savard, J., Clarke, A., Grant, P., Brandl, C. J., Pillus, L., Workman, J. L., & Côté, J. (1999). NuA4, an essential transcription adaptor/histone H4 acetyltransferase complex containing Esa1p and the ATM-related cofactor Tra1p [https://doi.org/10.1093/emboj/18.18.5108]. *The EMBO Journal*, *18*(18), 5108-5119. https://doi.org/https://doi.org/10.1093/emboj/18.18.5108

Alvino Gina, M., Collingwood, D., Murphy John, M., Delrow, J., Brewer Bonita, J., & Raghuraman, M. K. (2007). Replication in Hydroxyurea: It's a Matter of Time. *Molecular and Cellular Biology*, *27*(18), 6396-6406. https://doi.org/10.1128/MCB.00719-07

Arents, G., Burlingame, R. W., Wang, B. C., Love, W. E., & Moudrianakis, E. N. (1991). The nucleosomal core histone octamer at 3.1 A resolution: a tripartite protein assembly and a left-handed superhelix. *Proceedings of the National Academy of Sciences*, *88*(22), 10148-10152. https://doi.org/doi:10.1073/pnas.88.22.10148

Aricthota, S., Rana, P. P., & Haldar, D. (2022). Histone acetylation dynamics in repair of DNA double-strand breaks [Review]. *Frontiers in Genetics*, *13*. https://doi.org/10.3389/fgene.2022.926577

Awad, S., & Hassan, A. H. (2008). The Swi2/Snf2 bromodomain is important for the full binding and remodeling activity of the SWI/SNF complex on H3- and H4-acetylated nucleosomes. *Ann N Y Acad Sci*, *1138*, 366-375. https://doi.org/10.1196/annals.1414.038

Bar-Ziv, R., Brodsky, S., Chapal, M., & Barkai, N. (2020). Transcription Factor Binding to Replicated DNA. *Cell Reports*, *30*(12), 3989-3995.e3984. https://doi.org/https://doi.org/10.1016/j.celrep.2020.02.114

Bednar, J., Horowitz, R. A., Grigoryev, S. A., Carruthers, L. M., Hansen, J. C., Koster, A. J., & Woodcock, C. L. (1998). Nucleosomes, linker DNA, and linker histone form a unique structural motif that directs the higher-order folding and compaction of chromatin. *Proceedings of the National Academy of Sciences*, *95*(24), 14173-14178. https://doi.org/doi:10.1073/pnas.95.24.14173

Bensasson, D., Zarowiecki, M., Burt, A., & Koufopanou, V. (2008). Rapid evolution of yeast centromeres in the absence of drive. *Genetics*, *178*(4), 2161-2167. https://doi.org/10.1534/genetics.107.083980

Buitrago, D., Labrador, M., Arcon, J. P., Lema, R., Flores, O., Esteve-Codina, A., Blanc, J., Villegas, N., Bellido, D., Gut, M., Dans, P. D., Heath, S. C., Gut, I. G., Brun Heath, I., & Orozco, M. (2021). Impact of DNA methylation on 3D genome structure. *Nature Communications*, *12*(1). https://doi.org/10.1038/s41467-021-23142-8

Carrozza, M. J., Li, B., Florens, L., Suganuma, T., Swanson, S. K., Lee, K. K., Shia, W.-J., Anderson, S., Yates, J., Washburn, M. P., & Workman, J. L. (2005). Histone H3 Methylation by Set2 Directs Deacetylation of Coding Regions by Rpd3S to Suppress Spurious Intragenic Transcription. *Cell*, *123*(4), 581-592. https://doi.org/10.1016/j.cell.2005.10.023

Chen, C.-C., Carson, J. J., Feser, J., Tamburini, B., Zabaronick, S., Linger, J., & Tyler, J. K. (2008). Acetylated Lysine 56 on Histone H3 Drives Chromatin Assembly after Repair and Signals for the Completion of Repair. *Cell*, *134*(2), 231-243. https://doi.org/10.1016/j.cell.2008.06.035

Cheng, T. H., Chang, C. R., Joy, P., Yablok, S., & Gartenberg, M. R. (2000). Controlling gene expression in yeast by inducible site-specific recombination. *Nucleic Acids Res*, *28*(24), E108. https://doi.org/10.1093/nar/28.24.e108

Dechassa, M. L., Zhang, B., Horowitz-Scherer, R., Persinger, J., Woodcock, C. L., Peterson, C. L., & Bartholomew, B. (2008). Architecture of the SWI/SNF-Nucleosome Complex. *Molecular and Cellular Biology*, *28*(19), 6010-6021. https://doi.org/10.1128/mcb.00693-08

Dronamraju, R., Jha, D. K., Eser, U., Adams, A. T., Dominguez, D., Choudhury, R., Chiang, Y.-C., Rathmell, W. K., Emanuele, M. J., Churchman, L. S., & Strahl, B. D. (2018). Set2 methyltransferase facilitates cell cycle progression by maintaining transcriptional fidelity. *Nucleic Acids Research*, *46*(3), 1331-1344. https://doi.org/10.1093/nar/gkx1276

Dungrawala, H., Hua, H., Wright, J., Abraham, L., Kasemsri, T., McDowell, A., Stilwell, J., & Schneider, B. L. (2012). Identification of new cell size control genes in S. cerevisiae. *Cell Division*, *7*(1), 24. https://doi.org/10.1186/1747-1028-7-24

Dörter, I., & Momany, M. (2016). Fungal Cell Cycle: A Unicellular versus Multicellular Comparison. *Microbiology Spectrum*, *4*(6), 4.6.28. https://doi.org/10.1128/microbiolspec.FUNK-0025-2016

Eckert-Boulet, N., Rothstein, R., & Lisby, M. (2011). Cell Biology of Homologous Recombination in Yeast. In (pp. 523-536). Humana Press. https://doi.org/10.1007/978-1-61779-129-1_30

Efroni, S., Duttagupta, R., Cheng, J., Dehghani, H., Hoeppner, D. J., Dash, C., Bazett-Jones, D. P., Le Grice, S., McKay, R. D. G., Buetow, K. H., Gingeras, T. R., Misteli, T., & Meshorer, E. (2008). Global Transcription in Pluripotent Embryonic Stem Cells. *Cell Stem Cell*, *2*(5), 437-447. https://doi.org/https://doi.org/10.1016/j.stem.2008.03.021

Ehrentraut, S. (2010). Rpd3-dependent boundary formation at telomeres by removal of Sir2 substrate. *Proceedings of the National Academy of Sciences*. https://doi.org/https://dx.doi.org/10.1073/pnas.0909169107

Etier, A., Dumetz, F., Chéreau, S., & Ponts, N. (2022). Post-Translational Modifications of Histones Are Versatile Regulators of Fungal Development and Secondary Metabolism. *Toxins*, *14*(5), 317. https://doi.org/10.3390/toxins14050317

Finch, J. T., & Klug, A. (1976). Solenoidal model for superstructure in chromatin. *Proceedings of the National Academy of Sciences*, *73*(6), 1897-1901. https://doi.org/doi:10.1073/pnas.73.6.1897

Frenkel, N., Jonas, F., Carmi, M., Yaakov, G., & Barkai, N. (2021). Rtt109 slows replication speed by histone N-terminal acetylation. *Genome Res*, *31*(3), 426-435. https://doi.org/10.1101/gr.266510.120

Frigerio, C., Di Nisio, E., Galli, M., Colombo, C. V., Negri, R., & Clerici, M. (2023). The Chromatin Landscape around DNA Double-Strand Breaks in Yeast and Its Influence on DNA Repair Pathway Choice. *International Journal of Molecular Sciences*, *24*(4), 3248. https://www.mdpi.com/1422-0067/24/4/3248

Fu, Y., Pastushok, L., & Xiao, W. (2008). DNA damage-induced gene expression in Saccharomyces cerevisiae. *FEMS Microbiology Reviews*, *32*(6), 908-926. https://doi.org/10.1111/j.1574-6976.2008.00126.x

Fyodorov, D. V., Zhou, B.-R., Skoultchi, A. I., & Bai, Y. (2018). Emerging roles of linker histones in regulating chromatin structure and function. *Nature Reviews Molecular Cell Biology*, *19*(3), 192-206. https://doi.org/10.1038/nrm.2017.94

Gershon, L., & Kupiec, M. (2021). The Amazing Acrobat: Yeast's Histone H3K56 Juggles Several Important Roles While Maintaining Perfect Balance. *Genes*, *12*(3), 342. https://doi.org/10.3390/genes12030342

Gilbert, T., McDaniel, S., Byrum, S., Cades, J., Dancy, B., Wade, H., Tackett, A., Strahl, B., & Taverna, S. (2014). A PWWP Domain-Containing Protein Targets the NuA3 Acetyltransferase Complex via Histone H3 Lysine 36 trimethylation to Coordinate Transcriptional Elongation at Coding Regions. *Molecular & cellular proteomics : MCP*, *13*. https://doi.org/10.1074/mcp.M114.038224

Goloborodko, A., Marko, J. F., & Mirny, L. A. (2016). Chromosome compaction by active loop extrusion. *Biophysical Journal*, *110*(10), 2162-2168.

Gordon, F., Luger, K., & Hansen, J. C. (2005). The core histone N-terminal tail domains function independently and additively during salt-dependent oligomerization of nucleosomal arrays. *Journal of Biological Chemistry*, *280*(40), 33701-33706.

Gotta, M., Laroche, T., Formenton, A., Maillet, L., Scherthan, H., & Gasser, S. M. (1996). The clustering of telomeres and colocalization with Rap1, Sir3, and Sir4 proteins in wild-type Saccharomyces cerevisiae. *J Cell Biol*, *134*(6), 1349-1363. https://doi.org/10.1083/jcb.134.6.1349

Grunstein, M., & Gasser, S. M. (2013). Epigenetics in Saccharomyces cerevisiae. *Cold Spring Harbor Perspectives in Biology*, *5*(7), a017491-a017491. https://doi.org/10.1101/cshperspect.a017491

Guillemette, B., Drogaris, P., Lin, H.-H. S., Armstrong, H., Hiragami-Hamada, K., Imhof, A., Bonneil, É., Thibault, P., Verreault, A., & Festenstein, R. J. (2011). H3 Lysine 4 Is Acetylated at Active Gene Promoters and Is Regulated by H3 Lysine 4 Methylation. *PLoS Genetics*, *7*(3), e1001354. https://doi.org/10.1371/journal.pgen.1001354

Hammond, C. M., Strømme, C. B., Huang, H., Patel, D. J., & Groth, A. (2017). Histone chaperone networks shaping chromatin function. *Nature Reviews Molecular Cell Biology*, *18*(3), 141-158. https://doi.org/10.1038/nrm.2016.159

Hassan, A. H., Awad, S., & Prochasson, P. (2006). The Swi2/Snf2 Bromodomain Is Required for the Displacement of SAGA and the Octamer Transfer of SAGA-acetylated Nucleosomes. *Journal of Biological Chemistry*, *281*(26), 18126-18134. https://doi.org/10.1074/jbc.m602851200

Henikoff, S., Ahmad, K., & Malik, H. S. (2001). The Centromere Paradox: Stable Inheritance with Rapidly Evolving DNA. *Science*, *293*(5532), 1098-1102. https://doi.org/10.1126/science.1062939

Howe, L., Auston, D., Grant, P., John, S., Cook, R. G., Workman, J. L., & Pillus, L. (2001). Histone H3 specific acetyltransferases are essential for cell cycle progression. *Genes & Development*, *15*(23), 3144-3154. https://doi.org/10.1101/gad.931401

Jacq, C., Alt-Mörbe, J., Andre, B., Arnold, W., Bahr, A., Ballesta, J. P., Bargues, M., Baron, L., Becker, A., Biteau, N., Blöcker, H., Blugeon, C., Boskovic, J., Brandt, P., Brückner, M., Buitrago, M. J., Coster, F., Delaveau, T., del Rey, F., . . . et al. (1997). The nucleotide sequence of Saccharomyces cerevisiae chromosome IV. *Nature*, *387*(6632 Suppl), 75-78.

Jain, N., Janning, P., & Neumann, H. (2021). 14-3-3 Protein Bmh1 triggers short-range compaction of mitotic chromosomes by recruiting sirtuin deacetylase Hst2. *Journal of Biological Chemistry*, *296*, 100078. https://doi.org/https://doi.org/10.1074/jbc.AC120.014758

Janke, C., Magiera, M. M., Rathfelder, N., Taxis, C., Reber, S., Maekawa, H., Moreno-Borchart, A., Doenges, G., Schwob, E., Schiebel, E., & Knop, M. (2004). A versatile toolbox for PCR-based tagging of yeast genes: new fluorescent proteins, more markers and promoter substitution cassettes. *Yeast*, *21*(11), 947-962. https://doi.org/10.1002/yea.1142

Jenni, S., Dimitrova, Y. N., Valverde, R., Hinshaw, S. M., & Harrison, S. C. (2017). Molecular Structures of Yeast Kinetochore Subcomplexes and Their Roles in Chromosome Segregation. *Cold Spring Harbor Symposia on Quantitative Biology*, *82*, 83-89. https://doi.org/10.1101/sqb.2017.82.033738

Jin, Q. W., Fuchs, J., & Loidl, J. (2000). Centromere clustering is a major determinant of yeast interphase nuclear organization. *Journal of Cell Science*, *113*(11), 1903-1912. https://doi.org/10.1242/jcs.113.11.1903

Kawai, S., Phan, T. A., Kono, E., Harada, K., Okai, C., Fukusaki, E., & Murata, K. (2009). Transcriptional and metabolic response in yeast Saccharomyces cerevisiae cells during polyethylene glycol-dependent transformation. *J Basic Microbiol*, *49*(1), 73-81. https://doi.org/10.1002/jobm.200800123

Kishkevich, A., Cooke, S. L., Harris, M. R. A., & de Bruin, R. A. M. (2019). Gcn5 and Rpd3 have a limited role in the regulation of cell cycle transcripts during the G1 and S phases in Saccharomyces cerevisiae. *Sci Rep*, *9*(1), 10686. https://doi.org/10.1038/s41598-019-47170-z

Kitamura, E., Tanaka, K., Kitamura, Y., & Tanaka, T. U. (2007). Kinetochore microtubule interaction during S phase in Saccharomyces cerevisiae. *Genes Dev*, *21*(24), 3319-3330. https://doi.org/10.1101/gad.449407

Kornberg, R. D. (1977). Structure of Chromatin. *Annual Review of Biochemistry*, *46*(1), 931-954. https://doi.org/10.1146/annurev.bi.46.070177.004435

Krebs, J. E. (2007). Moving marks: Dynamic histone modifications in yeast. *Molecular BioSystems*, *3*(9), 590. https://doi.org/10.1039/b703923a

Kruitwagen, T., Chymkowitch, P., Denoth-Lippuner, A., Enserink, J., & Barral, Y. (2018). Centromeres License the Mitotic Condensation of Yeast Chromosome Arms. *Cell*, *175*(3), 780-795.e715. https://doi.org/10.1016/j.cell.2018.09.012

Kruitwagen, T., Denoth-Lippuner, A., Wilkins, B. J., Neumann, H., & Barral, Y. (2015). Axial contraction and short-range compaction of chromatin synergistically promote mitotic chromosome condensation. *eLife*, *4*. https://doi.org/10.7554/elife.10396

Lafon, A., Petty, E., & Pillus, L. (2012). Functional Antagonism between Sas3 and Gcn5 Acetyltransferases and ISWI Chromatin Remodelers. *PLoS Genetics*, *8*, e1002994. https://doi.org/10.1371/journal.pgen.1002994

Lee, J. S., Shukla, A., Schneider, J., Swanson, S. K., Washburn, M. P., Florens, L., Bhaumik, S. R., & Shilatifard, A. (2007). Histone crosstalk between H2B monoubiquitination and H3 methylation mediated by COMPASS. *Cell*, *131*(6), 1084-1096. https://doi.org/10.1016/j.cell.2007.09.046

Lindstrom, D. L., & Gottschling, D. E. (2009). The Mother Enrichment Program: A Genetic System for Facile Replicative Life Span Analysis in Saccharomyces cerevisiae. *Genetics*, *183*(2), 413-422. https://doi.org/10.1534/genetics.109.106229

Ling, Y. H., & Yuen, K. W. Y. (2019). Point centromere activity requires an optimal level of centromeric noncoding RNA. *Proceedings of the National Academy of Sciences*, *116*(13), 6270-6279. https://doi.org/10.1073/pnas.1821384116

Lowell, J. E., & Pillus, L. (1998). Telomere tales: chromatin, telomerase and telomere function in Saccharomyces cerevisiae. *Cellular and Molecular Life Sciences (CMLS)*, *54*(1), 32-49. https://doi.org/10.1007/s000180050123

Luger, K., Mäder, A. W., Richmond, R. K., Sargent, D. F., & Richmond, T. J. (1997). Crystal structure of the nucleosome core particle at 2.8 Å resolution. *Nature*, *389*(6648), 251-260. https://doi.org/10.1038/38444

Maeshima, K., Rogge, R., Tamura, S., Joti, Y., Hikima, T., Szerlong, H., Krause, C., Herman, J., Seidel, E., Deluca, J., Ishikawa, T., & Hansen, J. C. (2016). Nucleosomal arrays self-assemble into supramolecular globular structures lacking 30-nm fibers. *The EMBO Journal*, *35*(10), 1115-1132. https://doi.org/10.15252/embj.201592660

Mao, F., Leung, W.-Y., & Xin, X. (2007). Characterization of EvaGreen and the implication of its physicochemical properties for qPCR applications. *BMC Biotechnology*, *7*(1), 76. https://doi.org/10.1186/1472-6750-7-76

McDaniel, S. L., & Strahl, B. D. (2013). Stress-free with Rpd3: a unique chromatin complex mediates the response to oxidative stress. *Mol Cell Biol*, *33*(19), 3726-3727. https://doi.org/10.1128/mcb.01000-13

Millar, C. B., & Grunstein, M. (2006). Genome-wide patterns of histone modifications in yeast. *Nature Reviews Molecular Cell Biology*, *7*(9), 657-666. https://doi.org/10.1038/nrm1986

Morgan, D. O. (2014). Sgo1 recruits PP2A to chromosomes to ensure sister chromatid bi-orientation during mitosis [Article]. *Journal of Cell Science*, *127*(22), 4974-4983. https://doi.org/10.1242/jcs.161273

Nakanishi, S., Lee, J. S., Gardner, K. E., Gardner, J. M., Takahashi, Y.-H., Chandrasekharan, M. B., Sun, Z.-W., Osley, M. A., Strahl, B. D., Jaspersen, S. L., & Shilatifard, A. (2009). Histone H2BK123 monoubiquitination is the critical determinant for H3K4 and H3K79 trimethylation by COMPASS and Dot1. *Journal of Cell Biology*, *186*(3), 371-377. https://doi.org/10.1083/jcb.200906005

O'Kane, C. J., & Hyland, E. M. (2019). *Yeast epigenetics: the inheritance of histone modification states* [BSR20182006]. [New York, N.Y.] :.

Obradovic, J., Jurisic, V., Tosic, N., Mrdjanovic, J., Perin, B., Pavlovic, S., & Djordjevic, N. (2013). Optimization of PCR Conditions for Amplification of GC-RichEGFRPromoter Sequence. *Journal of Clinical Laboratory Analysis*, *27*(6), 487-493. https://doi.org/10.1002/jcla.21632

Palozola, K. C., Donahue, G., Liu, H., Grant, G. R., Becker, J. S., Cote, A., Yu, H., Raj, A., & Zaret, K. S. (2017). Mitotic transcription and waves of gene reactivation during mitotic exit. *Science*, *358*(6359), 119-122. https://doi.org/10.1126/science.aal4671

Perrod, S., Cockell, M. M., Laroche, T., Renauld, H., Ducrest, A. L., Bonnard, C., & Gasser, S. M. (2001). A cytosolic NAD-dependent deacetylase, Hst2p, can modulate nucleolar and telomeric silencing in yeast. *Embo j*, *20*(1-2), 197-209. https://doi.org/10.1093/emboj/20.1.197

Proffitt, J. H., Davie, J. R., Swinton, D., & Hattman, S. (1984). 5-Methylcytosine is not detectable in Saccharomyces cerevisiae DNA. *Molecular and Cellular Biology*, *4*(5), 985-988. https://doi.org/10.1128/mcb.4.5.985

Pryde, F., Jain, D., Kerr, A., Curley, R., Mariotti, F. R., & Vogelauer, M. (2009). H3 K36 Methylation Helps Determine the Timing of Cdc45 Association with Replication Origins. *PLoS ONE*, *4*(6), e5882. https://doi.org/10.1371/journal.pone.0005882

Pöpsel, J. (2015). *Characterization of a novel lysine acetylation site in the N-terminal domain of the centromeric histone variant Cse4 in Saccharomyces cerevisiae* Humboldt-Universität zu Berlin, Lebenswissenschaftliche Fakultät].

Ramos Alonso, L., Holland, P., Le Gras, S., Zhao, X., Jost, B., Bjørås, M., Barral, Y., Enserink, J., & Chymkowitch, P. (2023). Mitotic chromosome condensation resets chromatin to safeguard transcriptional homeostasis during interphase. *Proceedings of the National Academy of Sciences of the United States of America*, *120*, e2210593120. https://doi.org/10.1073/pnas.2210593120

Rando, O. J., & Winston, F. (2012). Chromatin and Transcription in Yeast. *Genetics*, *190*(2), 351-387. https://doi.org/10.1534/genetics.111.132266

Ricci, Maria A., Manzo, C., García-Parajo, M. F., Lakadamyali, M., & Cosma, Maria P. (2015). Chromatin Fibers Are Formed by Heterogeneous Groups of Nucleosomes In Vivo. *Cell*, *160*(6), 1145-1158. https://doi.org/https://doi.org/10.1016/j.cell.2015.01.054

Ruiz-Roig, C., Viéitez, C., Posas, F., & de Nadal, E. (2010). The Rpd3L HDAC complex is essential for the heat stress response in yeast. *Mol Microbiol*, *76*(4), 1049-1062. https://doi.org/10.1111/j.1365-2958.2010.07167.x

Schibler, A., Koutelou, E., Tomida, J., Wilson-Pham, M., Wang, L., Lu, Y., Cabrera, A. P., Chosed, R. J., Li, W., Li, B., Shi, X., Wood, R. D., & Dent, S. Y. R. (2016). Histone H3K4 methylation regulates deactivation of the spindle assembly checkpoint through direct binding of Mad2. *Genes & Development*, *30*(10), 1187-1197. https://doi.org/10.1101/gad.278887.116

Separovich, R. J., & Wilkins, M. R. (2021). Ready, SET, Go: Post-translational regulation of the histone lysine methylation network in budding yeast. *Journal of Biological Chemistry*, *297*(2), 100939. https://doi.org/https://doi.org/10.1016/j.jbc.2021.100939

Shahbazian, M. D., Zhang, K., & Grunstein, M. (2005). Histone H2B Ubiquitylation Controls Processive Methylation but Not Monomethylation by Dot1 and Set1. *Molecular Cell*, *19*(2), 271-277. https://doi.org/10.1016/j.molcel.2005.06.010

Song, F., Chen, P., Sun, D., Wang, M., Dong, L., Liang, D., Xu, R.-M., Zhu, P., & Li, G. (2014). Cryo-EM Study of the Chromatin Fiber Reveals a Double Helix Twisted by Tetranucleosomal Units. *Science*, *344*(6182), 376-380. https://doi.org/10.1126/science.1251413

Strahl, B. D., & Briggs, S. D. (2021). The SAGA continues: The rise of cis- and trans-histone crosstalk pathways. *Biochimica et Biophysica Acta (BBA) - Gene Regulatory Mechanisms*, *1864*(2), 194600. https://doi.org/https://doi.org/10.1016/j.bbagrm.2020.194600

Straight, A. F., Marshall, W. F., Sedat, J. W., & Murray, A. W. (1997). Mitosis in living budding yeast: anaphase A but no metaphase plate. *Science*, *277*(5325), 574-578. https://doi.org/10.1126/science.277.5325.574

Taddei, A., & Gasser, S. M. (2012). Structure and function in the budding yeast nucleus. *Genetics*, *192*(1), 107-129. https://doi.org/10.1534/genetics.112.140608

Tang, Y., Gao, X.-D., Wang, Y., Yuan, B.-F., & Feng, Y.-Q. (2012). Widespread Existence of Cytosine Methylation in Yeast DNA Measured by Gas Chromatography/Mass Spectrometry. *Analytical Chemistry*, *84*(16), 7249-7255. https://doi.org/10.1021/ac301727c

Tolomeo, D., Capozzi, O., Stanyon, R. R., Archidiacono, N., D'Addabbo, P., Catacchio, C. R., Purgato, S., Perini, G., Schempp, W., Huddleston, J., Malig, M., Eichler, E. E., & Rocchi, M. (2017). Epigenetic origin of evolutionary novel centromeres. *Scientific Reports*, *7*(1), 41980. https://doi.org/10.1038/srep41980

Tompa, R., & Madhani, H. D. (2007). Histone H3 Lysine 36 Methylation Antagonizes Silencing in Saccharomyces cerevisiae Independently of the Rpd3S Histone Deacetylase Complex. *Genetics*, *175*(2), 585-593. https://doi.org/10.1534/genetics.106.067751

Vagnarelli, P. (2013). Chapter Six - Chromatin Reorganization Through Mitosis. In R. Donev (Ed.), *Advances in Protein Chemistry and Structural Biology* (Vol. 90, pp. 179-224). Academic Press. https://doi.org/https://doi.org/10.1016/B978-0-12-410523-2.00006-7

Venkatesh, S., Li, H., Gogol, M. M., & Workman, J. L. (2016). Selective suppression of antisense transcription by Set2-mediated H3K36 methylation. *Nature Communications*, *7*(1), 13610. https://doi.org/10.1038/ncomms13610

Voichek, Y., Bar-Ziv, R., & Barkai, N. (2016). Expression homeostasis during DNA replication. *Science*, *351*(6277), 1087-1090. https://doi.org/10.1126/science.aad1162

Voichek, Y., Mittelman, K., Gordon, Y., Bar-Ziv, R., Lifshitz Smit, D., Shenhav, R., & Barkai, N. (2018). Epigenetic Control of Expression Homeostasis during Replication Is Stabilized by the Replication Checkpoint. *Molecular Cell*, *70*(6), 1121-1133.e1129. https://doi.org/https://doi.org/10.1016/j.molcel.2018.05.015

Warsi, T. H., Navarro, M. S., & Bachant, J. (2008). DNA Topoisomerase II Is a Determinant of the Tensile Properties of Yeast Centromeric Chromatin and the Tension Checkpoint. *Molecular Biology of the Cell*, *19*(10), 4421-4433. https://doi.org/10.1091/mbc.e08-05-0547

Zhang, K., Lin, W., Latham, J. A., Riefler, G. M., Schumacher, J. M., Chan, C., Tatchell, K., Hawke, D. H., Kobayashi, R., & Dent, S. Y. (2005). The Set1 methyltransferase opposes Ipl1 aurora kinase functions in chromosome segregation. *Cell*, *122*(5), 723-734. https://doi.org/10.1016/j.cell.2005.06.021

Zhang, Q., Yoon, Y., Yu, Y., Parnell, E. J., Garay, J. A. R., Mwangi, M. M., Cross, F. R., Stillman, D. J., & Bai, L. (2013). Stochastic expression and epigenetic memory at the yeast HO promoter. *Proceedings of the National Academy of Sciences*, *110*(34), 14012-14017. https://doi.org/doi:10.1073/pnas.1306113110

Zhou, B. R., Jiang, J., Feng, H., Ghirlando, R., Xiao, T. S., & Bai, Y. (2015). Structural Mechanisms of Nucleosome Recognition by Linker Histones. *Mol Cell*, *59*(4), 628-638. https://doi.org/10.1016/j.molcel.2015.06.025

Zhou, J., Zhou, B. O., Lenzmeier, B. A., & Zhou, J.-Q. (2009). *Histone deacetylase Rpd3 antagonizes Sir2-dependent silent chromatin propagation* [3699-3713]. [Oxford].